

AD A115232

ELECTRON DOSE ATTENUATION KERNELS FOR SLAB AND SPHERICAL GEOMETRIES

T. M. Jordon

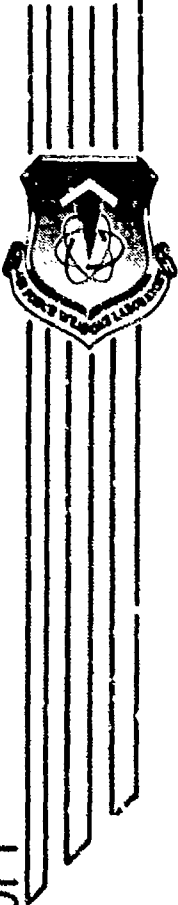
Experimental & Math Physics Consultants
Santa Monica, CA 90403

November 1981

Final Report

Approved for public release; distribution unlimited.

DTIC FILE COPY



AIR FORCE WEAPONS LABORATORY
Air Force Systems Command
Kirtland Air Force Base, NM 87117

DTIC
ELECTE
JUN 7 1982
S B D

This final report was prepared by Experimental Physics Consultants, Santa Monica, California, under Contract F29650-78-M-2320, Job Order 88091901. Dr Joseph F. Janni (NTYC) was the Laboratory Project Officer-in-Charge.

When US Government drawings, specifications, or other data are used for any purpose other than a definitely related Government procurement operation, the Government thereby incurs no responsibility nor any obligation whatsoever, and the fact that the Government may have formulated, furnished, or in any way supplied the said drawings, specifications, or other data, is not to be regarded by implication or otherwise, as in any manner licensing the holder or any other person or corporation, or conveying any rights or permission to manufacture, use or sell any patented invention that may in any way be related thereto.

This report has been authored by a contractor of the United States Government. Accordingly, the United States Government retains a nonexclusive, royalty-free license to publish or reproduce the material contained herein, or allow others to do so, for the United States Government purposes.

The Public Affairs Office has reviewed this report, and it is releasable to the National Technical Information Service, where it will be available to the general public, including foreign nationals.

If your address has changed, if you wish to be removed from our mailing list, or if your organization no longer employs the addressee, please notify AFWL/NTYC, Kirtland AFB, NM 87117 to help us maintain a current mailing list.

This technical report has been reviewed and is approved for publication.

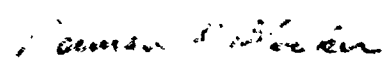


JOSEPH F. JANNI, PhD
Project Officer



MARION F. SCHNEIDER
Lt Colonel, USAF
Chief, Satellite and C³ Branch

FOR THE COMMANDER



NORMAN K. BLOCKER
Colonel, USAF
Chief, Applied Physics Division

DO NOT RETURN COPIES OF THIS REPORT UNLESS CONTRACTUAL OBLIGATIONS OR NOTICE ON A SPECIFIC DOCUMENT REQUIRES THAT IT BE RETURNED.

UNCLASSIFIED

SECURITY CLASSIFICATION OF THIS PAGE (When Data Entered)

REPORT DOCUMENTATION PAGE		READ INSTRUCTIONS BEFORE COMPLETING FORM
1. REPORT NUMBER AFWL-TR-81-43	2. GOVT ACCESSION NO. AD-A745 232	3. RECIPIENT'S CATALOG NUMBER
4. TITLE (and Subtitle) ELECTRON DOSE ATTENUATION KERNELS FOR SLAB AND SPHERICAL GEOMETRIES	5. TYPE OF REPORT & PERIOD COVERED Final Report	
	6. PERFORMING ORG. REPORT NUMBER	
7. AUTHOR(s) T. M. Jordan	8. CONTRACT OR GRANT NUMBER(s) F29650-78-M-2320	
9. PERFORMING ORGANIZATION NAME AND ADDRESS Experimental & Math Physics Consultants San Francisco, CA 90403	10. PROGRAM ELEMENT, PROJECT, TASK AREA & WORK UNIT NUMBERS 62601F/88091901	
11. CONTROLLING OFFICE NAME AND ADDRESS Air Force Weapons Laboratory (NTYC) Kirtland Air Force Base, NM 87117	12. REPORT DATE November 1981	
	13. NUMBER OF PAGES 120	
14. MONITORING AGENCY NAME & ADDRESS (if different from Controlling Office)	15. SECURITY CLASS. (of this report) Unclassified	
	15a. DECLASSIFICATION DOWNGRADING SCHEDULE	
16. DISTRIBUTION STATEMENT (of this Report) Approved for public release; distribution unlimited.		
17. DISTRIBUTION STATEMENT (of the abstract entered in Block 20, if different from Report)		
18. SUPPLEMENTARY NOTES		
19. KEY WORDS (Continue on reverse side if necessary and identify by block number) Electron Shielding Space Satellites Electron Attenuation Bremsstrahlung Depth Dose Space Radiation Dose Attenuation Slab-to-Sphere Conversion Fission Spectrum Monte Carlo		
20. ABSTRACT (Continue on reverse side if necessary and identify by block number) Dose attenuation kernels are given for fission spectrum electrons in aluminum shields with slab and spherical geometries. Sectoring methods used for satellites and space vehicles are discussed and several mathematical relationships are summarized. Dose attenuation data for monoenergetic electrons are presented for several shield materials and geometrics. ↑		

CONTENTS

<u>Section</u>		<u>Page</u>
I	INTRODUCTION	3
II	KERNELS	4
III	SECTORING	14
IV	MANIPULATIONS	20
V	ANOTHER SECTORING KERNEL	32
VI	SECTORING KERNEL SELECTION	40
	APPENDIX A. MONOENERGETIC ELECTRON ATTENUATION DATA	63



Accession For	
NTIS GRA&I	<input checked="" type="checkbox"/>
DTIC TAB	<input type="checkbox"/>
Unannounced	<input type="checkbox"/>
Justification	
By	
Distribution/	
Availability Codes	
Avail and/or	
Dist	Special
A	

ILLUSTRATIONS

<u>Figure</u>		<u>Page</u>
1	Aluminum Dose Attenuation, Back-scatter Effects	8
2	Aluminum Dose Attenuation, Geometry Effects	10
3	Comparison of Slab Kernels	12
4	Solid Sphere Kernels, Jovian Electrons	17
5	Solid Sphere Kernels, Fission Electrons	18
6	Flux Tube Geometry	22
7	Spherical Shield Geometry	31
8	Minimum Path Geometry	37

I. INTRODUCTION

Monte Carlo dose attenuation kernels for the transport of fission electrons through aluminum have been calculated for simple slab and spherical geometries. These kernels are presented in Section II.

Solid angle sectoring methods are commonly used for complex geometry calculations. The selection of kernels appropriate to sectoring calculations is discussed in Section III.

Several factors of 2 are sometimes handled incorrectly in space radiation dose calculations. These factors and some mathematical relationships are presented in Section IV.

Section V derives several relationships for spherical shields and describes sectoring kernels that predict correct results in two simple shield geometries.

Section VI reiterates prior information on sectoring kernels and includes a scheme for predicting shield curvature effects.

Dose attenuation data for slab, sphere, and shell, and solid sphere shields are presented in the appendix. These data span the energy range of 0.1 to 8 MeV and materials from hydrogen through uranium.

II. KERNELS

Attenuation kernels are denoted as functions of shield thickness t ; e.g., $K(t)$ is the response behind a shield of thickness t . The units of t are given variously as cm, mils, and g/cm^2 ,

All kernels are presented in the form used for sectoring analyses. If R denotes the total response e.g., dose

$$R_{\text{complex geometry}} = \sum_{\text{solid angle sectors}} \left(\frac{\text{sector solid angle}}{4\pi} \right) K(t \text{ of sector}) \quad (1)$$

This implies that slab shield kernels which have a source incident on only one side are multiplied by 2 to form $K(t)$. Thus, source-shield configurations have mirror symmetry in the dose plane.

For example, a dose point between two slab shields of thicknesses t_1 and t_2 would have the response computed as

$$R_{\text{total}} = \frac{1}{2} K(t_1) + \frac{1}{2} K(t_2) \quad (2)$$

and if t_2 becomes infinite

$$R_{\text{total}} = \frac{1}{2} K(t_1) \quad (3)$$

The geometry of the shield is denoted by a subscript on the kernel K :

$K_{-}(t)$ is two times the dose behind a slab shield of thickness, t . No backscatter material is present. Radiation is incident from one side only.

$K_{\infty}(t)$ is two times the dose behind a slab shield of thickness, t , with an infinite backscatter material. Radiation is incident from one side only.

$K_{=}(t)$ is the dose between two slab shields each of thickness, t . Radiation is incident from both sides. The symmetry makes $K_{=}(t)$ equivalent to two times the dose behind a shield of thickness, t , with a backscatterer of thickness t .

$K_{0}(t)$ is the dose at the center of a spherical shell shield of thickness, t . The inner radius of the spherical shell is essentially infinite. Radiation is incident on the outside of the shell. Radiation transmitted through the shell can backscatter from the shell.

$K.(t)$ is the dose at the center of a solid spherical shield of thickness, t , with radiation incident on the outer surface of the sphere.

The dose for zero shield thickness is the same for geometries without a backscatterer

$$K_{-}(0) = K_{=}(0) = K_{0}(0) = K.(0) = K_{\text{free space}} \quad (4)$$

The double slab shield configuration is equivalent to an infinite backscatterer for large thickness so that

$$K_{\infty}(t) = K_{\underline{}}(t) \quad \text{for large } t \quad (5)$$

CALCULATION TECHNIQUES

An isotropic radiation field ϕ^0 in particles/cm² is described as a transport problem by a surface source or current of strength $\phi^0/4$ particles/cm². The surface on which the source is defined must be exterior to the shield geometry. A cosine angular distribution relative to the inward surface normal is required to reproduce an isotropic flux inside the source surface.

A fission electron energy distribution was used in the dose calculations. The energy variation of this spectrum was represented by (normalizing constants suppressed)

$$\begin{aligned} f(E) &= \exp(-0.575 E - 0.055 E^2) \quad \text{particles/MeV} \\ &= \exp\left(-\left[\frac{E + 5.227}{4.264}\right]^2\right) \end{aligned} \quad (6)$$

where E is the electron energy in MeV, restricted to the range $0 < E < 7$ MeV. This energy dependence was integrated numerically for normalization to a fluence of one electron/cm².

The Monte Carlo calculations were performed using adjoint methods described in Reference 1. Histories were generated for

1. Jordan, T.W., An Adjoint Charged Particle Transport Method, EMP.L76.072, July 1976.

an infinite medium of aluminum. Shield geometries of various thicknesses were overlaid onto the infinite medium electron tracks to obtain a dose contribution for each geometry (Ref. 2). The production calculation required 5 minutes (CDC 7600) to obtain simultaneous results for the five geometries and 40 shield thicknesses. Calculated standard deviations less than 2 percent were obtained for most data points.

CALCULATION RESULTS

Dose rates are expressed as point results in rad (Si) units. No silicon was actually included in the calculations. The flux spectrum obtained in aluminum was LET weighted, i.e., folded with the restricted linear energy transfer function for silicon. The restricted energy transfer excluded energy loss mechanisms included in the transport simulation, i.e., radiative energy loss and energy losses corresponding to high energy secondary electrons.

The effect of including a backscatter material in dose calculations is shown in Figure 1. The lower curve is for a one side slab without a backscatterer, $K_-(t)$, and the upper curve is for the two slab shield $K_+(t)$, i.e., backscatter thickness equal to shield thickness. For shield thicknesses greater than 10 mils aluminum, the backscattered electrons add about 30 percent to the dose. Restated, the absence of a backscatter material reduces the dose by approximately 35 percent.

2. Jordan, T.W., Parametric Adjoint Electron Transport in 1-D Geometries, EMP.L76.097, September 1976.

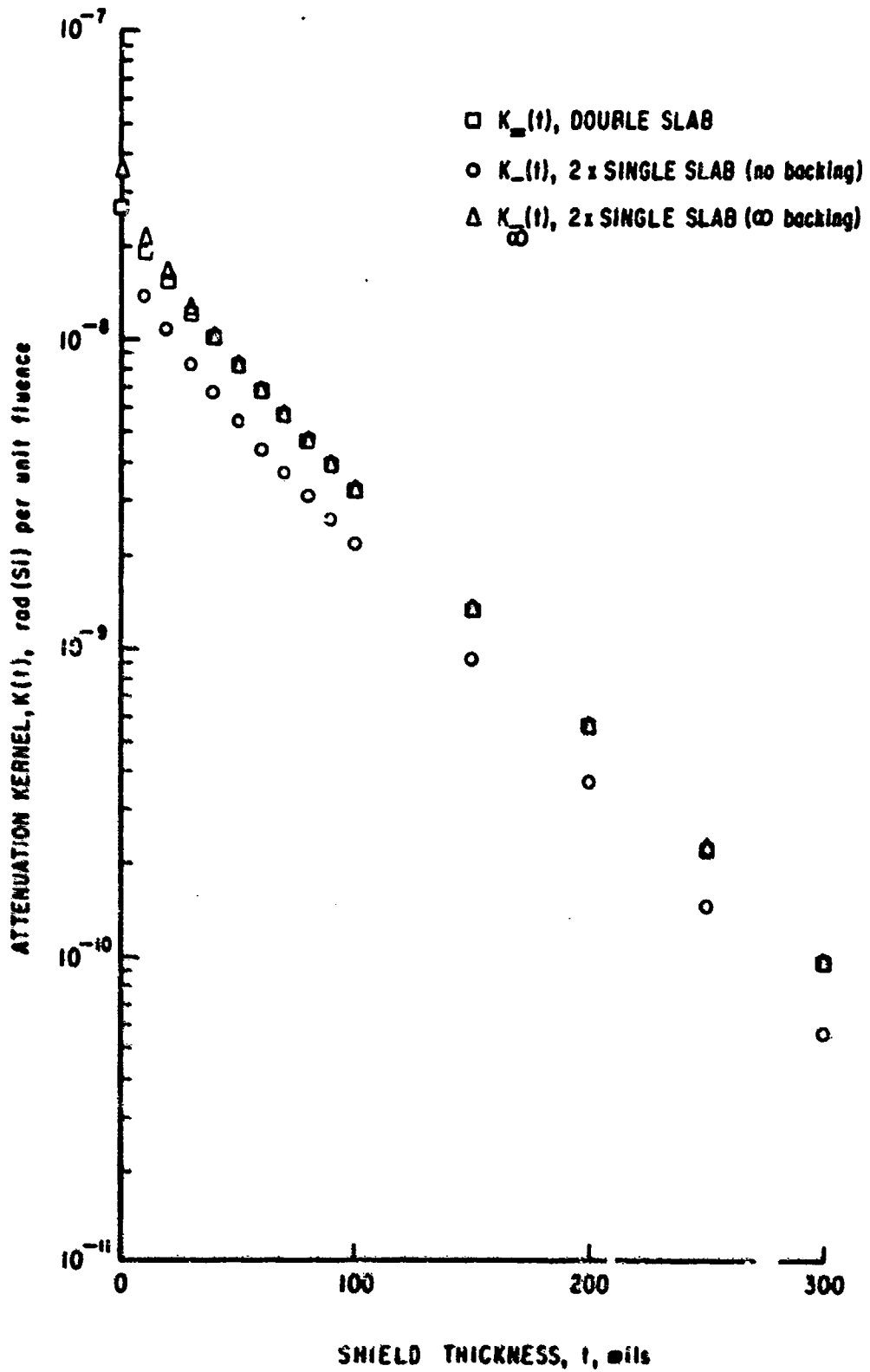


Figure 1. Aluminum Dose Attenuation - Backscatter effects
Fission Electrons, Unit Free Space Fluence

The effect of infinite backing is most notable at zero thickness where the slab dose is increased by approximately 30 percent. This is indicated by the highest curve in the vicinity of zero shield thickness. The infinite backing curve cannot be distinguished from the double shield curve for thicknesses greater than 25 mils.

The effect of shield geometry on dose is shown in Figure 2. The lowest curves are for the slab geometry shields which have backing.

The intermediate curve is for spherical shell shields. The shell shield curve roughly parallels the slab shield curve for thicknesses of 30 mils or more. The shell shield dose is higher by 30 to 50 percent. The parallel nature of the slab and shell curves implies that the angular distribution of the electrons has an approximate equilibrium since, for an infinite spherical shell radius

$$K_0(t) = 4\pi K_{\Omega}(t,1) \quad (7)$$

where $K_{\Omega}(t,\mu)$ is the dose per steradian for slab geometry as a function of μ , the cosine of the angle between the slab normal and the particle direction.

The highest dose curve is for a solid sphere shield geometry. For this geometry, the dose curve diverges from the other curves as the shield thickness increases.

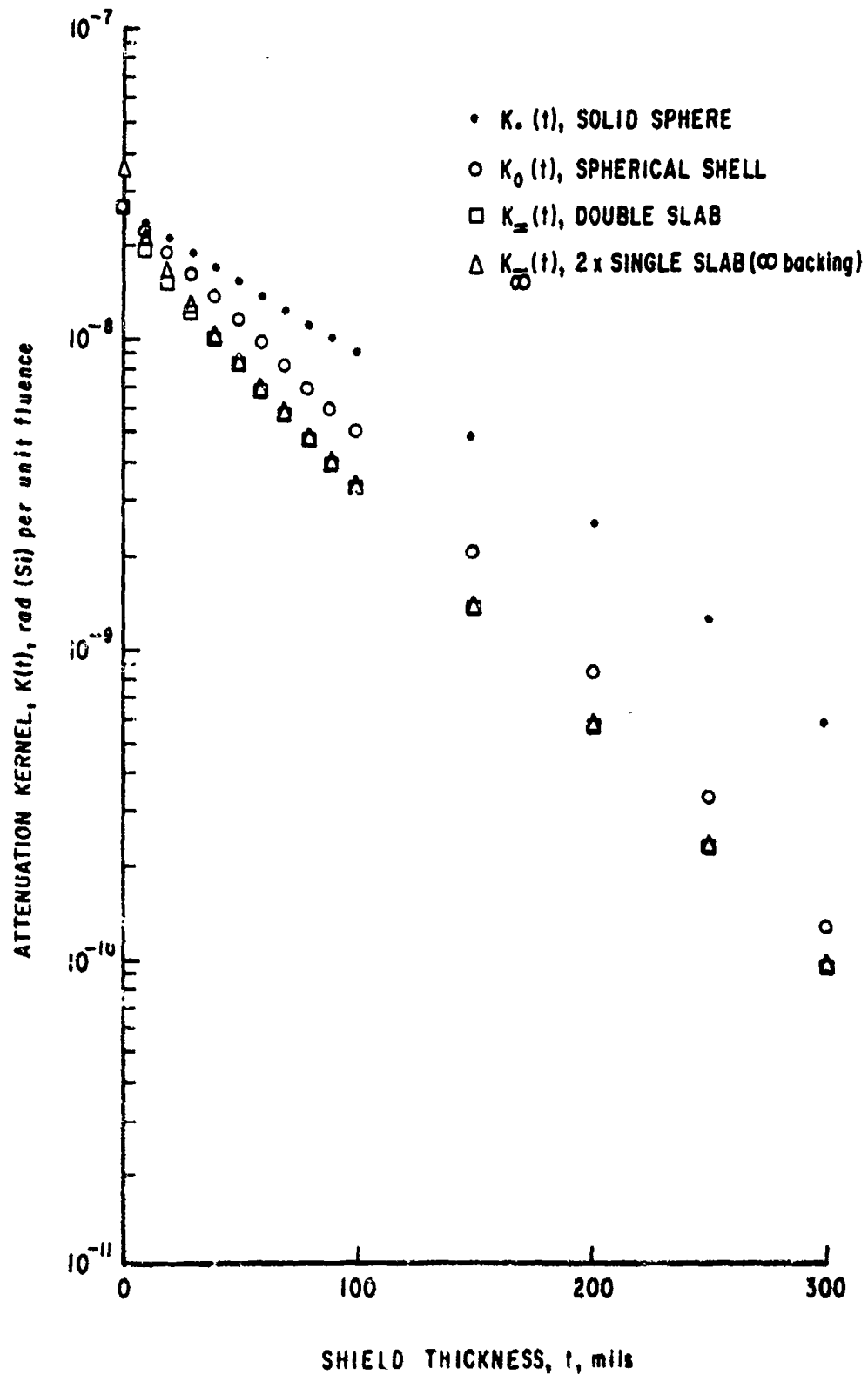


Figure 2. Aluminum Dose Attenuation - Geometry Effects
Fission Electrons, Unit Free Space Fluence

The enhanced dose, or focusing, results from the shorter average particle paths traversed in the spherical geometry. More of the external source electrons are able to penetrate the shield in the solid sphere geometry. As the shield thickness approaches the end of the effective particle range, only a small ~~spot of area on~~ the slab shield surface can contribute to the dose. For the same shield thickness, the entire surface of the solid sphere will contribute to the dose.

ACCURACY

The accuracy of these curves is determined partially by comparisons with other calculations. Figure 3 is a comparison of the infinite backed dose (slab shield) with Morel's Monte Carlo calculations reported in Reference 3.

The calculated results in Reference 3 have been multiplied by 2 in correspondence with the terminology used here (all one side slab results multiplied by 2 to correspond with 4π source incidence). These data are for the average dose in a silicon device 1 mm thick with infinite backing in contrast to the point dose results reported earlier. Silicon and aluminum have very similar cross sections. Therefore, the 1 mm Si is comparable to 23 mils of aluminum. This average dose data has been plotted in histogram form.

3. Morel, J.E., Doses to a Thin Silicon Slab Behind Aluminum, Aluminum-Tantalum, and Aluminum-Lead Shields for Isotropic Fission Electrons, AFWL-DYT-TN-75-1, Air Force Weapons Laboratory, Kirtland AFB, NMex, July 1975.

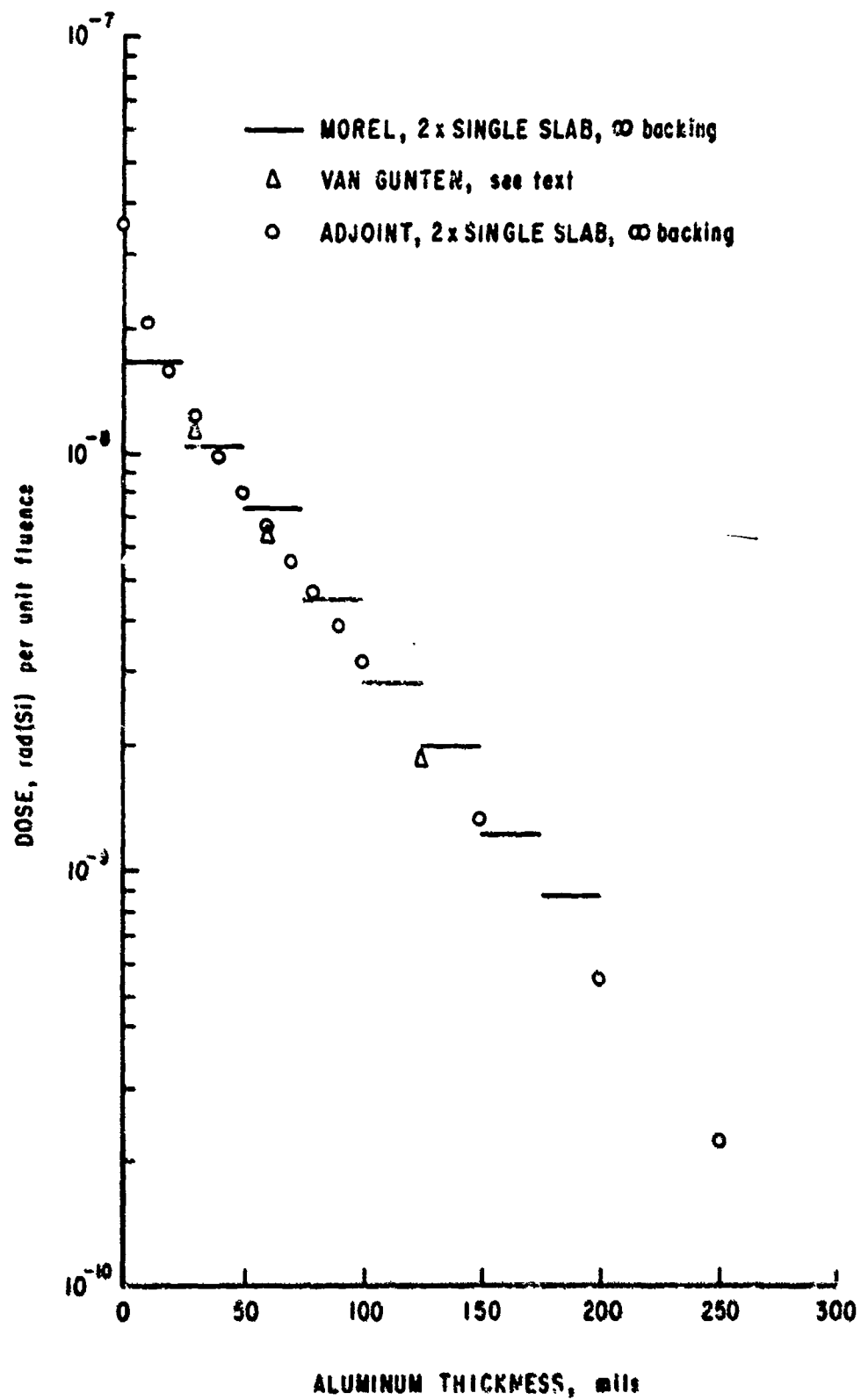


Figure 3. Comparison of Slab Kernels
Fission Spectrum Electrons, Unit Free Space Fluence

There is a definite divergence of the calculations which approaches 30 percent at 175 to 200 mils. The reason for the divergence cannot be identified from material at hand.

The experimental results shown in Reference 4* have been used in previous validations of the adjoint method. These results were obtained from hollow boxes of various aluminum wall thicknesses. The data for 30, 60, and 124 mil walls are used for comparison by the following steps: near and far wall doses are added, then the sum is doubled. The experimental data are for a source incident on one wall. Adding near and far wall dose accounts approximately for backscatter. Doubling accounts for two side incidence.

BREMSSTRAHLUNG

The infinite medium tracking models used for these calculations did not produce sufficient photons to yield accurate photon dose results in the small shield geometries. Peripheral numerical calculation indicates a peak bremsstrahlung dose of approximately 5×10^{-12} rad (Si) per unit free space electron fluence in the slab geometries.

4. Van Gunten, O.O., Three Dimensional Electron Dose Distribution Measurements, University of Maryland Thesis, 1971.

* Van Gunten, O.O., Private Communication on reduction of experimental data by two, February 1976.

III. SECTORING

Complex geometry dose calculations can be performed efficiently by adjoint Monte Carlo. The most usual calculation method, however, is solid angle sectoring.

Sectoring calculations must neglect details of the particle transport. However, these approximate methods should yield the correct answer when applied to simple geometries.

The usual sectoring method is to integrate numerically

$$R = \frac{1}{4\pi} \int_{4\pi} K(t(\underline{u})) \, d\underline{u} \quad (8)$$

where $t(\underline{u})$ is the mass thickness encountered between the detector point and the exterior of the vehicle along the direction \underline{u} . The $K(t)$ is a response attenuation kernel either tabulated or curve fit as a function of mass thickness t .

By requiring that sectoring methods yield the correct dose at the center of a solid sphere of radius t , it follows that $K(t)$ must be the solid sphere kernel $K.(t)$.

Requiring that sectoring also produce the correct dose at the center of a semi-infinite slab of thickness $2t$, it follows that

$$R = K_{\infty}(t) = \int_0^1 K.(t/\mu) \, d\mu \quad (9)$$

Calculating partial derivatives with respect to t (easier if the integration variable is first changed to $r = t/\mu$) yields

$$K.(t) = K_{\underline{}}(t) - t \frac{dK_{\underline{}}(t)}{dt} \quad (10)$$

This relationship must be satisfied by the kernels if sectoring analysis gives the correct answer for the limiting cases of simple slab or solid sphere shields. The relationship has been reported in a private communication.*

The relationship is exact for cosine sources and the straight ahead approximation, i.e., particle transport with energy loss but no angular deflections. The straight ahead approximation is applicable to and used for heavy charged particles. Application to electron problems is suspect for energies less than tens of MeV.

Equation 10 is also exact for the following hypothetical transport problem: a uniform infinite medium and a cosine angular distribution surface source which emits positive (real) particles into the hemisphere towards the detector and negative (not real) particles into the hemisphere away from the detector.

The hypothetical problem has two aspects not encountered in real problems. Source particles emitted into the forward (detector) hemisphere may make multiple passes across the source plane, enhancing response kernels. Negative particles emitted

* Smith, E.C., Private Communication, Hughes, 1976.
Radke, G., Private Communication, AFWL, 1977.

into the backward hemisphere may also cross the source plane one or more times, contributing and, thereby, decreasing the kernel. The net effect is a kernel decrease.

Arguing that particles reflected across the source plane are a second order effect gives credence to using the relationship generally. More support is obtained by checking the equation for problems where both slab and sphere kernels are available.

Slab and sphere kernels have been calculated for Jovian electron spectra. Testing of Equation 10 for Jovian kernels is shown in Figure 4. The agreement is good for both aluminum and tungsten. However, the Jovian spectrum has appreciable content above 10 MeV where the straight ahead approximation also starts to apply.

Equation 10 can be tested on the fission electron kernels with the results shown in Figure 5. Again, the agreement is good. The fission electron spectrum is harder than radiation belt spectra. However, it has sufficient low energy content, less than 2 MeV, to suggest that Equation 10 holds under fairly general conditions.

The following steps are suggested for sectoring analysis:

- (1) evaluate $K_{\underline{}}(t)$; i.e., a Monte Carlo calculation for a source emitting $\frac{1}{2}$ particle with a cosine distribution in the forward hemisphere incident on a slab shield of infinite thickness.

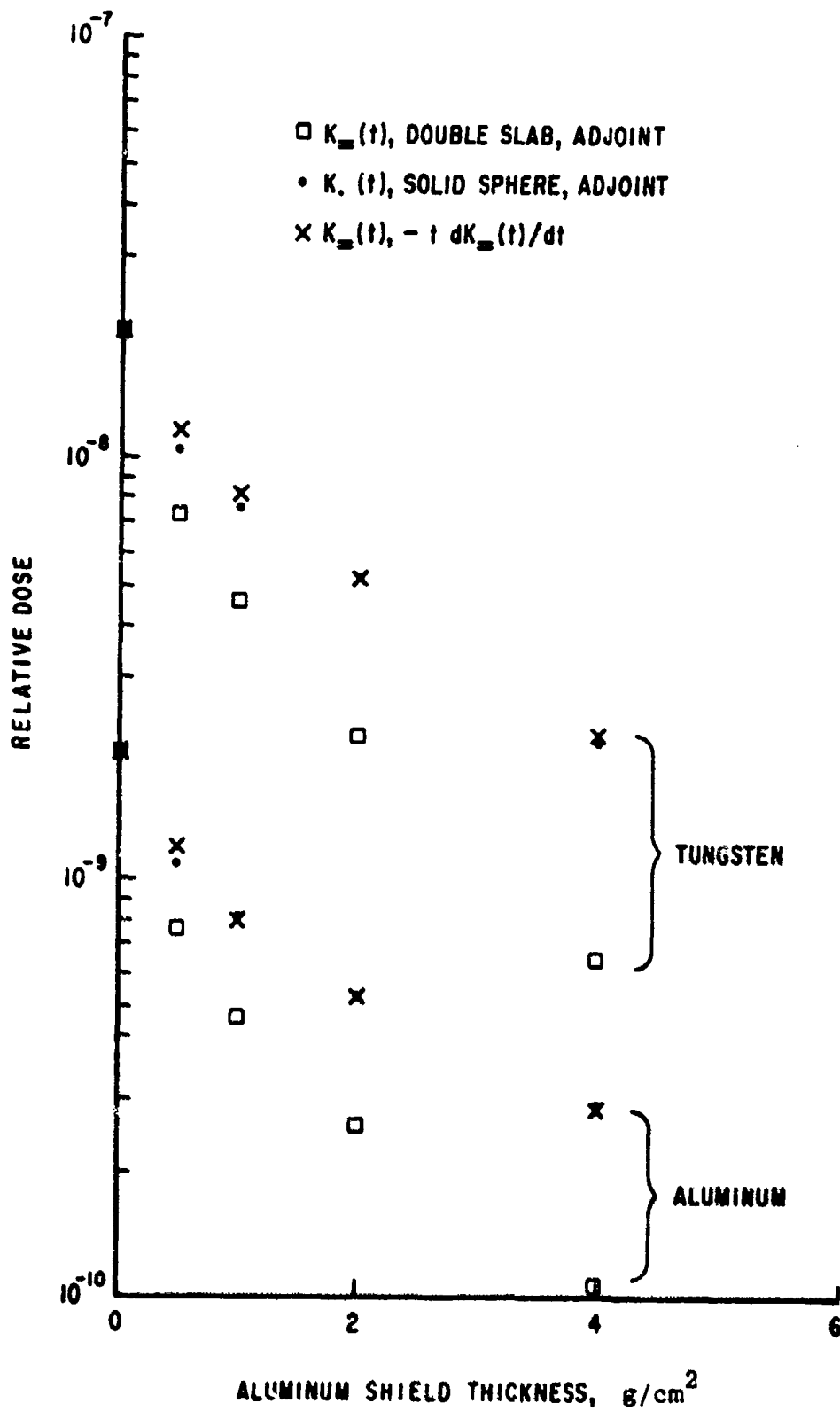


Figure 4. Solid Sphere Kernels - Jovian Electrons

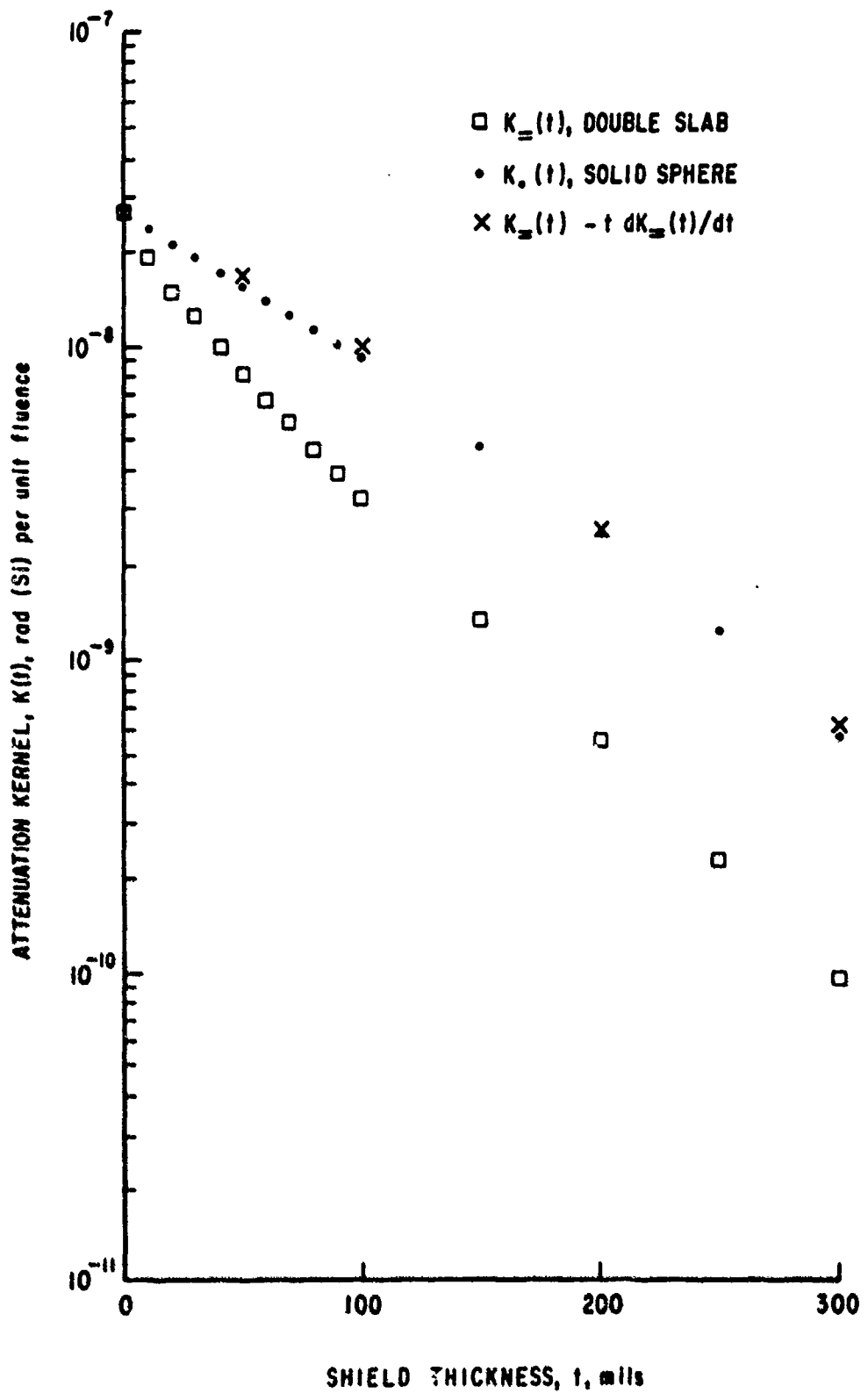


Figure 5. Solid Sphere Kernels - Fission Electrons

- (2) calculate $K.(t)$ using Equation 10;
- (3) use $K.(t)$ in the sectoring analysis.

The infinite slab thickness ensures that backscattered particles are accounted for in the analysis. The kernel $K_{\infty}(t)$ is calculated as basic data since almost all Monte Carlo codes can compute it. Nonadjoint methods have difficulties when computing $K.(t)$ directly.

The relationship between slab and sphere kernels applies to solid spheres and not spherical shells. From the adjoint calculations for spherical geometries, it is seen that the solid sphere response is greater than the spherical shell response. However, the solid sphere kernel will yield solid sphere response at the center of a spherical shell. This over estimate for one simple geometry is deemed better than using kernels which under estimate the response in other simple geometries.

A more complicated sectoring kernel is given in Section V. This kernel requires modifications to the sectoring program. The kernel eliminates the conservatism of the solid sphere kernel when applied to shell geometries and produces the correct response when applied to simple geometry solid shields, slabs, and the interior of spherical shells.

IV. MANIPULATIONS

A space radiation environment is usually expressed as a scalar fluence (or flux) differential in energy

$$\phi(E) \quad (\text{particles/cm}^2 \text{ MeV}) \quad (11)$$

or, equivalently, by the integral scalar fluence

$$\phi(>E) = \int_E^{\infty} \phi(E') \, dE' \quad (12)$$

where

$$\phi(E) = - \frac{d\phi}{dE} (>E) \quad (13)$$

This fluence environment has inverse area units which is often misleading. The density per unit area is measured on a surface perpendicular to the direction of particle motion. A scalar fluence implies integration over all particle directions. Therefore, the density per unit area of a surface with fixed orientation cannot always be determined.

With isotropy, the differential angular flux can be written as

$$\phi(\underline{x}, \underline{u}, E) = \frac{\phi(E)}{4\pi} \text{ particles/cm}^2 \text{ MeV steradian second} \quad (14)$$

where \underline{x} denotes position and \underline{u} is a unit vector in the direction of particle motion.

A more basic definition of the differential angular flux is the particle density

$$\rho(\underline{x}, \underline{u}, E) \quad (\text{particles/cm}^3 \text{ MeV steradian}) \quad (15)$$

multiplied by the particle speed $v(E)$ in cm/s

$$\phi(\underline{x}, \underline{u}, E) = \rho(\underline{x}, \underline{u}, E) v(E) \quad (16)$$

The vector current is defined as the flux times the particle direction vector \underline{u}

$$\underline{j}(\underline{x}, \underline{u}, E) = \underline{u} \phi(\underline{x}, \underline{u}, E) \quad (17)$$

the differential vector current can also be written as the particle density times the vector velocity $\underline{v}(E) = \underline{u} v(E)$

$$\underline{j}(\underline{x}, \underline{u}, E) = \underline{v}(E) \rho(\underline{x}, \underline{u}, E) \quad (18)$$

Defining a fixed unit area in space and letting \underline{n} denote the unit normal to this area (on the side containing the projection of \underline{u}), then the number of particles crossing this unit area is the component of the current \underline{j} along \underline{n}

$$j_n(\underline{x}, \underline{u}, E) = \underline{n} \cdot \underline{j}(\underline{x}, \underline{u}, E) \quad (19)$$

$$= \underline{n} \cdot \underline{v}(E) \rho(\underline{x}, \underline{u}, E) \quad (20)$$

$$= \underline{n} \cdot \underline{u} \phi(\underline{x}, \underline{u}, E) \quad (21)$$

This same relationship can be obtained by considering the number of particles which cross the area per unit time. For a time interval dt , all particles closer than $v(E) dt$ will cross the surface (ignoring interactions). The volume of particles with direction \underline{u} that cross the surface is a tube of length $v(E) dt$ and cross sectional area $dA = dA_n \underline{n} \cdot \underline{u}$ where dA_n is the differential area perpendicular to \underline{n} .

$$dV = dA_n \underline{n} \cdot \underline{u} v(E) dt \quad (22)$$

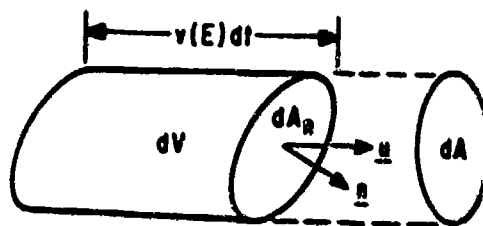


Figure 6. Flux Tube Geometry

multiplying the volume by the particle density gives the total number of particles crossing the area dA_n . Dividing by the area and the time interval dt yields the total number of particles crossing per unit area and per unit time

$$\begin{aligned} J_n(\underline{x}, \underline{u}, E) &= \rho(\underline{x}, \underline{u}, E) dV/dA_n dt = \underline{n} \cdot \underline{u} v(E) \rho(\underline{x}, \underline{u}, E) \\ &= \underline{n} \cdot \underline{u} \phi(\underline{x}, \underline{u}, E) \end{aligned} \quad (23)$$

Thus, the number of particles crossing a surface with orientation \underline{n} is equal to the flux only for particle directions \underline{u} parallel to \underline{n} so that $\underline{n} \cdot \underline{u} = 1$. For all other particle directions, the particles crossing per unit area perpendicular to \underline{n} is the flux reduced by the factor $\underline{n} \cdot \underline{u}$.

For space radiation problems, the initial population of particles is specified by the particle current entering a surface which surrounds the vehicle

$$j_n(\underline{x}, \underline{u}, E) = \frac{\phi(E)}{4\pi} \underline{u} \cdot \underline{n} \quad (24)$$

The number of particles entering this surface per unit area is given by an integration over entering directions

$$j_n(\underline{x}, E) = \int_{\underline{u} \cdot \underline{n} > 0} \frac{\phi(E)}{4\pi} \underline{u} \cdot \underline{n} \, d\underline{u} \quad (25)$$

Using the cosine of the polar angle measured from \underline{n} , μ , and the azimuthal angle measured around \underline{n} , θ ,

$$j_n(\underline{x}, E) = \int_0^{2\pi} \int_0^1 \frac{\phi(E)}{4\pi} \mu \, d\mu \, d\theta = \frac{\phi(E)}{4} \quad (26)$$

Thus, the number of particles entering the surface per unit area is $\phi/4$. Similarly, in the absence of interactions inside the surface, the number of particles leaving the surface per unit area is $\phi/4$ for a net flow of zero. Both the entrance and exit currents have a cosine distribution relative to the surface normal.

TRANSPORT KERNELS

The response at a component is determined by an integration of the form

$$R = \iint S^0(P) M(P, P') D^0(P') \, dP \, dP' \quad (27)$$

where $S^0(P)$ denotes the density of source particles, $M(P,P')$ is the flux at P' per unit source at P and $D^0(P')$ is the response per unit flux at P' . An abbreviated notation has been used for particle coordinates

$$\begin{aligned} P &= \underline{x}, \underline{u}, E & P' &= \underline{x}', \underline{u}', E' \\ dP &= d\underline{x} \, d\underline{u} \, dE & dP' &= d\underline{x}' \, d\underline{u}' \, dE' \end{aligned} \quad (28)$$

The discussion is now limited to a fixed source with a separable energy dependence

$$S^0(\underline{x}, \underline{u}, E) = S^0(\underline{x}, \underline{u}) f(E) \quad (29)$$

where $f(E)$ is the normalized source spectrum, and a point isotropic detector

$$D^0(\underline{x}', \underline{u}', E') = \delta(\underline{x}' - \underline{x}_0) g(E') \quad (30)$$

where δ is the Dirac delta function and $g(E')$ is the energy dependence of the response per unit flux.

For a uniform infinite medium, the total response can now be written as

$$R = \iint S^0(\underline{x}, \underline{u}) \bar{M}(\underline{x}, \underline{u}, \underline{x}_0) d\underline{x} \, d\underline{u} \quad (31)$$

where the kernel \bar{M} is the response at \underline{x}_0 per source particle emitted at \underline{x} in the direction \underline{u} integrated over source energy, and energy and direction at the detector

$$\bar{M}(\underline{x}, \underline{u}, \underline{x}_0) = \iiint f(E) M(\underline{x}, \underline{u}, E, \underline{x}_0, \underline{u}', E') g(E') dE' d\underline{u}' dE \quad (32)$$

\bar{M} can be represented by

$$\bar{M}(\underline{x}, \underline{u}, \underline{x}_0) = K(r, \underline{u} \cdot \underline{u}') / r^2 \quad r = |\underline{x}_0 - \underline{x}|$$

$$\underline{u}' = (\underline{x}_0 - \underline{x}) / r \quad (33)$$

since only the source and detector separation r and relative orientation $\underline{u} \cdot \underline{u}'$ are pertinent parameters for an infinite medium.

The response kernel K can be determined by any number of methods, e.g., Monte Carlo. For the following discussions, the method of calculation and the actual variation with distance and direction is not required.

The volume spatial integration over the source for the integral response can be written in spherical coordinates

$$d\underline{x} = r^2 dr d\underline{u}' \quad (34)$$

with an origin at the detector point \underline{x}_0 . The R integral becomes

$$R = \iiint S^0(\underline{x}_0 - r\underline{u}', \underline{u}) K(r, \underline{u} \cdot \underline{u}') d\underline{u}' d\underline{u} dr \quad (35)$$

For a surface source, the source density can be written

$$S^0(\underline{x}, \underline{u}) = S^0(\underline{x}, \underline{u}) \delta(p) \quad (36)$$

where $\delta(p)$ is a one-dimensional delta function in a thickness variable p measured perpendicular to the surface, i.e., measured along \underline{n} . Using a delta function transformation

$$\delta(p) = \delta(r - s) \frac{dr}{dp} = \delta(r - s) \frac{1}{\underline{n} \cdot \underline{u}'} \quad (37)$$

where s is the distance to the surface along $-\underline{u}'$. Substituting into the integral response equation and performing the integration over r yields

$$R = \iint S^0(\underline{x}_0 - s\underline{u}', \underline{u}) K(s, \underline{u} \cdot \underline{u}') \frac{du \, du'}{\underline{n} \cdot \underline{u}'} \quad (38)$$

If the source per unit area is spatially constant

$$S^0(\underline{x}_0 - s\underline{u}', \underline{u}) = S^0(\underline{u})$$

$$R = \iint S^0(\underline{u}) K(s, \underline{u} \cdot \underline{u}') \frac{du \, du'}{\underline{n} \cdot \underline{u}'} \quad (39)$$

If the source is azimuthally symmetric around \underline{n}

$$S^0(\underline{u}) = S^0(\underline{n} \cdot \underline{u}) / 2\pi$$

$$R = \frac{1}{2\pi} \iint S^0(\underline{n} \cdot \underline{u}) K(s, \underline{u} \cdot \underline{u}') \frac{du \, du'}{\underline{n} \cdot \underline{u}'} \quad (40)$$

If the angular dependence relative to the surface normal is cosine and the total emission in the forward hemisphere is $\frac{1}{2}$ particles/cm², then

$$S^0(\underline{n} \cdot \underline{u}) = \underline{n} \cdot \underline{u} / 2$$

$$R = \frac{1}{4\pi} \iint \underline{n} \cdot \underline{u} K(s, \underline{u} \cdot \underline{u}') \frac{d\underline{u} d\underline{u}'}{\underline{n} \cdot \underline{u}'} \quad (41)$$

If particles transport straight ahead (no deflections) then

$$\begin{aligned} K(s, \underline{u} \cdot \underline{u}') &= K(s) \delta(\underline{u} \cdot \underline{u}' - 1) / 2\pi \\ &= K(s) \delta(\underline{u} - \underline{u}') \end{aligned} \quad (42)$$

$$\begin{aligned} \int \underline{n} \cdot \underline{u} K(s, \underline{u} \cdot \underline{u}') d\underline{u} &= K(s) \underline{n} \cdot \underline{u}' \\ R &= \frac{1}{4\pi} \int K(s) d\underline{u}' \end{aligned} \quad (43)$$

If the uniform infinite medium is a void

$$\begin{aligned} K(s) &= 1 \\ R &= \frac{1}{4\pi} \int d\underline{u}' = 1 \end{aligned} \quad (44)$$

For general problems, K and S^0 are expanded as Legendre series

$$K(s, \underline{u} \cdot \underline{u}') = \frac{1}{4\pi} \sum_{i=0}^{\infty} (2i+1) K_i(s) P_i(\underline{u} \cdot \underline{u}') \quad (45)$$

$$S^0(\underline{u}) = \frac{1}{4\pi} \sum_{j=0}^{\infty} (2j+1) S_j^0 P_j(\underline{u} \cdot \underline{n}) \quad (46)$$

where $P_k(\mu)$ is the k th Legendre polynomial and the expansion coefficients are

$$K_i(s) = 2\pi \int_{-1}^1 K(s, \mu) P_i(\mu) d\mu \quad (47)$$

$$S_j^0 = 2\pi \int_{-1}^1 S^0(\underline{u}) P_j(\underline{u} \cdot \underline{n}) d(\underline{u} \cdot \underline{n}) \quad (48)$$

Substitution of the series into the response integral yields

$$R = \sum_{i,j} \frac{2i+1}{4\pi} \frac{2j+1}{4\pi} S_j^0 \int K_i(s) \int P_j(\underline{u} \cdot \underline{n}) P_i(\underline{u} \cdot \underline{n}) \frac{d\underline{u} d\underline{u}'}{\underline{n} \cdot \underline{u}'} \quad (49)$$

The addition theorem for Legendre polynomials allows writing

$$P_i'(\underline{u} \cdot \underline{u}') = P_i(\underline{u} \cdot \underline{n}) P_i(\underline{n} \cdot \underline{u}') + f(\theta) \quad (50)$$

where θ is an azimuthal angle measured around \underline{u} and $f(\theta)$ is 2π periodic. Integrating over \underline{u}

$$\begin{aligned} \int P_j(\underline{u} \cdot \underline{n}) \left[P_i(\underline{u} \cdot \underline{n}) P_i(\underline{n} \cdot \underline{u}') + f(\theta) \right] d\underline{u} \\ = \frac{4\pi}{2i+1} P_i(\underline{n} \cdot \underline{u}') \delta_{ij} \end{aligned} \quad (51)$$

where δ_{ij} is the Kronecker delta, and the integral response is

$$R = \sum_{i=0} \frac{2i+1}{4\pi} S_i^0 \int K_i(s) P_i(\underline{n} \cdot \underline{u}') \frac{d\underline{u}'}{\underline{n} \cdot \underline{u}'} \quad (52)$$

For a hypothetical cosine surface source emitting $\frac{1}{3}$ particle in the forward hemisphere, and $-\frac{1}{3}$ particle in the backward hemisphere

$$S^0(\underline{u}) = \underline{u} \cdot \underline{n} / 4\pi \quad S_j^0 = \delta_{j,1} / 3 \quad (53)$$

i.e., only the first expansion coefficient is nonzero. The integral response becomes

$$R = \frac{1}{4\pi} \int K_1(s) P_1(\underline{n} \cdot \underline{u}') \frac{d\underline{u}'}{\underline{n} \cdot \underline{u}'} \quad (54)$$

$$= \frac{1}{4\pi} \int K_1(s) d\underline{u}' \quad (55)$$

since $P_1(\underline{n} \cdot \underline{u}') = \underline{n} \cdot \underline{u}'$.

For a point in the center of a sphere, $s = t$ (the radius) for all directions so that

$$R(t) = K_1(t) \quad (56)$$

For a point midway between two planes separated by $2t$, $s = t/\mu$ where μ is the cosine of the angle measured from the normal to the planes, and

$$\begin{aligned} R(t) &= 2 \frac{1}{4\pi} \int_0^{2\pi} \int_0^1 K_1(t/\mu) d\mu d\theta \\ &= t \int_t^\infty K_1(s) \frac{ds}{s^2} \quad (57) \end{aligned}$$

Differentiating with respect to t

$$\frac{dR_{\equiv}}{dT} = \frac{R_{\equiv}}{t} - \frac{K_1(t)}{t} = (R_{\equiv} - R_{\cdot})/t \quad (58)$$

or

$$R_{\cdot}(t) = R_{\equiv}(t) - t \frac{dR_{\equiv}}{dt}(t) \quad (59)$$

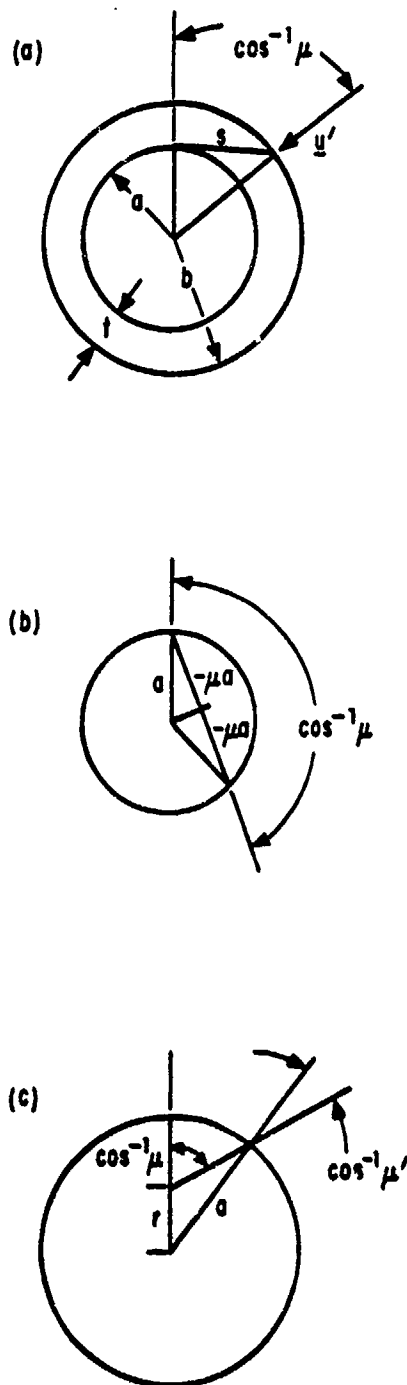


Figure 7. Spherical Shield Geometry

V. ANOTHER SECTORING KERNEL

The dose at a point at radius a inside a solid sphere of radius $b = a + t$, is denoted by $R_o(a, t)$, where the cosine source is applied at the larger radius, $a + t$, and the sphere is a subset of a uniform infinite medium. It follows from Equation 52 that

$$\begin{aligned} R_o(a, t) &= \frac{1}{4\pi} \int_{4\pi} K_1(s) d\underline{u}' \\ &= \frac{1}{2} \int_{-1}^1 K_1(s(\mu)) d\mu \end{aligned} \quad (60)$$

where the law of cosines yields

$$b^2 = a^2 + s^2 + 2 a s \mu \Rightarrow s = -\mu a + \sqrt{b^2 - a^2 (1 - \mu^2)} \quad (61)$$

Assuming the sphere is hollow for $r < a$ and that the cavity has little effect on the inward dose kernel

$$R_o(a, t) = \frac{1}{2} \int_0^1 K_1(s) d\mu + \frac{1}{2} \int_{-1}^0 K_1(s) d\mu \quad (62)$$

inward directed particles
particles traversing cavity

For the particles traversing the cavity, the distance through material is now

$$\begin{aligned} s &= -\mu a + \sqrt{b^2 - a^2 (1 - \mu^2)} - (-2\mu a) \\ &= \mu a + \sqrt{b^2 - a^2 (1 - \mu^2)} \end{aligned} \quad (63)$$

so that the upper and lower hemisphere integrations are equal and

$$R_0(a, t) = \int_0^1 K_1(s(\mu)) d\mu \quad (64)$$

The angular integration is transformed to an integration over distance using

$$\frac{-d\mu}{ds} = \frac{-d}{ds} \left[\frac{b^2 - a^2 - s^2}{2as} \right] = \frac{b^2 - a^2 + s^2}{2as^2} = \frac{h^2 + s^2}{2as^2} \quad (65)$$

where

$$h^2 = b^2 - a^2 = (t + a)^2 - a^2 = t^2 + 2at \quad (66)$$

so that

$$R_0(a, t) = \frac{h^2}{2a} \int_t^h K_1(s) \frac{ds}{s^2} + \frac{1}{2a} \int_t^h K_1(s) ds \quad (67)$$

Assuming

$$K_1(s) = K_2(s) - s \frac{dK_2}{ds}(s) \quad (68)$$

still holds, integration by parts yields

$$R_0(a, t) = K_-(t) + \frac{1}{a} \left[t K_-(t) - h K_-(h) + \int_t^h K_-(s) ds \right] \quad (69)$$

For large a ,

$$R_0(\infty, t) = K_-(t) \quad (70)$$

as expected; i.e., the inside surface of the spherical shell looks like a slab to the transporting particles.

For an inside radius much less than the shell thickness, $a \ll t$

$$h = \sqrt{t^2 + 2at} = t \sqrt{1 + 2a/t} = t(1 + \frac{1}{2}(2a/t)) \\ = t + a$$

$$K_-(s) = K_-(t) + \frac{dK_-}{dt}(t) (s - t), \text{ first term expansion}$$

$$K_-(h) = K_-(t) + a \frac{dK_-}{dt}(t) \quad \text{since } h - t = a \quad (71)$$

Substitution and evaluation of the integral yields

$$R_0(a, t) = K_-(t) - t \frac{dK_-}{dt}(t) - \frac{a}{2} \frac{dK_-}{dt}(t) \quad (72)$$

and for $a = 0$,

$$R_0(0, t) = K_-(t) - t \frac{dK_-}{dt}(t) = K_-(t) \quad (73)$$

the solid sphere kernel, as expected.

The forward/backward symmetry of the angular flux on the cavity surface can be seen from the geometry. For every particle entering the cavity in the direction \underline{u} there is an equivalent particle hitting the entrance point with direction $-\underline{u}$.

The dose inside the spherical cavity can be obtained by an angular dose current integration, where

$$J_0(a, t, \mu) = J_0(a, t, -\mu) \quad \text{dose/steradian/cm}^2 \quad (74)$$

In fact, for large inner radii

$$J_0(\infty, t, \mu) = J_-(t, \mu) \quad (75)$$

where $J_-(t, \mu)$ is the angular dose current in the semi-infinite slab geometry, with or without a void at the detector plane.

In terms of angular dose current

$$R_0(a, t) = 4\pi \int_0^1 J_0(a, t, \mu) \frac{d\mu}{\mu} \quad (76)$$

$$R_-(t) = 4\pi \int_0^1 J_-(t, \mu) \frac{d\mu}{\mu} \quad (77)$$

since the angular flux and current are related by

$$J(\mu) = \mu\phi(\mu) \quad \text{or} \quad \phi(\mu) = J(\mu)/\mu \quad (78)$$

Assuming the transmitted dose current varies as

$$J_0(a, t, \mu') = \frac{1}{4\pi} A(t) \mu'^{\alpha(t)} \quad (79)$$

and if $R_0(r, a, t)$ denotes the dose at radius r in a spherical cavity of radius $a > r$, the dose can be calculated as

$$R_0(r, a, t) = 4\pi \int_0^1 J_0(a, t, \mu') \frac{d\mu}{\mu^2} \quad (80)$$

For $r = a$, $\mu' = \mu$ (Fig. 7c) and

$$R_0(a, a, t) = A(t) \int_0^1 \mu^{\alpha(t)-1} d\mu = \frac{A(t)}{\alpha(t)} \quad (81)$$

For $r = 0$, $\mu' = 1$, and

$$R_0(0, a, t) = A(t) \int_0^1 d\mu = A(t) \quad (82)$$

In the limit of large a

$$R_0(\infty, \infty, t) = R_-(t) \quad \text{and} \quad R_0(0, \infty, t) = R_0(t) \quad (83)$$

which implies that

$$A(t) = K_0(t) \quad (84)$$

$$\alpha(t) = K_0(t) / K_-(t) \quad (85)$$

This transmitted dose kernel is applied in complicated geometries by assuming that materials traversed are sections of a spherical shell. This requires dose attenuation kernel evaluations based on t_0 where t_0 is an estimate of the minimum path traversed by the radiation

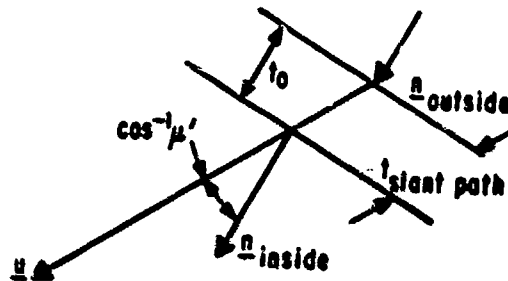


Figure 8. Minimum Path Geometry

$$t_0 = t(\text{slant path}) \frac{1}{2} (\underline{u} \cdot \underline{n}_{\text{inside}} + \underline{u} \cdot \underline{n}_{\text{outside}}) \quad (86)$$

A combined kernel which accounts for both shell and solid shield geometry effects is

$$K(t) = K_{\text{shell}}(t) \left[\alpha(t_0) \mu' \alpha(t_0) - 1 \right] \left[1 - \tau \frac{\frac{dK_{\text{solid}}(t)}{dt} K_{\text{solid}}(t.)}{K_{\text{solid}}(t) K_{\text{solid}}(t)} \right] \quad (87)$$

shell shield term solid shield term

where it is assumed that

$$\frac{dK_{\text{solid}}}{dt}(t.) = \frac{dK_{\text{solid}}}{dt}(t) \frac{K_{\text{solid}}(t.)}{K_{\text{solid}}(t)} \quad (88)$$

t_s is the distance through solid material surrounding the dose point, zero if the point is in a cavity

t_0 is the estimated minimum distance through all the other shell like shields, zero if only a solid shield

$$t = t_1 + t_0$$

$$\alpha(t_0) = K_0(t) / K_-(t_0)$$

$$= 1 \text{ if } t_0 \text{ is zero} \tag{89}$$

No attempt has been made to include curvature effects for the shell shields. For $t_0 = 0$, the solid shield kernel results and for $t_1 = 0$, the angular dose, spherical shell kernel accrues.

The following steps are used to generate kernel information using conventional slab geometry codes

- (1) $K_{\infty}(t)$ is generated rather than $K_-(t)$ to properly account for backscattered particles. The problem has a cosine source emitting $\frac{1}{2}$ particle into an infinitely thick slab.
- (2) The backward and forward angular doses (response weighted angular fluxes) are obtained from the same calculation.

Assuming a Monte Carlo calculation

$$J_{\infty}(t, \mu < -\mu_0) = \frac{1}{2\pi(1 - \mu_0)} \sum_{-1 \leq \mu < -\mu_0} \text{backward traveling histories with directions} \tag{90}$$

$$J_{\infty}(t, \mu > \mu_0) = \frac{1}{2\pi(1 - \mu_0)} \sum_{\mu_0 < \mu \leq 1} \text{forward traveling histories with directions} \tag{91}$$

(3) Estimate the center of spherical shell kernel using

$$\begin{aligned} J_0(t, \mu > \mu_0) &= J_0(t, \mu < -\mu_0) \\ &= \frac{1}{2} \left[J_{\frac{\pi}{2}}(t, \mu > \mu_0) + J_{\frac{\pi}{2}}(t, \mu < -\mu_0) \right] \end{aligned} \quad (92)$$

i.e.

$$\begin{aligned} K_0(t) &= 4\pi J_0(t, \mu = 1) \\ &= 2\pi \left[J_{\frac{\pi}{2}}(t, \mu > \mu_0) + J_{\frac{\pi}{2}}(t, \mu < -\mu_0) \right] \end{aligned} \quad (93)$$

(4) Calculate the ratio of spherical shell to slab geometry dose

$$\alpha(t) = K_0(t) / K_{\frac{\pi}{2}}(t) \geq 1 \quad (94)$$

VI. SECTORING KERNEL SELECTION

Charged particle dose predictions for satellite and deep space probes are usually performed by sectoring calculations. The accuracy of these predictions is controlled partially by one-dimensional dose attenuation kernels. This section discusses kernel selection in the energy domains where particles have straight line paths and where the particles have significant angular deflections.

Sectoring calculations assume an explicit three-dimensional analytic geometry mockup of the spacecraft. The dose, D , at critical points in the spacecraft is computed as

$$D = \int_{4\pi} \frac{K(t(\underline{u}))}{4\pi} d^2 \underline{u} \quad (95)$$

where \underline{u} is a direction from the point to the outside of the vehicle, $t(\underline{u})$ is the material thickness encountered along \underline{u} , $d^2 \underline{u}$ is the differential solid angle, and $K(t)$ is a dose attenuation kernel.

This integration is performed numerically by defining many solid angle sectors; e.g., I total sectors each of size $4\pi/I$ steradians, for each sector i defining an average direction \underline{u}_i , and evaluating

$$D = \sum_{i=1}^I \frac{4\pi}{I} \frac{K(t(\underline{u}_i))}{4\pi} \quad (96)$$

Sum over sectors sector solid angle dose per steradian for thickness $t(\underline{u}_i)$

The thickness $t(\underline{u}_i)$ is determined by a ray trace from the dose point along the direction \underline{u}_i . Three sources of error in this type of analysis are:

- (1) The fineness of the angular integration which determines how well thin vehicle sections are resolved (or if they are seen at all).
- (2) The degree to which the radiation arriving from the direction \underline{u}_i actually traverses the materials comprising the thickness $t(\underline{u}_i)$. This approximation neglects the scatter and change of direction as the particles traverse the materials.
- (3) The extent that simple geometry used in deriving the attenuation kernel $K(t)$ approximates the actual geometry of the sector.

The first error source will not be discussed farther here. It can be investigated in most codes by parameters controlling the size of the solid angle sectors.

The latter two error sources are related since they both require knowledge of how particles really get from the outside of the vehicle to the dose point. A definitive answer to the error magnitude is outside the realm of sectoring analysis and

requires numerical methods such as adjoint Monte Carlo (which provides a realistic simulation of all the processes working on the particles as they progress towards the detector point).

However, it is possible by examining some typical one-dimensional geometry problems, to get some insight into the potential magnitude of the errors in sectoring analysis and to select one dimensional kernels that will provide both upper and lower bounds on the dose for most three-dimensional geometries.

The capability of bracketing the true dose--by sectoring with upper and lower bound kernels--will alleviate the accuracy question for many dose points. When the upper/lower bound kernels are in substantial agreement, differing by less than a factor of 2, then a good dose prediction can be assumed (using the upper bound kernel for conservatism in design). When there is substantial disagreement between the upper and lower bound dose estimates--more than a factor of 2 disagreement--further analysis is required.

Additional analysis can include adjoint Monte Carlo, or an in-depth review of the dose point and its surroundings. By reviewing the local geometry of the dose point, it may be possible to identify which of the kernel estimates is expected to best represent a particular dose point.

The remainder of this document covers one-dimensional kernels in some depth with the following intent:

- (1) Identify the correct kernels for specific particle types;
- (2) identify the difference in dose predicted by different kernels and the source of that difference, and
- (3) provide some arguments for using specific kernels in particular circumstances.

STRAIGHT AHEAD MODELS

Sectoring is a straight ahead transport model since the particle transport is characterized only by the materials-- $t(\underline{u})$ --encountered along a specific direction \underline{u} .

The straight ahead method is reliable for some analyses, e.g.,

- (1) Dose from cosmic rays and protons, and
- (2) dose from electrons with energies exceeding 100 MeV.

Some sectoring codes do a complete particle energy analysis in the straight ahead approximation. The integral evaluated is, for a given sector

$$K(t) = \int_0^{\infty} \int_0^{\infty} \phi_0(E') M(E' \rightarrow E, t) D_0(E) dE' dE \quad (97)$$

where $K(t)$ is the dose at thickness t , $\phi_0(E')$ is the external environment (particles/cm² · MeV), $M(E' \rightarrow E, t)$ is the distribution in energy E at the detector point for a particle that starts with energy E' and traverses material thickness t , and $D_0(E)$ is the detector response (dose) to a particle of energy E .

In the straight ahead approximation, particles lose energy at a rate per unit path length s given by $L(E)$, i.e.

$$\frac{dE}{ds} = - L(E) \left(\frac{\text{MeV}}{\text{cm}} \right) \quad (98)$$

Therefore, after traversing the thickness t , a particle that starts at energy E' at the exterior of the satellite reaches the detector point with energy E given by

$$E = f(E', t) = E' - \int_0^t L(E(s)) ds \quad (99)$$

Neglecting all other processes, the basic transport kernel $M(E \rightarrow E', t)$ becomes

$$M(E' \rightarrow E, t) = \delta(E - f(E', t)) \quad (100)$$

where δ is the Dirac delta function, so that the dose $K(t)$ becomes

$$\begin{aligned} K(t) &= \int_0^{\infty} \int_0^{\infty} \phi_0(E') \delta(E - f(E', t)) D_0(E) dE dE' \\ &= \int_0^{\infty} \phi_0(E') D_0(f(E', t)) dE' \end{aligned} \quad (101)$$

The simplest and most often used method of evaluating this integral is to subdivide the energy domain into intervals called groups and evaluate

$$K(t) = \sum_{\text{groups } g} \underbrace{\phi_0(\bar{E}'_g) \Delta E_g}_{\text{particles in group } g \text{ impinging on vehicle}} \underbrace{D_0(\bar{E}_g(t))}_{\text{response to these particles at their degraded energy at the detector}} \quad (102)$$

where g is a group subscript, \bar{E}'_g is the average energy of the particles in group g , ΔE_g is the group width, $\bar{E}_g(t)$ is the energy the particles degrade to after traversing the thickness t

$$\bar{E}_g(t) = \bar{E}'_g - \int_0^t L(E(s)) ds \quad (103)$$

and $D_0(\bar{E}_g(t))$ is the response to these particles.

This simple method has one major problem. Since charged particles range out, all groups above some critical energy make it to the detector point while all those below that energy stop before getting there. This yes/no on groups can cause bumpy dose predictions unless a fine group structure is used.

An alternate way of evaluating the straight ahead dose is presented here because it eliminates the bump problem and is a major item that distinguishes adjoint Monte Carlo from conventional particle simulation Monte Carlo.

In the integral

$$K(t) = \int_0^{\infty} \phi_0(E') D_0(f(E', t)) dE' \quad (104)$$

make the change of variables

$$E = f(E', t) \iff E' = f^{-1}(E, t) \quad (105)$$

i.e.

$$E' = f^{-1}(E, t) = E + \int_0^t L(E'(s)) \, ds \quad (106)$$

then

$$K(t) = \int \phi_0(f^{-1}(E, t)) D_0(E) \left| \frac{dE'}{dE} \right| \, dE \quad (107)$$

where $|dE'/dE|$ is the Jacobian of the variable transformation. A careful evaluation of the Jacobian yields, for a single material,

$$\frac{dE'}{dE} = \frac{L(E')}{L(E)} \quad (108)$$

Therefore, the dose is also given by an integration over energy at the detector point in the form

$$K(t) = \int_0^\infty \phi_0(f^{-1}(E, t)) \left\{ \frac{L(f^{-1}(E, t))}{L(E)} \right\} D_0(E) \, dE \quad (109)$$

which can be evaluated using group terminology as

$$K(t) = \sum_{\substack{g \\ \text{groups}}} \phi_0(\bar{E}'_g(t)) \frac{L(\bar{E}'_g(t))}{L(\bar{E}_g)} D_0(\bar{E}_g) \Delta E_g \quad (110)$$

Now the groups are defined at the detector, \bar{E}_g is the average energy of the particle that arrive at the detector (preassigned)

in group g , $\bar{E}'_g(t)$ is the energy these particles need to hit the satellite with to arrive at the detector with energy \bar{E}_g , i.e.,

$$\bar{E}'_g(t) = \bar{E}_g + \int_0^t L(E'(s)) ds \quad (111)$$

This scheme eliminates any on/off bumps at the detector.

The major difference in this scheme is that particles speed up in backtracking from the detector point to the source, and that a factor $L(E')/L(E)$ is introduced into the equation for dose. The $L(E')/L(E)$ factor accounts for the contraction/expansion of particle group width during flight through the vehicle materials.

Generally, stopping powers $L(E)$ get larger at lower energies. This causes group widths to expand as particle travel from the source (outside the satellite) to the detector. Conversely, in tracking particle groups from the detector to the source, groups get narrower.

The factor $L(E'(t))/L(E)$ is the ratio of group width at the source to group width at the detector point for an infinitesimal width group. (Multiple materials require products of $L(E')/L(E)$ terms corresponding to the entrance energy and exit energy for each material layer.)

Most sectoring codes do not evaluate transport integrals explicitly. The integration is performed in a one-dimensional

code and results are supplied to the sectoring code as tabular data t_i , $K(t_i)$, $i = 1, 2, \dots$. The dose for a particular sector thickness $K(t(u))$ is then obtained by interpolation on thickness t .

As mentioned previously, the straight ahead method is accurate for heavy charged particles and very high energy electrons (> 100 MeV). However, some care must be used in selecting the kernel $K(t)$ since there are a variety of one-dimensional codes that can generate kernels for different source and material geometries. The applicable kernel is one of the following (they are all equal numerically because of the straight ahead model):

- (1) Dose at depth t in a slab for a source $\phi_0(E)$ normally incident on the slab,
- (2) dose at the center of a solid sphere of radius t for any source that has an angular strength of $\phi_0(E)/4\pi$ particles per unit area and per unit steradian normal to the sphere surface (particles incident at angles other than normal never get to the sphere center),
- (3) dose at the center of a spherical shell of thickness t with the same source conditions as 2, and
- (4) $4\pi t^2$ times the dose at the outside surface of a sphere of outer radius t with a point source of $\phi_0(E)$ particles MeV at the center of the sphere.

One kernel that must not be used is the dose at the center of a slab of thickness $2t$ where that slab is embedded in an isotropic flux field of $\phi_0(E)$.

Denoting this kernel by $K_{\underline{=}}(t)$ and the correct kernel by $K_{\underline{.}}(t)$ (the subscript look like a slab = and a sphere .), it is seen that

$$K_{\underline{=}}(t) = \int_{4\pi} \frac{K_{\underline{.}}(t(\underline{u}))}{4\pi} d^2\underline{u} \quad (112)$$

Writing $d^2\underline{u}$ as $da d\mu$ where a is azimuth around the slab normal and μ is the cosine of the angle between \underline{u} and the slab normal then

$$\begin{aligned} K_{\underline{=}}(t) &= \int_0^{2\pi} \int_{-1}^1 \frac{K_{\underline{.}}(t/|\mu|)}{4\pi} da d\mu \\ &= 2\pi \cdot 2 \int_0^1 \frac{K_{\underline{.}}(t/\mu)}{4\pi} d\mu = \int_0^1 K_{\underline{.}}(t/\mu) d\mu \quad (113) \end{aligned}$$

Since dose usually decreases with thickness, $K_{\underline{=}}(t)$ is less than $K_{\underline{.}}(t)$. Therefore, the use of a slab kernel in a sectoring code will result in an underestimate of the true dose. (Imagine applying the sectoring code to the sphere or slab--neither geometry gets the right answer if $K_{\underline{=}}(t)$ is the input kernel.)

Making the variable transformation

$$x = t/\mu \Rightarrow \mu = t/x \quad \text{and} \quad d\mu = (-t/x^2) d\nu \quad (114)$$

$$K_-(t) = t \int_t^\infty K_-(x) \frac{dx}{x^2} \quad (115)$$

Differentiating with respect to shield thickness t

$$\begin{aligned} \frac{d}{dt} K_-(t) &= \int_t^\infty K_-(x) \frac{dx}{x^2} + t \left(- \frac{K_-(x)}{x^2} \right)_{x=t} \\ &= \frac{1}{t} K_-(t) - \frac{K_-(t)}{t} \end{aligned} \quad (116)$$

thus

$$K_-(t) = K_-(t) - t \frac{d}{dt} K_-(t) \quad (117)$$

A comment on angular distributions is warranted because it leads naturally to the next subject. The slab kernel can be written as

$$K_-(t) = 4\pi \int_0^1 K_-(t, \nu) d\nu \quad (118)$$

where $K_-(t, \nu)$ is the dose per steradian for particles arriving at the detector at an angle $\cos^{-1} \nu$ relative to the slab normal.

Since

$$K_-(t) = \int_0^1 K_-(t/\nu) d\nu \quad (119)$$

it follows that

$$4\pi K_{\underline{z}}(t, \mu) = K_{\cdot}(t/\mu) \quad (120)$$

or

$$K_{\underline{z}}(t, \mu) = \frac{1}{4\pi} K_{\cdot}(t/\mu) \quad (121)$$

Therefore, for straight ahead dose attenuation kernels $K_{\cdot}(t)$ that decrease with thickness, the angular distribution of $K_{\underline{z}}(t, \mu)$ gets sharply peaked along the slab normal. ($K_{\cdot}(t/\mu) \ll K_{\cdot}(t)$ for values of μ less than 1.) Said another way, only those particles that are incident on the slab in some area around the normal contribute to the dose.

ELECTRONS

The transport of electrons below 10 MeV (typical earth environments) is not described by straight ahead models. The transmission of these electrons through materials is very close to a diffusion process; e.g., the angular distribution of particle transmitted through surfaces is almost isotropic. Moreover, the relative level of dose values is determined by the actual thickness of components such as box walls rather than the slant thickness seen by a sectoring code.

One indication of the effect of this diffuse transport can be seen in simple spherical geometries. The inside surface of a spherical shell of large radius looks like a slab to local incoming electrons (the electron range in the shell material is

much less than the shell radius). If the transmitted electrons retain their isotropic distribution, the dose at the center of the sphere, $K_0(t)$, and everywhere inside the shell is constant and equal to the slab dose $K_=(t)$.

In practice, the electrons transmitted through a slab of thickness, t , do become forward peaked, but not severely. The angular transmission can be approximated by

$$K_=(t, \mu) = 4\pi K_0(t) \mu^{\alpha(t)-1} \quad (122)$$

where

$$\alpha(t) = K_0(t)/K_=(t) \quad (123)$$

and is typically in the range 1 (isotropic) to 1.5. (Other angular distributions can be used but require more parameters. The above distribution suffers, for instance, by predicting $K_=(t, \mu=0) = 0$ if $\alpha(t) > 1$). Thus, in reality, the electron dose inside the sphere varies from $K_=(t)$ at the inside surface to $K_0(t)$ at the center, usually less than 50 percent.

This small variation of dose inside a spherical shell for electrons should be contrasted with the dose variation obtained for protons using straight ahead models. Since

$$K_=(t) = K_=(t) - t \frac{d}{dt} K_=(t) \quad (124)$$

the variation from inside surface ($K_=(t)$) to center (K_0) is often an order of magnitude or more for protons.

Dose enhancement is also seen for electrons as the inner radius of the spherical shell is shrunk to values on the order of the electron range or less--the dose remains roughly constant inside the cavity but is higher for the smaller cavity radius. Specifically, it has been shown that for a detector point inside a solid spherical shield, that the electron dose is given by $K_-(t)$ and not $\bar{K}_-(t)$ (remember that K_0 is the dose at the center of a very large, nearly infinite, radius sphere) where $K_-(t)$ is computed from $K_-(t) - t \frac{d}{dt} K_-(t)$. This result has also been demonstrated by adjoint Monte Carlo calculations.

Note that $K_0(t)$ and $K_-(t)$ are not equal for electrons (they are for straight ahead models). In fact, since $K_0(t)$ is on the order of $K_-(t)$ (or as much as 50 percent larger), and since $K_-(t)$ can be an order of magnitude larger than $K_-(t)$, the difference between $K_0(t)$ and $K_-(t)$ can also be an order of magnitude for electrons.

Reiterating the above, it is seen that the electron dose anywhere inside a large spherical cavity with shell thickness t is approximately $K_-(t)$. A sectoring code will yield this same result for the shell if $K_-(t)$ is supplied as input and the dose point is located at the center of the sphere. However, if the dose point is located near the inner surface of the shell, the sectoring code will underpredict the dose since an evaluation of

$$D = \int_0^1 K_-(t/u) du < K_-(t) \quad (125)$$

is effectively obtained. This type of conservatism (underprediction) cannot be tolerated in design calculations.

This tendency to underpredict cavity dose has been eliminated in the SIGMA-II sectoring code by forcing the program to estimate the minimum thickness, τ , seen by electrons. The usual slant thickness, t , calculated by the sectoring code is multiplied by cosine of the angle between the direction \underline{u} and the normal at entrance and exits of \underline{u} in the material

$$\tau = t \left(\frac{\underline{n}_1 \cdot \underline{u} + \underline{n}_2 \cdot \underline{u}}{2} \right) \quad (126)$$

The use of the minimum path, τ , as the thickness parameter is a much better characterization of the true transport characteristic of electrons. The additional use of the functional form $\mu^{\alpha(t)-1}$ to characterize departure from isotropic transmission through material layers results in a sectoring formalism that will reproduce the correct dose in two simple geometries:

- (1) dose inside a spherical shell, and
- (2) dose behind a slab shield.

However, the above kernel does not account for the dose enhancement seen in small solids containing dose points (or in small inner radius cavities). If the small solid is viewed separately--ignoring the effects of plates and voids prior to

reaching the solid--it has been shown* that the dose at points inside the solid is given by using $K_s(t)$ as the sectoring kernel.

Therefore, if $K_s(t)$ is used as a sectoring kernel with the usual slant path thickness, t , it will also predict the correct dose in two simple geometries:

- (1) dose inside a solid sphere, and
- (2) dose behind a slab shield.

The question remains as to which of these kernels is most appropriate in design calculations. In the limiting extreme of a spherical shell shield with a very small inner radius, the minimum path kernel underpredicts dose while in the other extreme of a very large inner radius the solid shield kernel overpredicts dose.

Since underestimates of dose can be critical to a mission, it would seem that using the solid sphere kernel is best. However, shield penalties associated with over conservative dose estimates can also jeopardize a mission. Consistency with earlier arguments would dictate using the solid sphere kernel and slant path sectoring. However, solid shield geometries are seldom encountered in practice--each sector usually involves

* "shown" by explicit adjoint Monte Carlo calculation and by an analytic derivation for an idealized problem that has, to first order, all the characteristics of the real problem and, to second order, cancelling terms that characterize the departure of the idealized problem from the real problem.

material layers separated by voids. Calculations on several typical points using adjoint Monte Carlo correlate much better with the minimum path kernel.

There is a way to combine the two kernels in a systematic method that accounts for peaking in small radius cavities. This combined kernel does not exist in any present code but could be added relatively easily to SIGMA-II for instance. The kernel is discussed at the end of this section.

The correct kernels for electron dose calculations can be obtained from one-dimensional Monte Carlo codes. Adjoint Monte Carlo can calculate the slab, solid sphere, and spherical shell configurations exactly.

Conventional particle simulation Monte Carlo is limited to calculations in slab geometry (it is hard to get particles to pass through a small volume at the center of the spheres). However, both the spherical shell and solid sphere kernels can be obtained from these slab geometries codes.

Specifically, the solid sphere electron dose kernel can be obtained by the formula

$$K_s(t) = K_m(t) - t \frac{dK_m(t)}{dt} \quad (127)$$

The validity of the formula has been demonstrated by explicit adjoint Monte Carlo calculations. (The formula is not exact, but any discrepancies are comparable to the Monte Carlo error bars). The spherical shell dose kernel can also be obtained

from a slab Monte Carlo calculation by requesting the angular dose (dose per steradian) in the direction along the slab normal. The 4π times this angular dose is the same as the spherical shell dose (the shell looks locally like a slab and the angular flux normal to the shell is the only flux that reaches the center of the sphere).

The source mockup is critical to the above calculations. The dose kernels are supposed to be representative of a shield embedded in an isotropic flux field. This isotropic flux field is simulated by a cosine source on the surface of the shield with a total particle source of $\frac{1}{2}$ for a unit isotropic flux. (It should be noted that data supplied by the National Space Sciences Data Center on dose attenuation is $\frac{1}{2}K_{\infty}(t)$ i.e., for $\frac{1}{2}$ of a particle--cosine incidence--a one sided slab result).

Slab geometry Monte Carlo calculations can be performed for finite thickness slabs or infinitely backed slabs. The better kernel is assumed to be the infinitely backed kernel since it includes a backscattering effect which also occurs in the satellite, and since it is conservatively higher.

HIGH ENERGY ELECTRONS

The final topic is a specific to the Jovian electron environment. This environment includes electrons > 100 MeV. Therefore, the basic transport mechanisms include combinations of straight ahead and diffusion mechanisms. Specifically,

electrons of high energy transport in an almost straight ahead manner and then diffuse after reduction to lower energies.

One way of handling this type problem is to use multiple kernels to describe the complete range of energies. Each band g would have a thickness t_g specified such that for thickness, t , less than t_g straight ahead models are employed while for $t > t_g$ the thickness $t' = (t - t_g)$ (closest to the detector) would use minimum thickness models. The thickness, t_g , would be defined by comparing one-dimensional calculations with straight ahead and with explicit transport models and defining t_g as the thickness where the calculations depart significantly in value. This logic does not exist in any sectoring code at this time.

A KERNEL WITH CURVATURE EFFECTS

The difference in dose obtained behind a solid sphere and a slab shield is geometrically obvious in the straight ahead approximation.

For the solid sphere, the point at the center of the sphere gets particle arriving from the entire 4π steradians and each particle has traversed the same thickness, t . For the slab, all particles except those traversing a path along the normal, traverse a path larger than t . The net affect is that only a part of the 4π steradians contributes to the dose at depth t .

The same geometric effect occurs for electrons even though the electron transport is more diffuse. The diffuse nature of the transport makes it more difficult--for the slab geometry--

to define a precise cone boundary within which particles traverse a thickness that allows them to reach the detector. However, this cone exists even though its boundaries are fuzzy.

The effect of curvature on cavity dose is predicted using the fact that electron dose is fairly uniform inside cavities and that the electron dose at the inner surface of a cavity can be predicted from $K_-(t)$ using slant thicknesses. Therefore, it is possible to compute a correction factor that accounts for the relative size of cavities encountered during sectoring since

$$K_-(t) = K_-(t) - t \frac{d}{dt} K_-(t) \quad (128)$$

in solid materials even when the straight ahead model does not apply.

Assume a is the inner radius of cavity and τ is the spherical shell thickness. Then the dose at the inner surface of the cavity is

$$K(\tau) = K_-(\tau) + \frac{1}{a} \left[\tau K_-(\tau) - h K_-(h) + \int_{\tau}^h K_-(x) dx \right] \quad (129)$$

where h is the maximum path in the shell

$$h = \sqrt{a^2 + 2a\tau} \quad (130)$$

If a is large, the evaluation gives $K_-(\tau)$ and if a is small, the value becomes $K_-(\tau)$. (Note that in the above equation a , t , τ , and h are all in equivalent units. Since a is an actual

dimension of a cavity, material thicknesses must be expressed in the same units as a (cm) except when interpolating the kernels).

Thus, every time a cavity is encountered, an enhancement factor can be computed for that cavity as

$$\text{enhancement factor} = \left[1 + \frac{1}{a} \left\{ \tau - h \left(\frac{K_{\tau}(h)}{K_{\tau}(\tau)} \right) + \frac{K_{\tau}(>\tau)}{K_{\tau}(\tau)} - \frac{K_{\tau}(>h)}{K_{\tau}(\tau)} \right\} \right] \quad (131)$$

where

$$K_{\tau}(>x) = \int_x^{\infty} K_{\tau}(x') dx' \quad (132)$$

Thus, an equation exists to predict the dose enhancement from solid shields surrounding dose points. This equation holds specifically for spherical geometry surrounding the detector point. A critical parameter is the radius of the cavity.

This section outlines a scheme for calculating an effective radius of cavities. No claim for correctness of the method is made except that it yields the correct results for the limiting extremes of slab and spherical shields.

The curvature in a plane containing x_i and x_j -- x_i, x_j denotes either (x,y), or (y,z), or (z,x) -- is given by

$$K_{ij} = \frac{d^2 x_j}{dx_i^2} / \left[1 + \left(\frac{dx_j}{dx_i} \right)^2 \right]^{3/2} \quad (133)$$

Therefore, when a ray crosses a surface, compute the curvature in the xy, yz, and zx planes from the surface equation and define an effective curvature as the average of these three values (or the square root of the average squares ...). Define the cavity radius a, as the reciprocal of this average curvature.

This process yields the following results for specific surfaces:

plane surface	$K = 0$	$\bar{a} = \infty$, correct
spherical surface	$K = 1/a$	$\bar{a} = a$, correct
cylindrical surface	$K = 1/2a$	$\bar{a} = 2a$, ?

Note that the correct curvature is obtained for slab and spherical geometries. Therefore, this prescription for cavity radius, in conjunction with the equation for dose enhancement as the cavity radius decreases, will give a kernel prescription that is correct for slabs, spherical shells, and solid spheres. The fact that the kernel will correctly predict these three geometries, including cavity radius effects, is a strong argument for its use in future calculations.

APPENDIX A

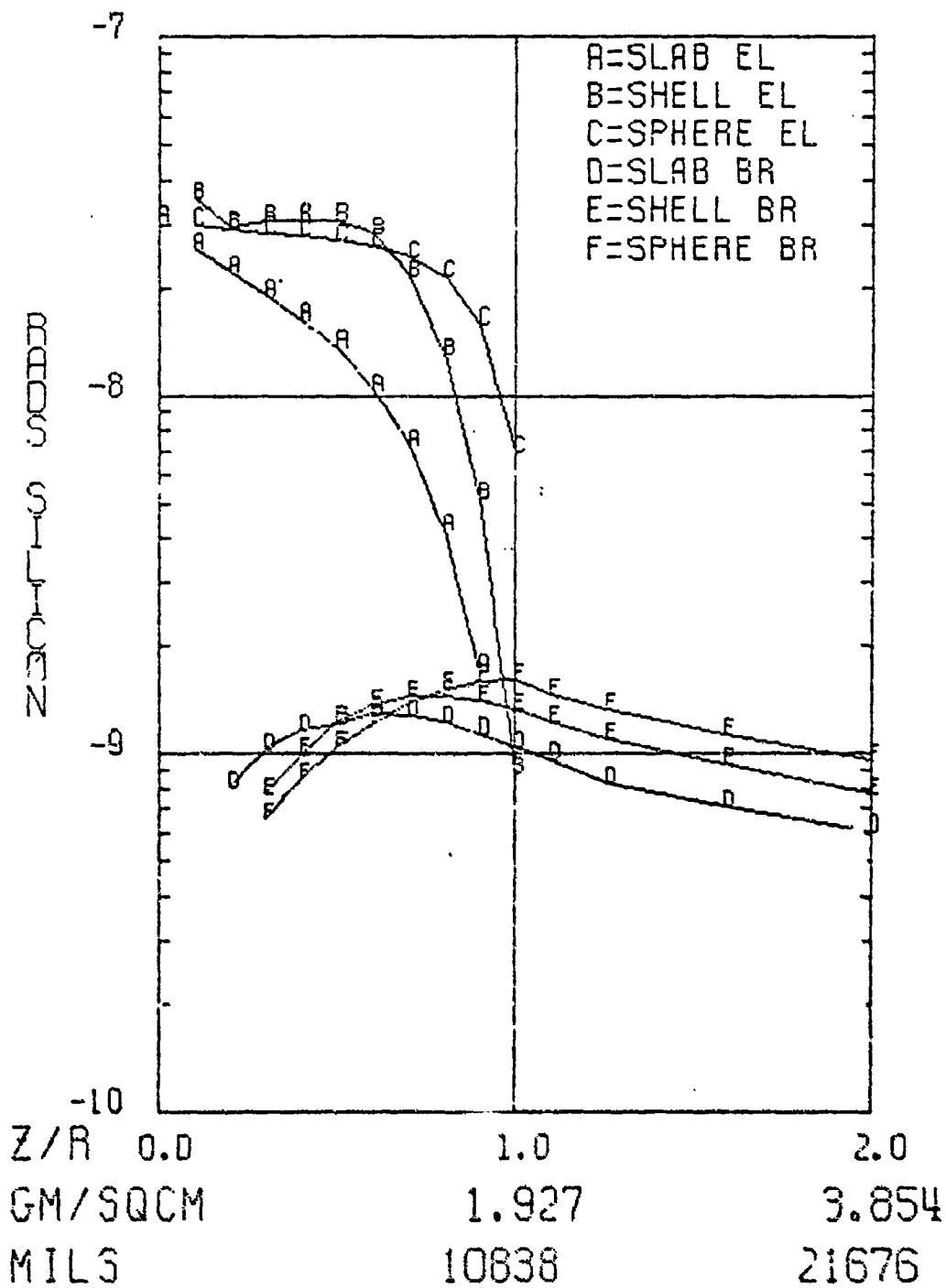
MONOENERGETIC ELECTRON ATTENUATION DATA

Dose attenuation curves are presented for monoenergetic electrons and their secondary bremsstrahlung. Electron energies are 8, 5, 3, 2, 1, 0.5, 0.25, and 0.1 MeV. Shield materials are hydrogen, helium, beryllium, aluminum, copper, tungsten, and uranium.

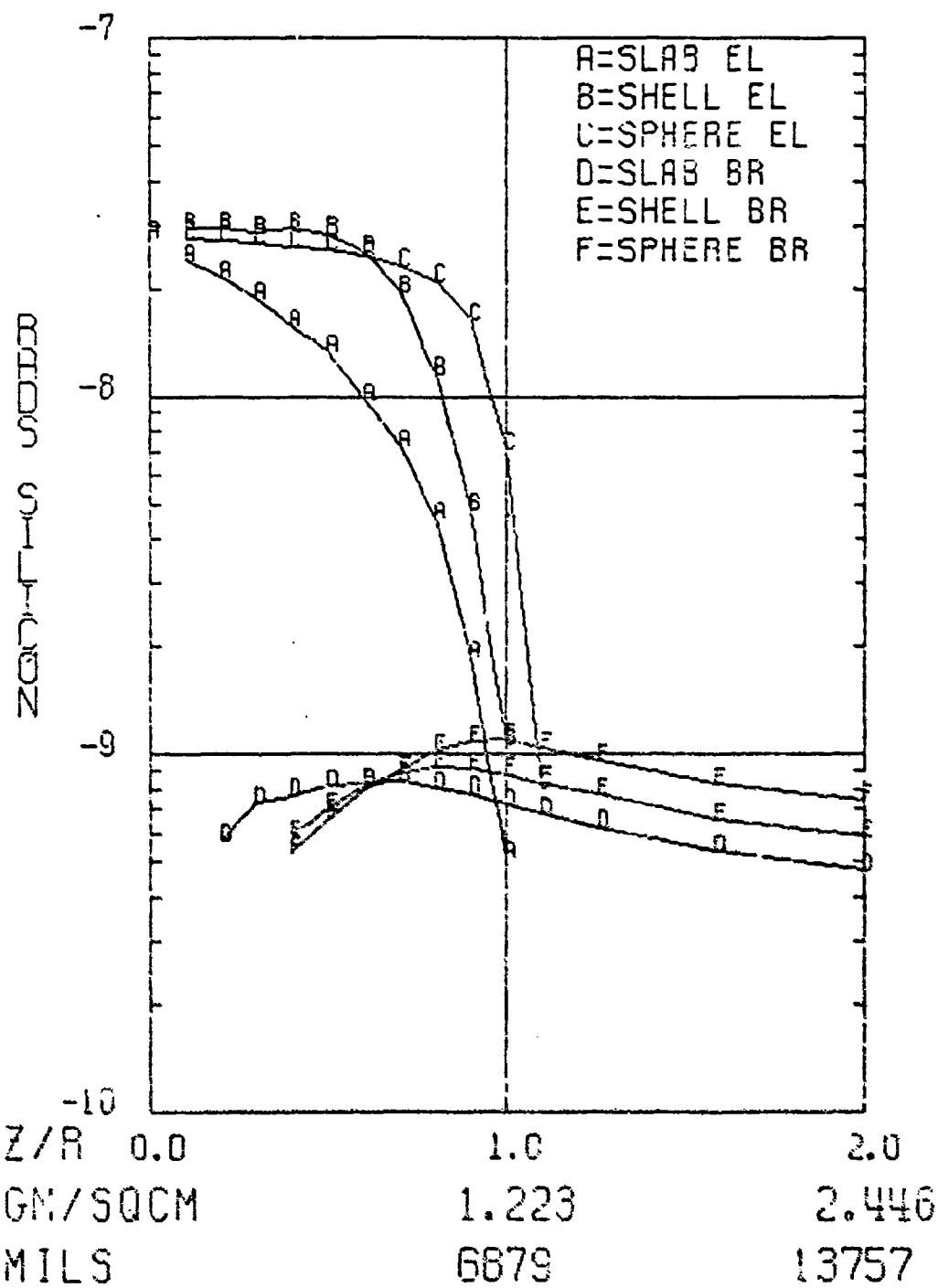
Attenuation curves are presented for three shield geometries, dose between two slabs each of thickness t , $D_{\text{slab}}(t)$, dose at the center of a spherical shell of very large inner radius $D_{\text{shell}}(t)$, and dose at the center of a solid spherical shield $D_{\text{solid}}(t)$. Each of the shields is imbedded in a unit isotropic free space fluence.

Electron and bremsstrahlung transport were simulated by a combination of analytic and Monte Carlo methods. Fluctuations in the computer results were not smoothed prior to plotting.

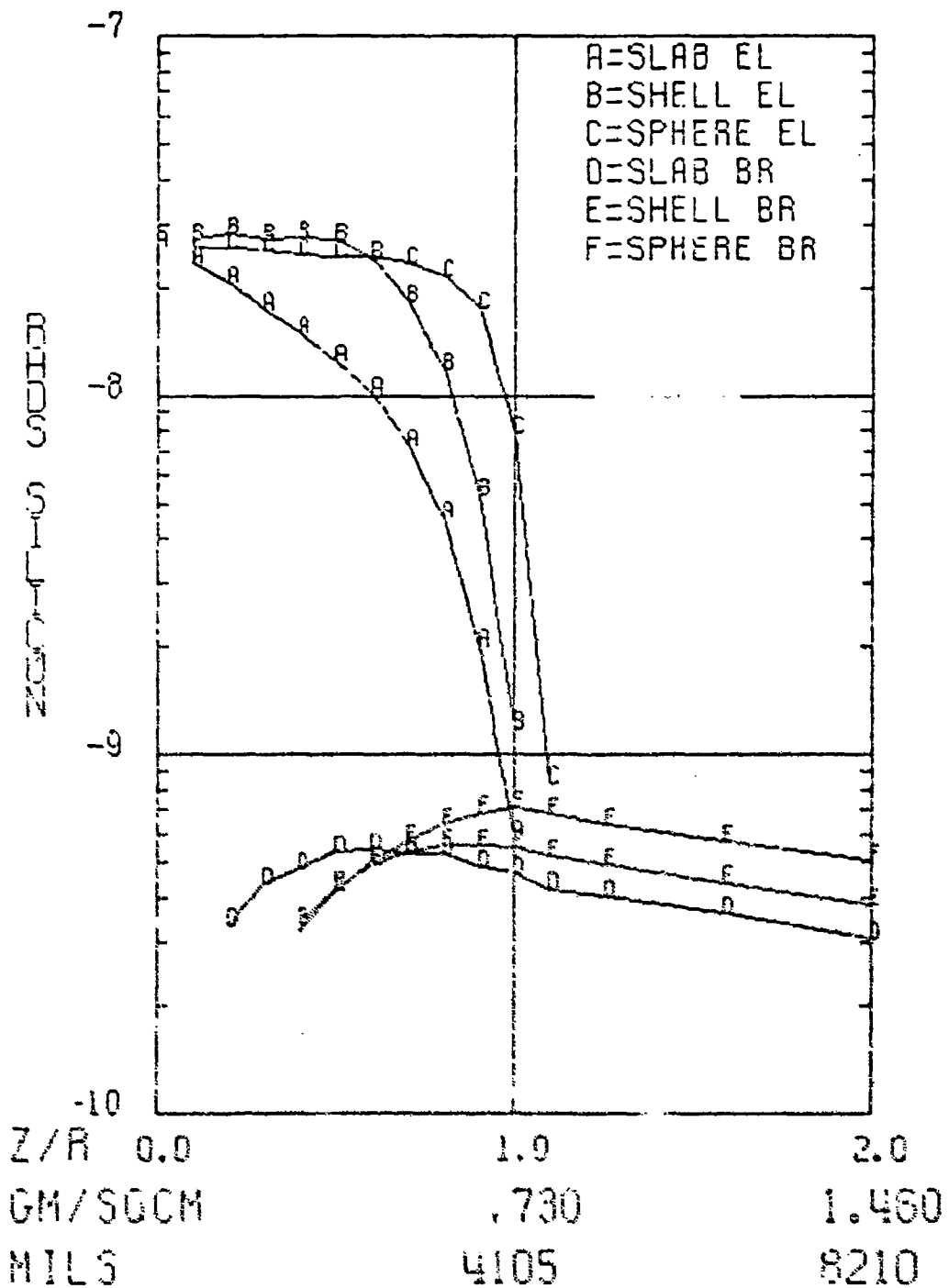
8 MEV, HYDROGEN



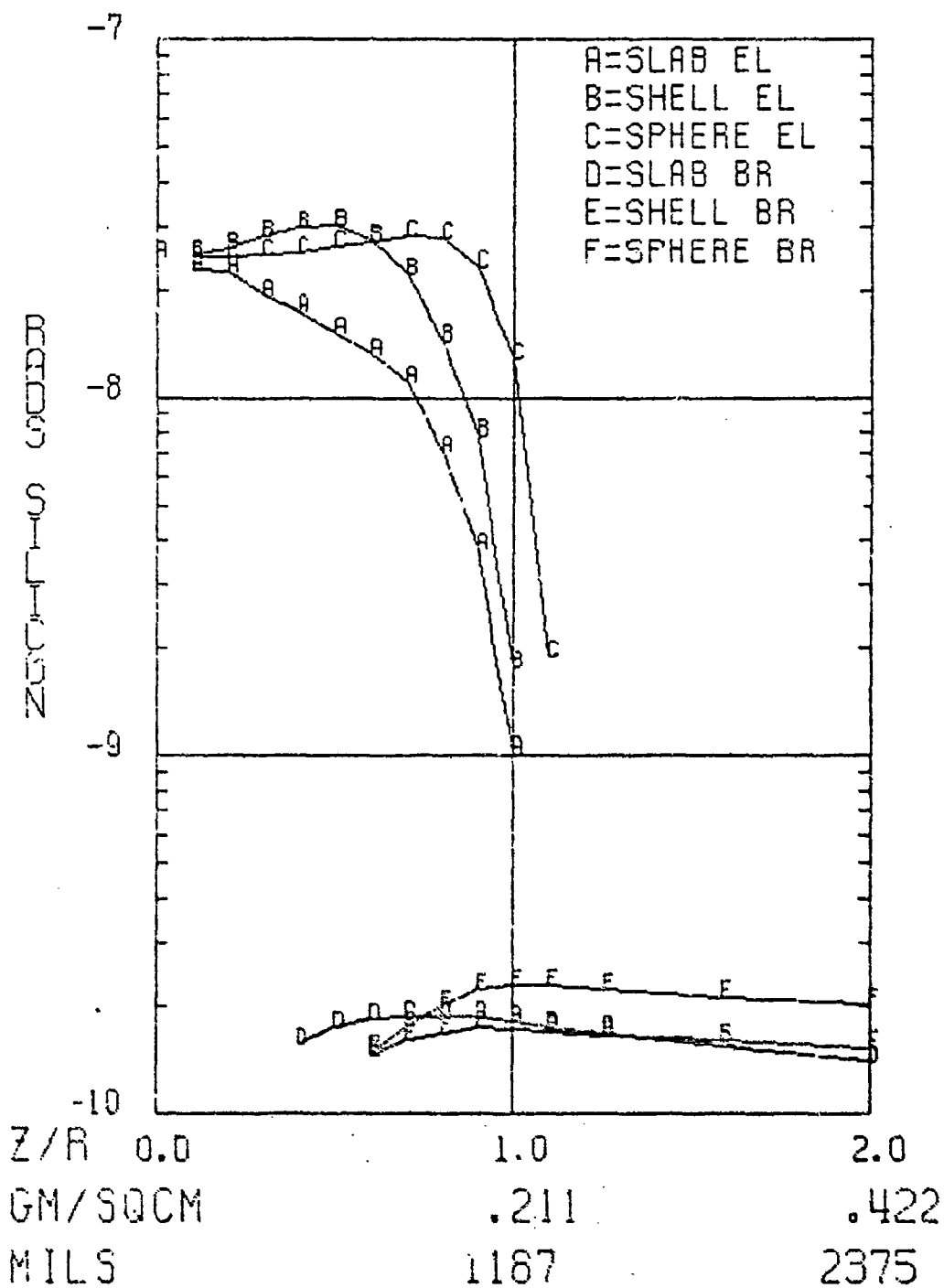
5 MEV, HYDROGEN



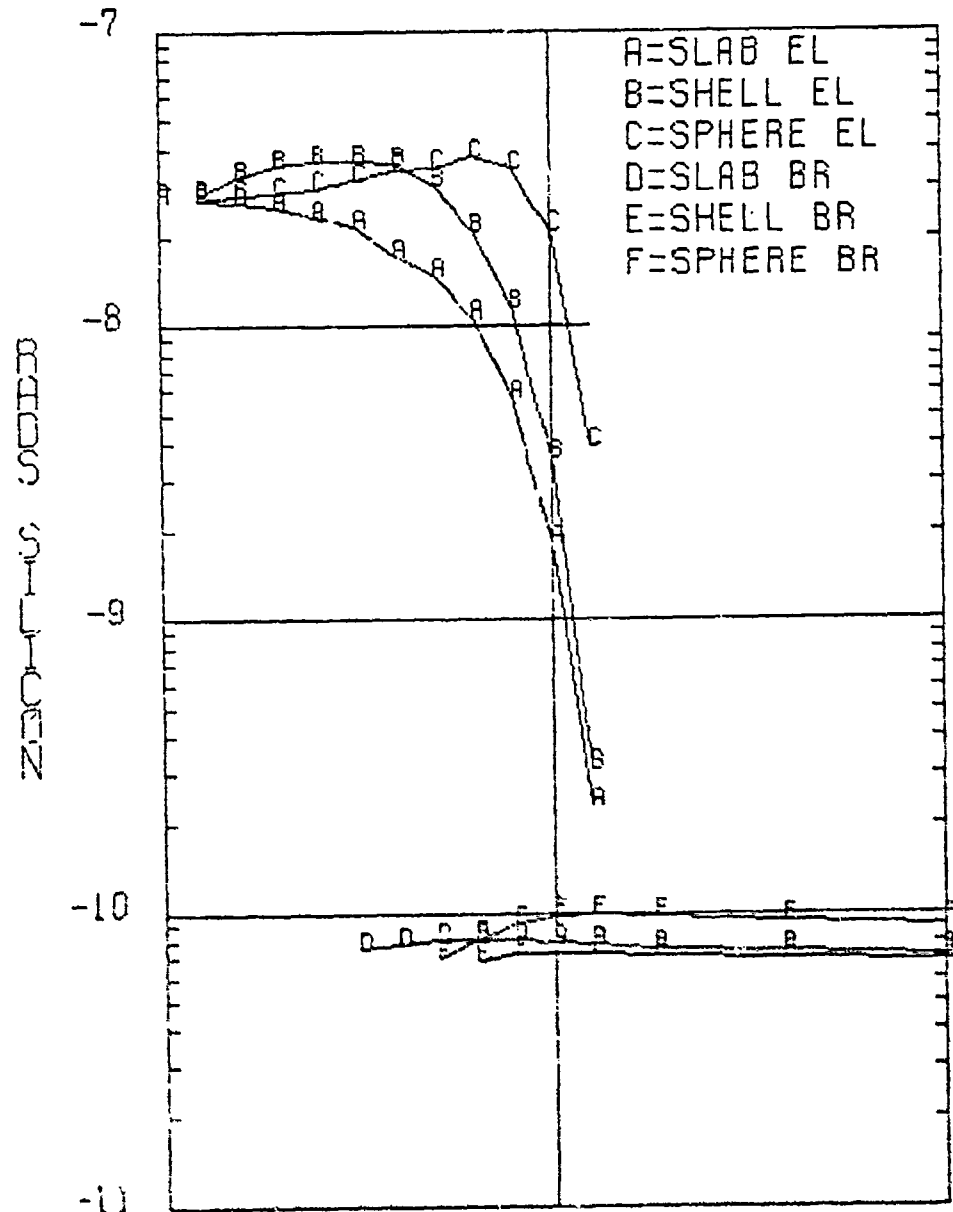
3 MEV, HYDROGEN



1 MEV, HYDROGEN



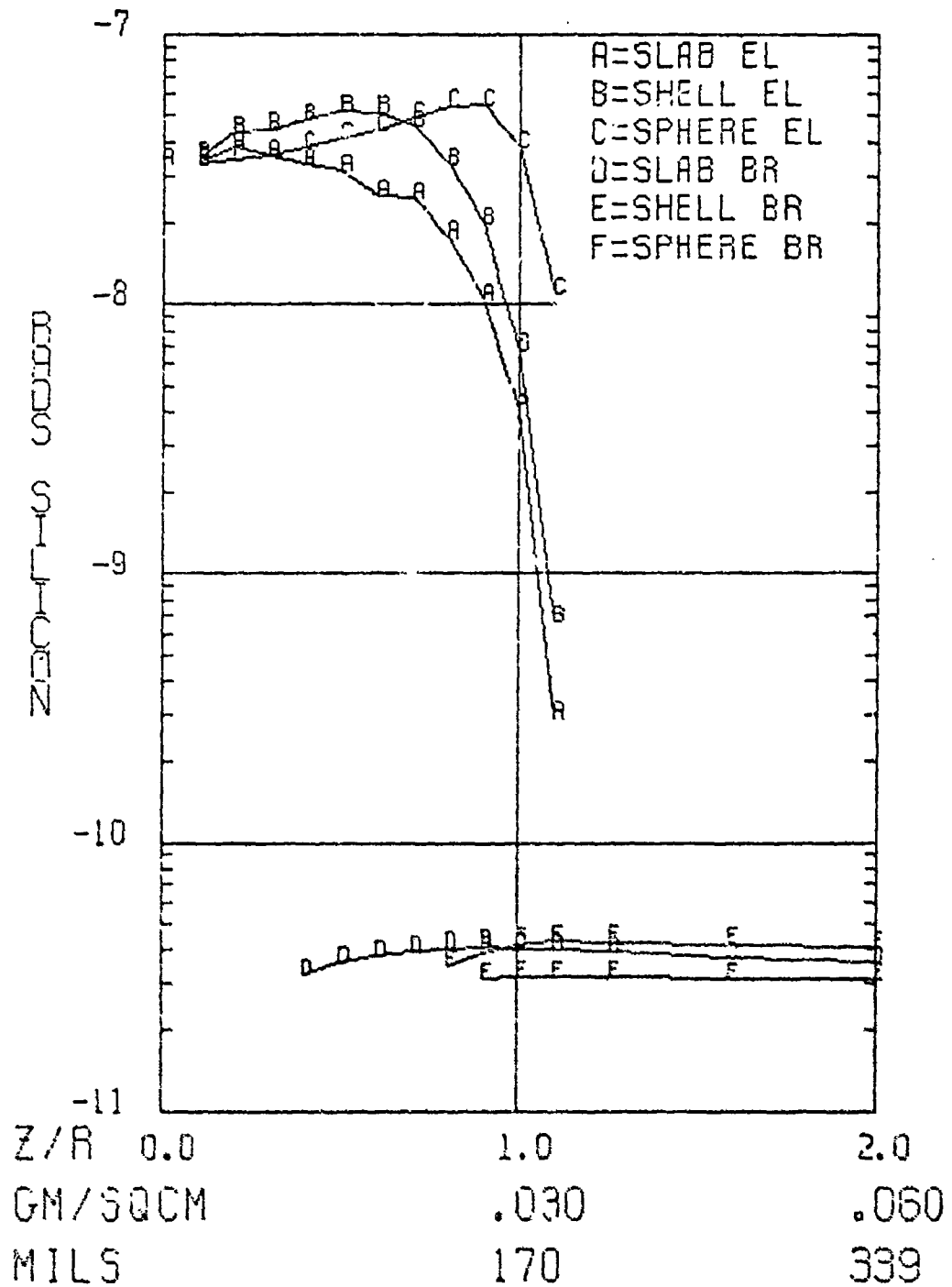
0.5 MEV, HYDROGEN



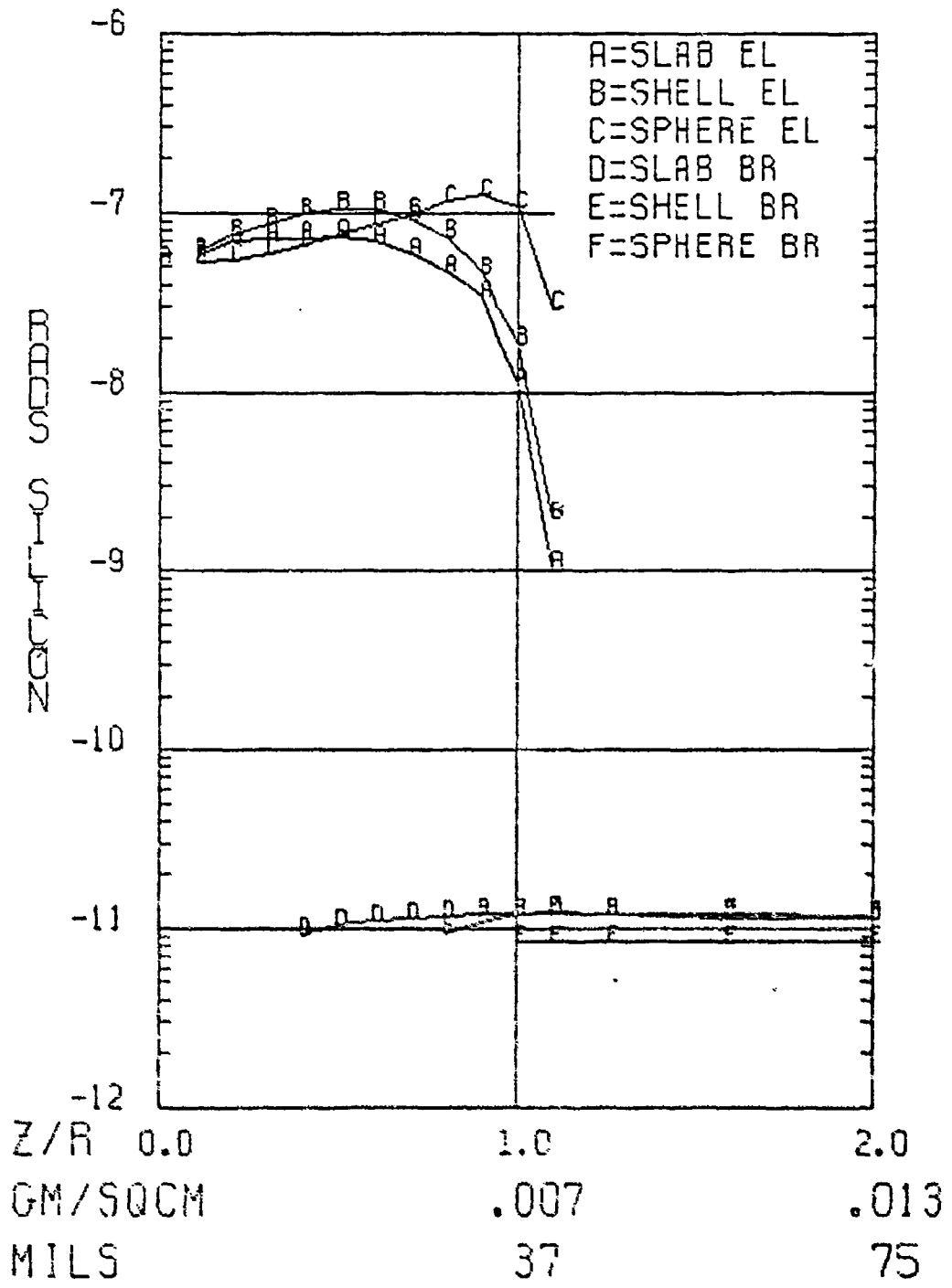
(1)

Z/R	0.0	1.0	2.0
GM/SQCM		.025	.169
MILS		476	952

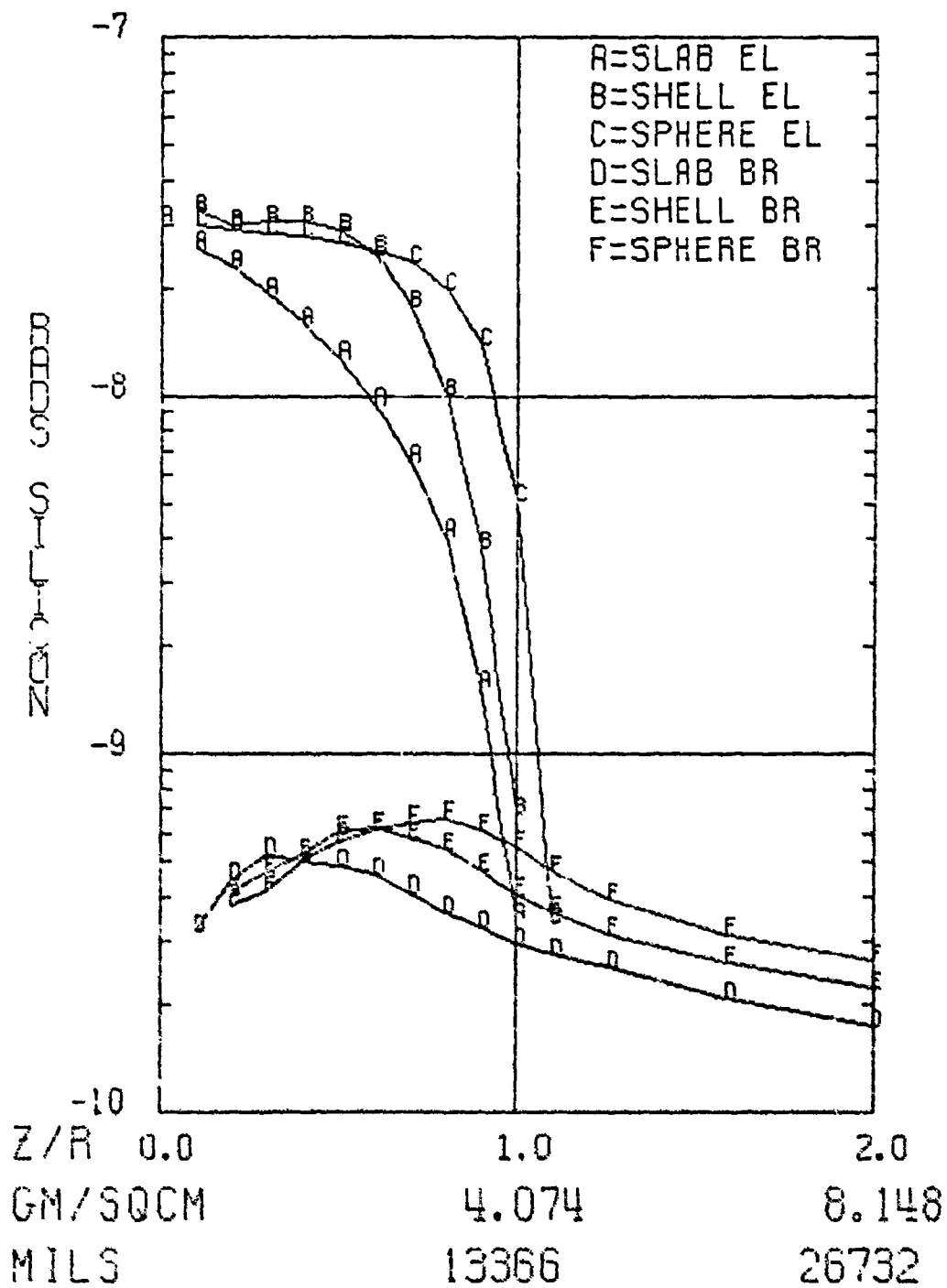
0.25 MEV, HYDROGEN



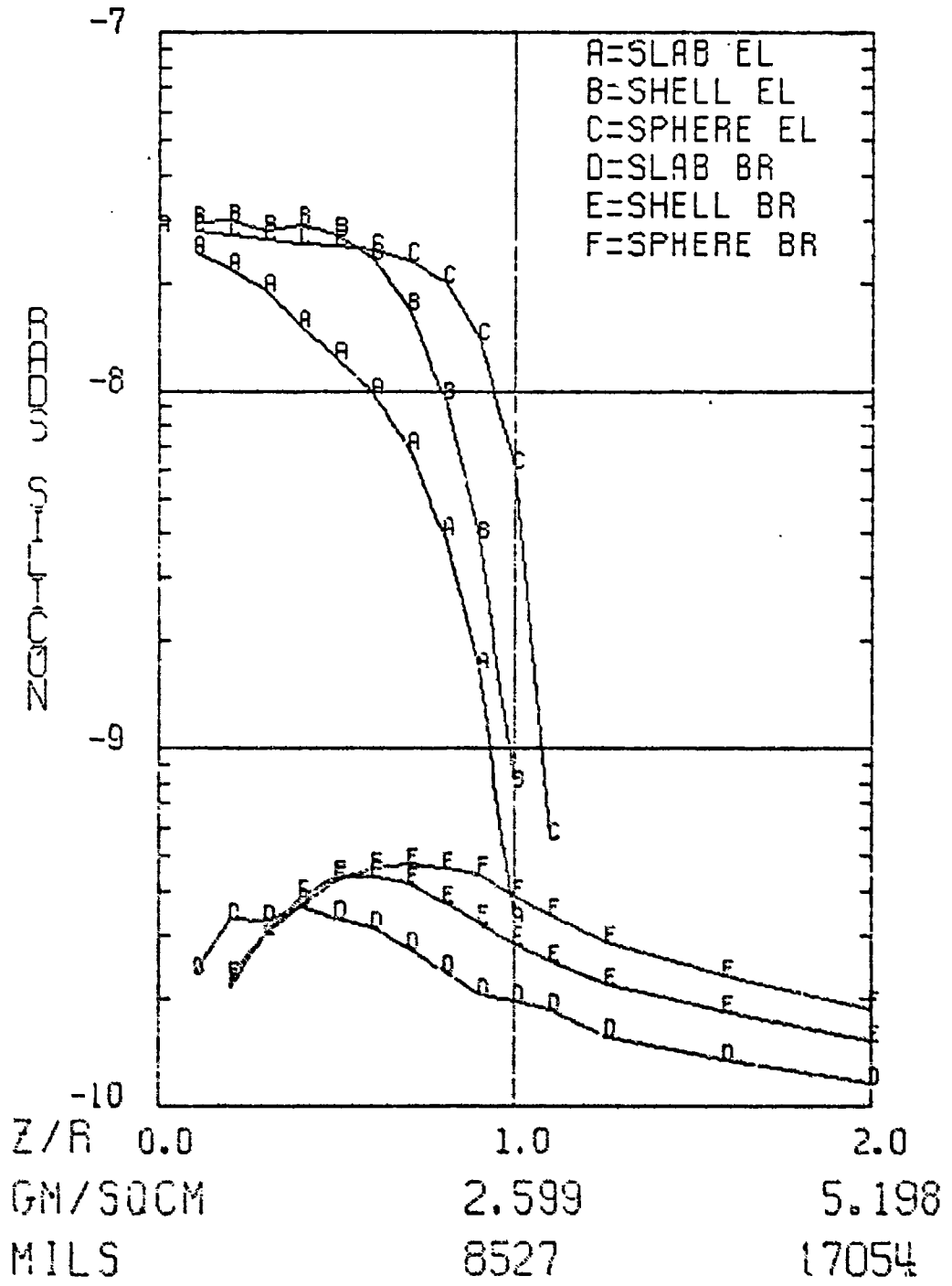
0.1 MEV, HYDROGEN



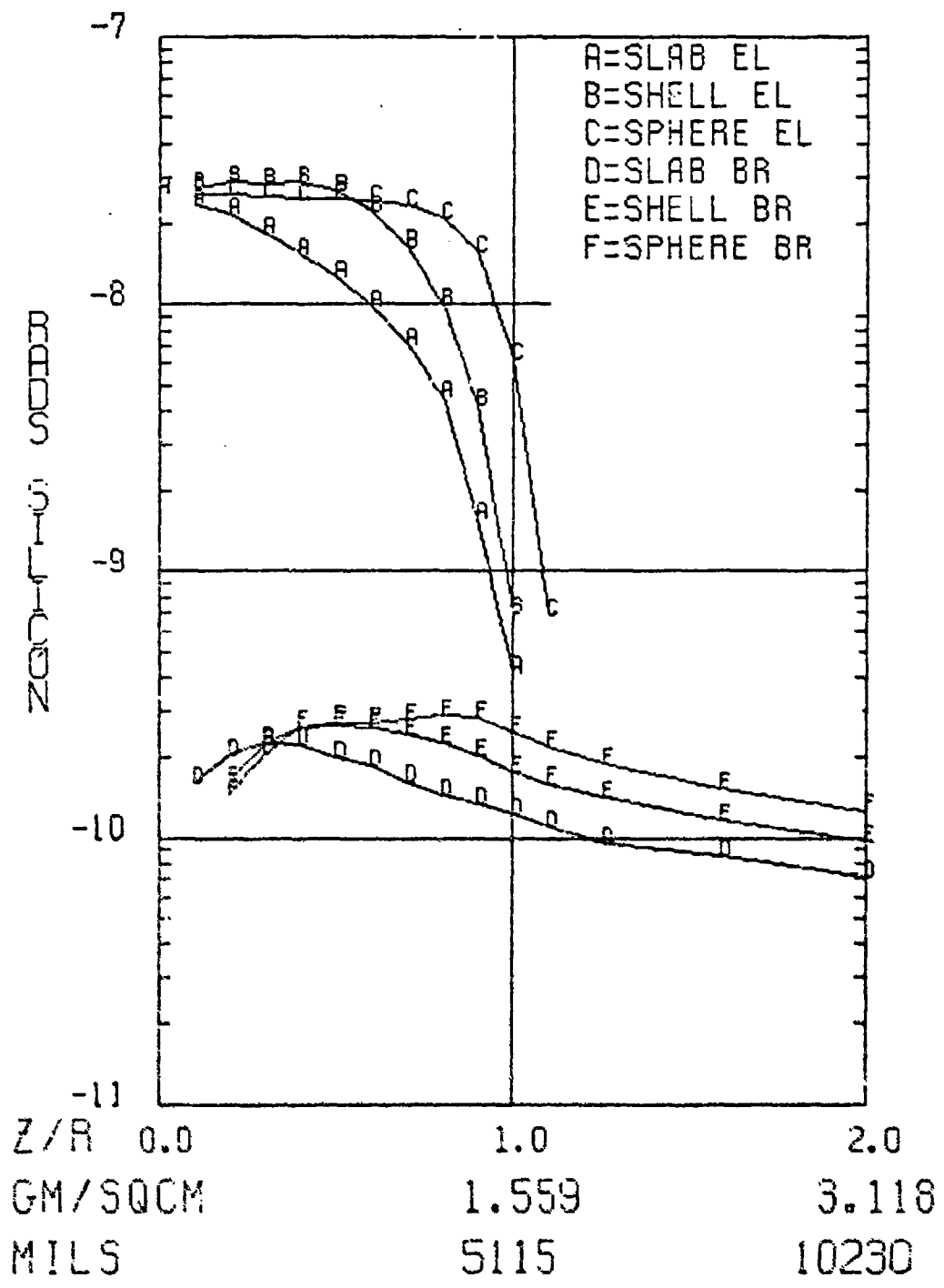
8 MEV, HELIUM



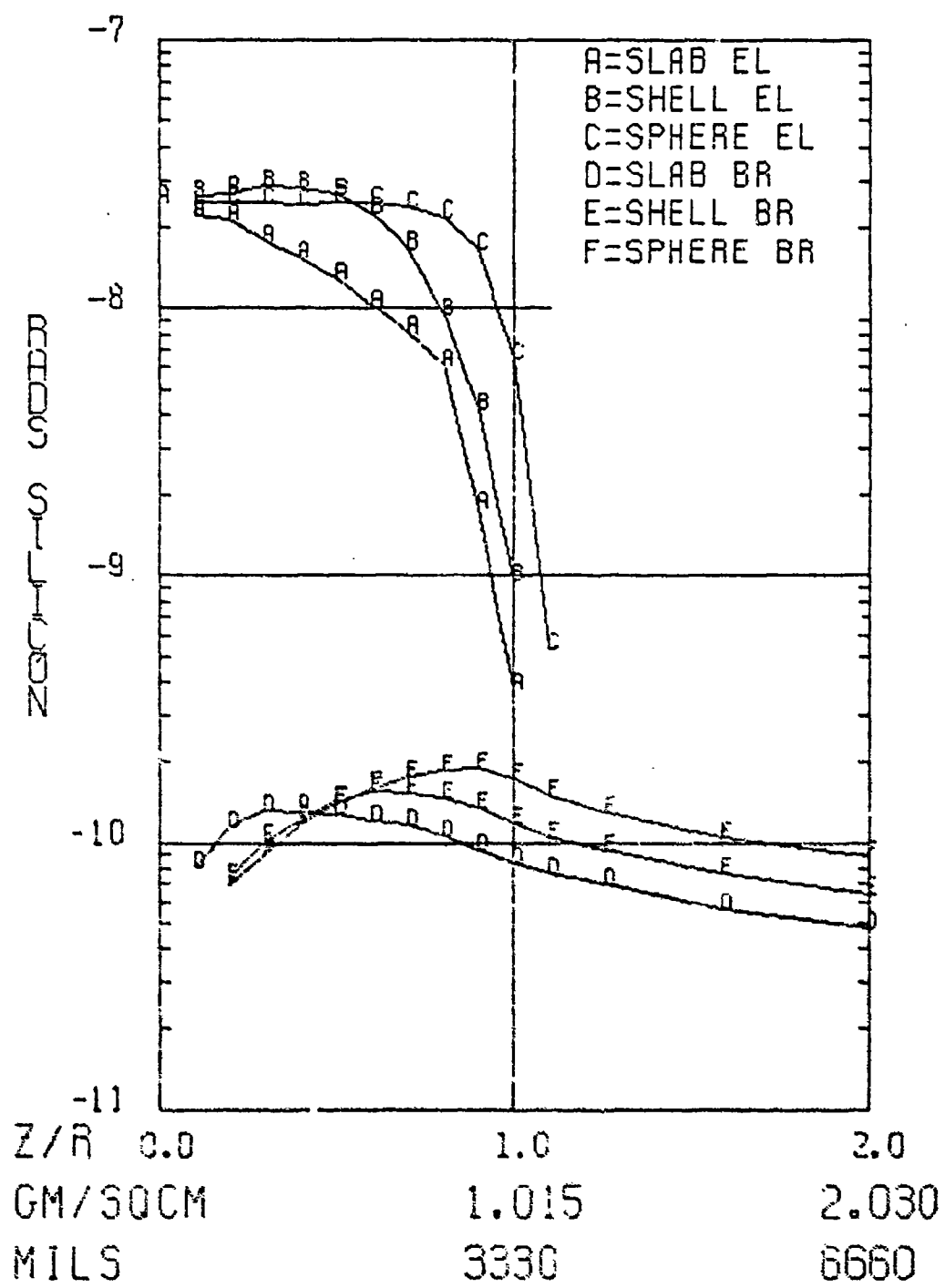
5 MEV, HELIUM



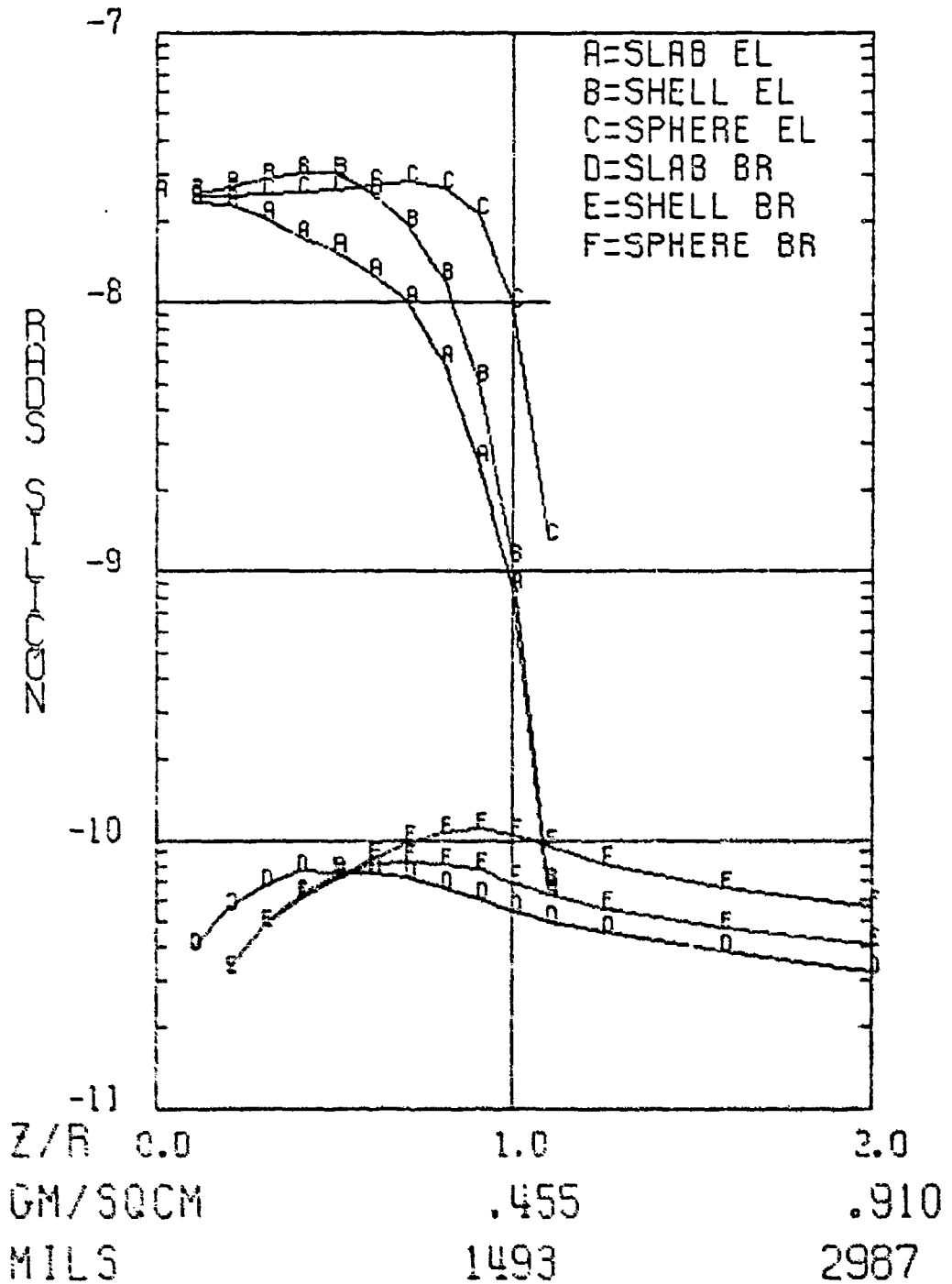
3 MEV, HELIUM



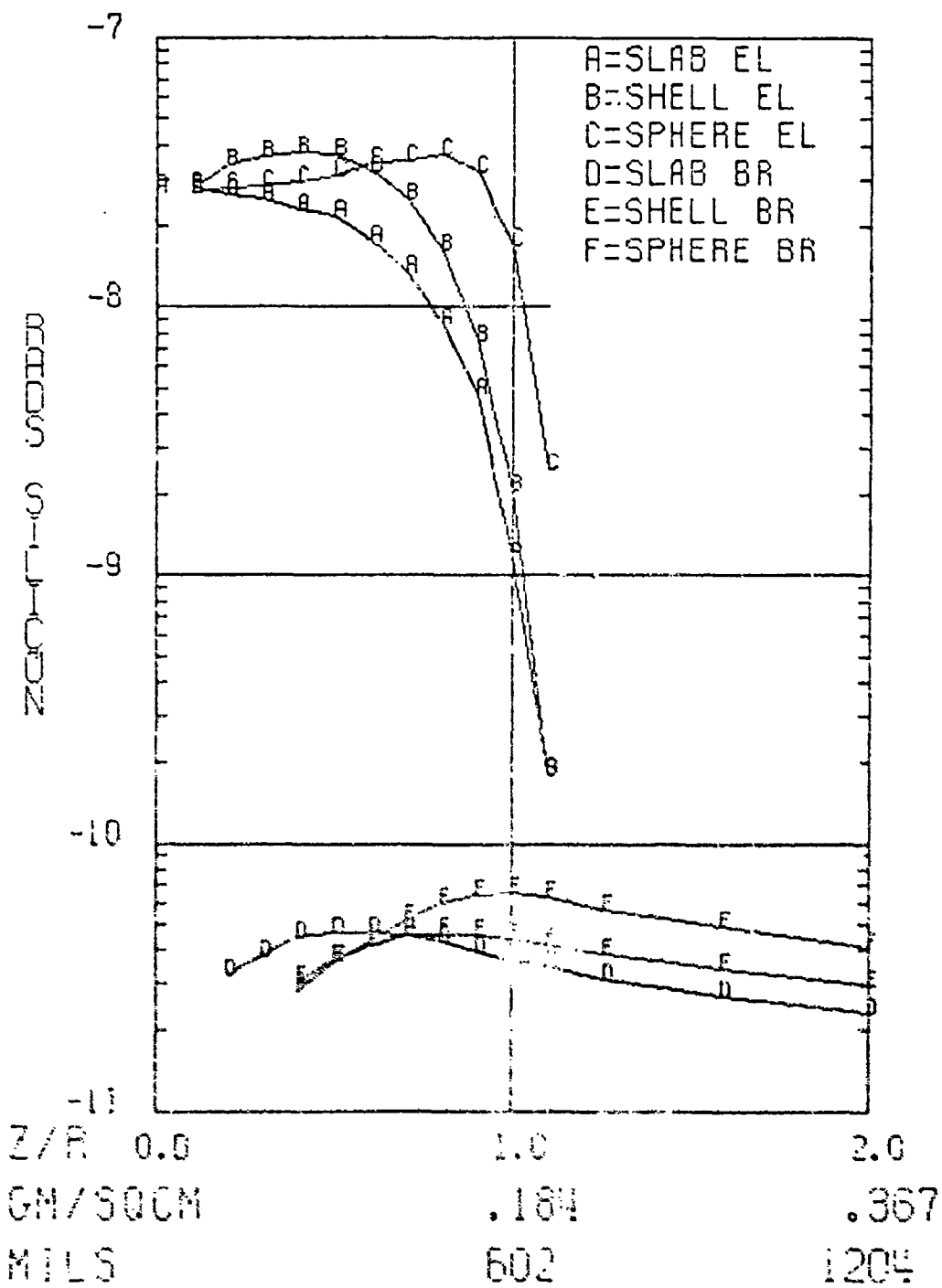
2 MEV, HELIUM



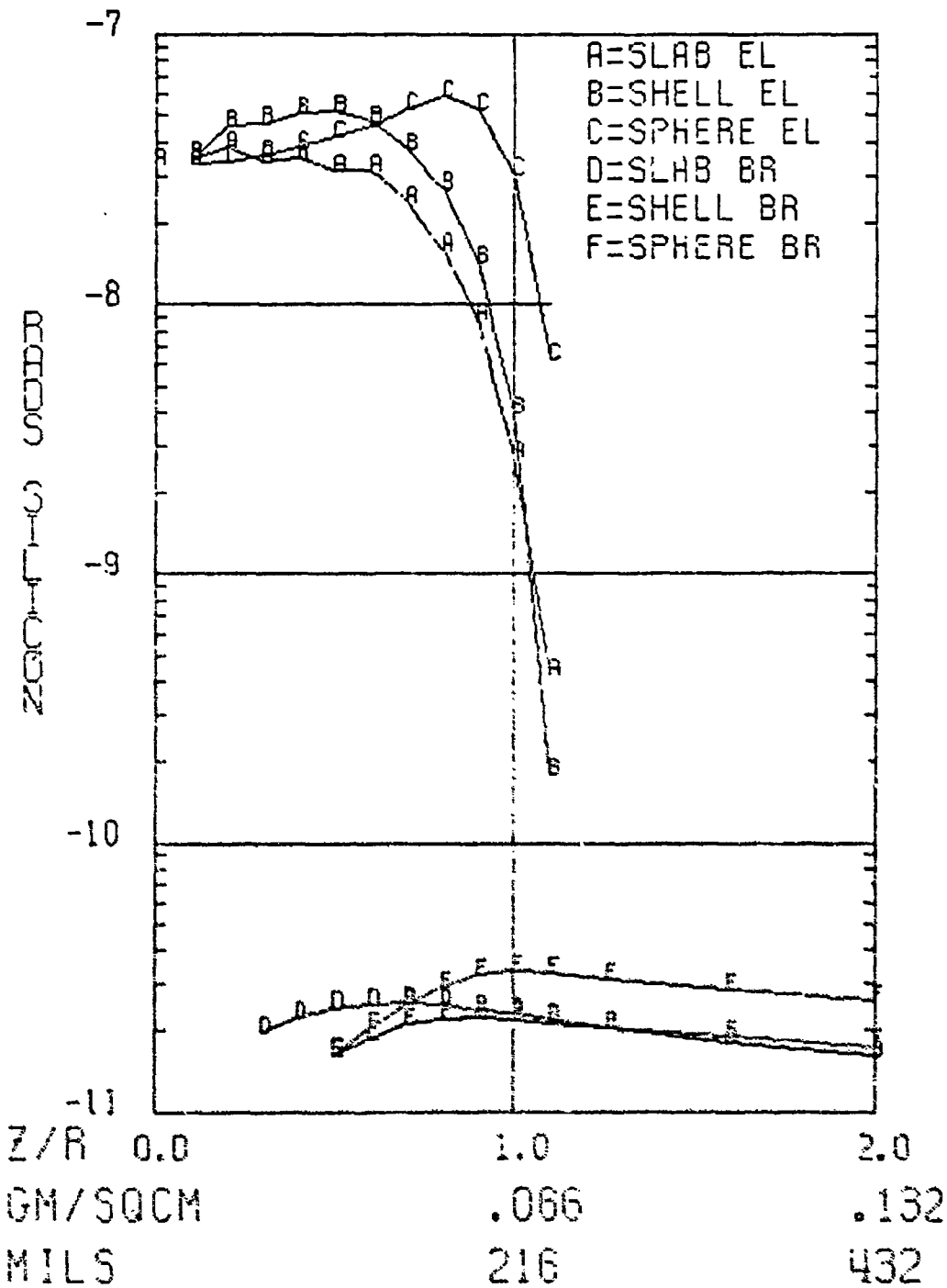
1 MEV, HELIUM



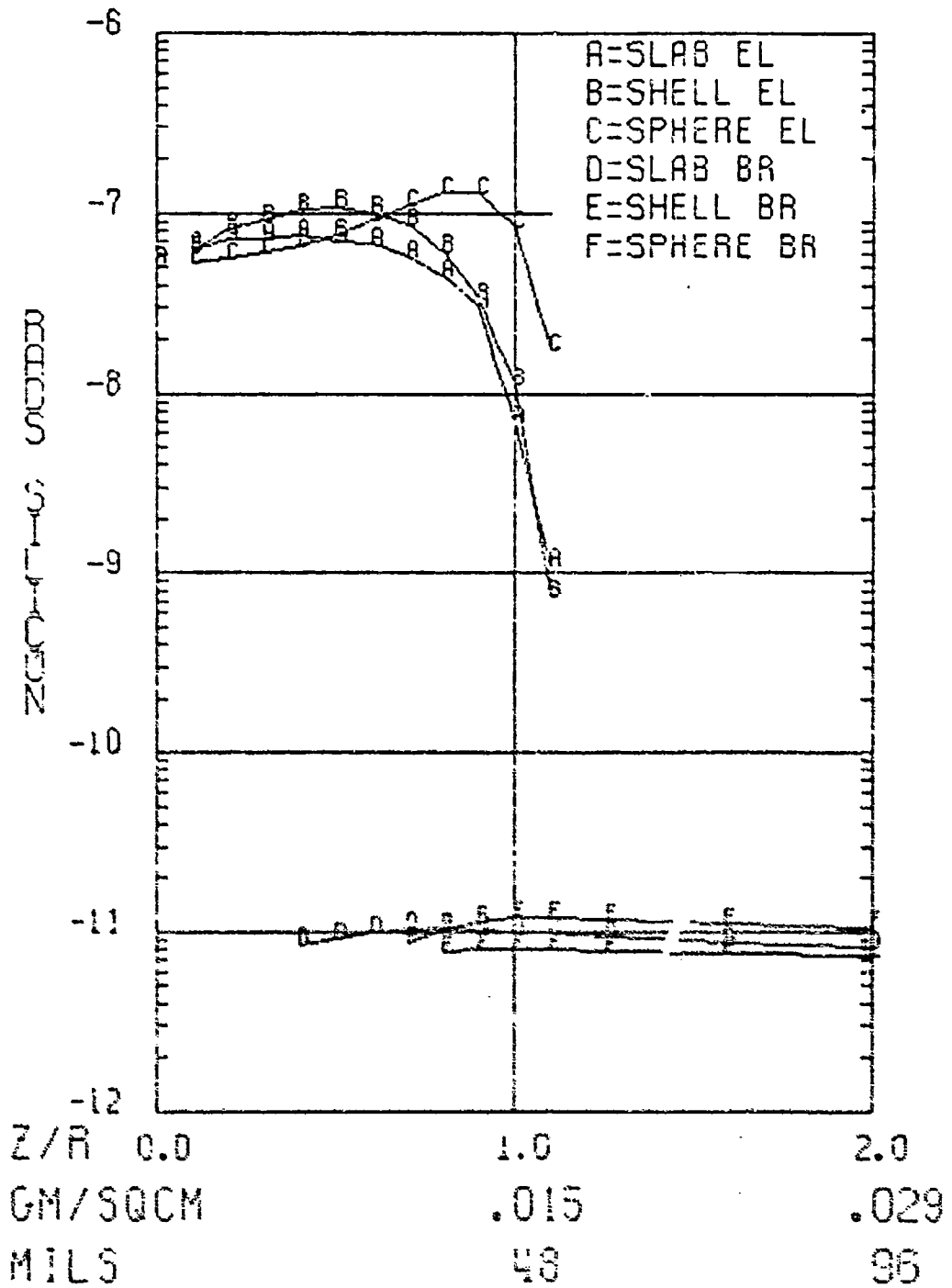
0.5 MEV, HELIUM



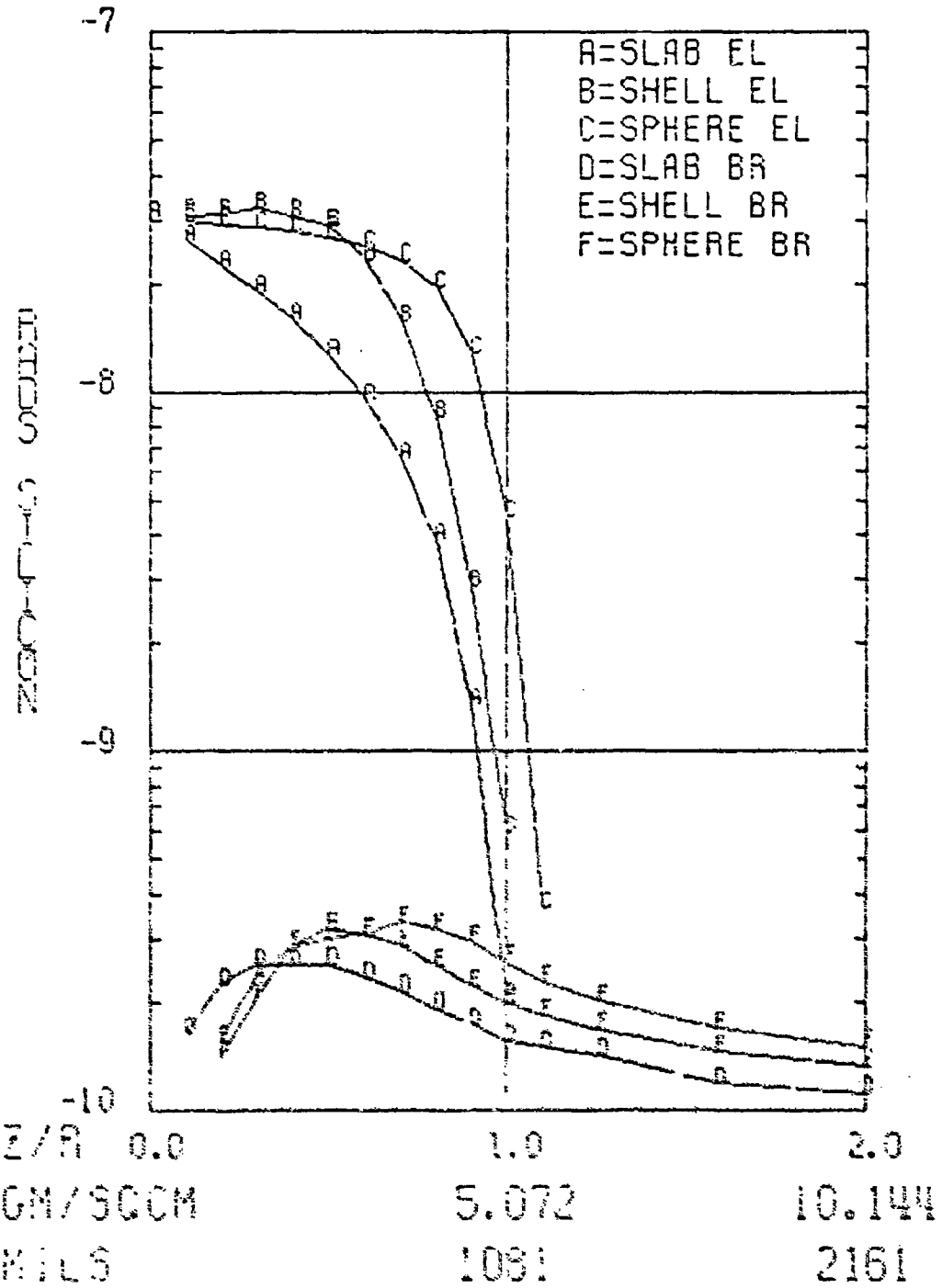
0.25 MEV, HELIUM



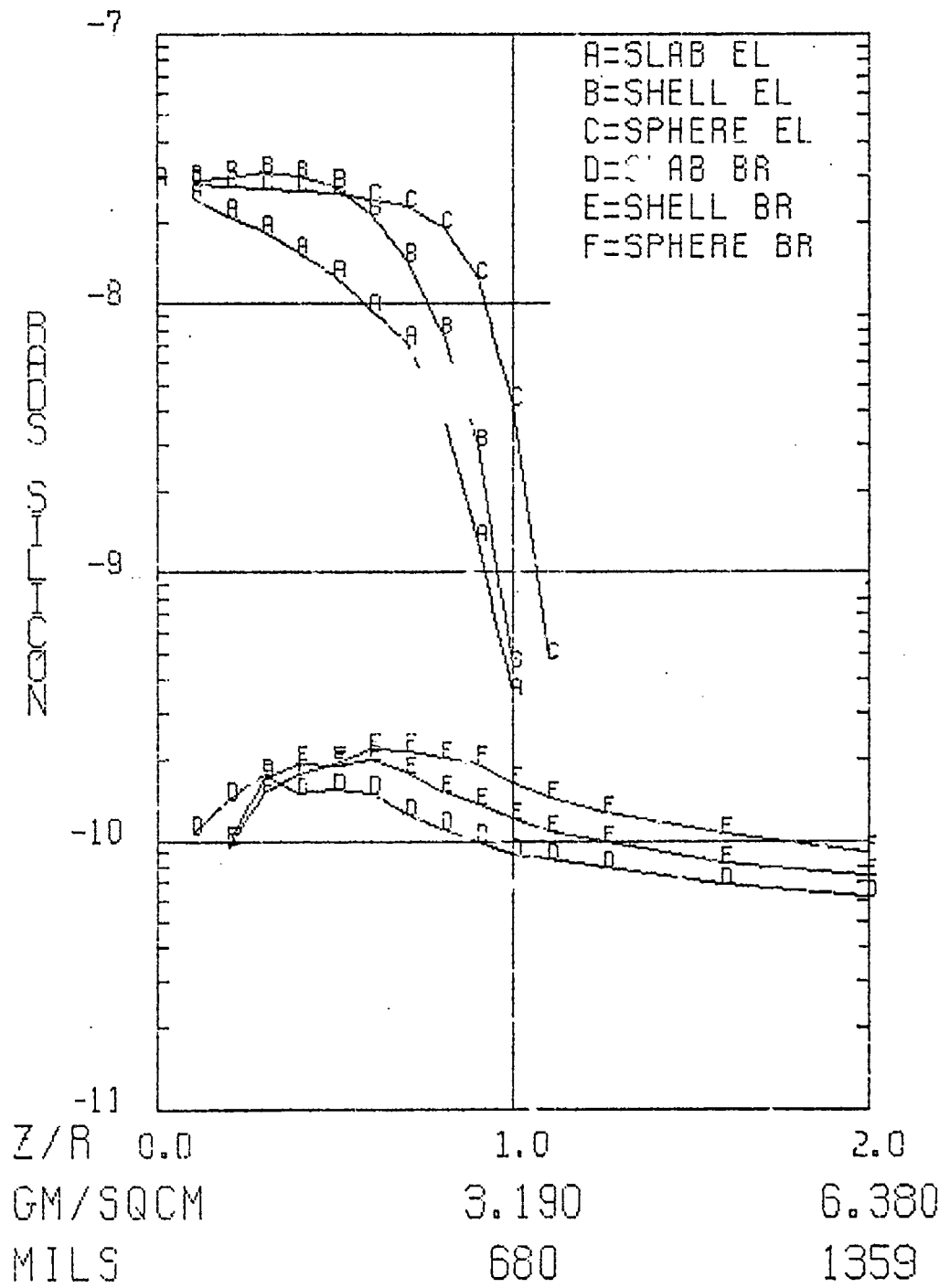
0.1 MEV, HELIUM



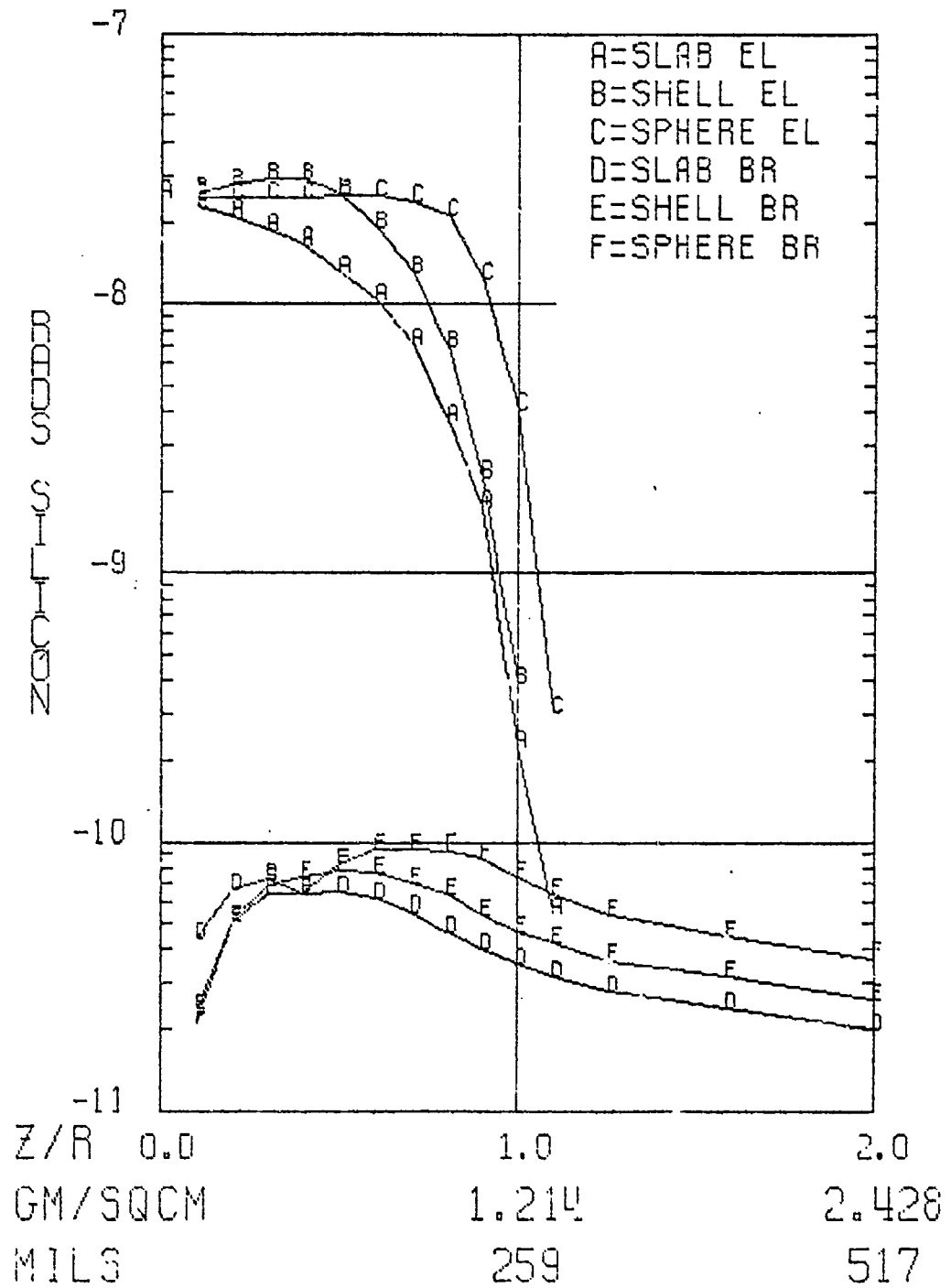
8 MEV, BERYLLIUM



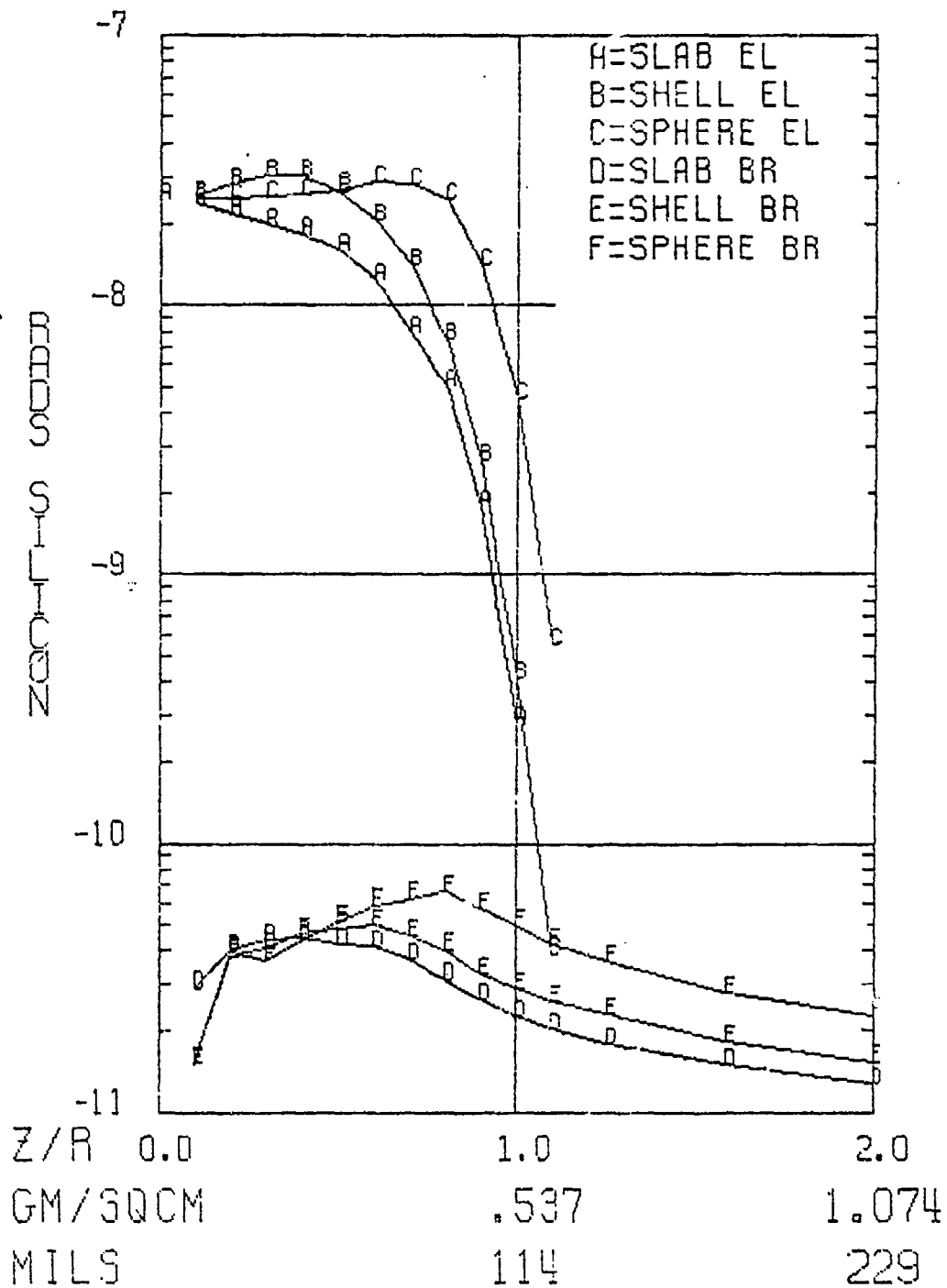
5 MEV, BERYLLIUM



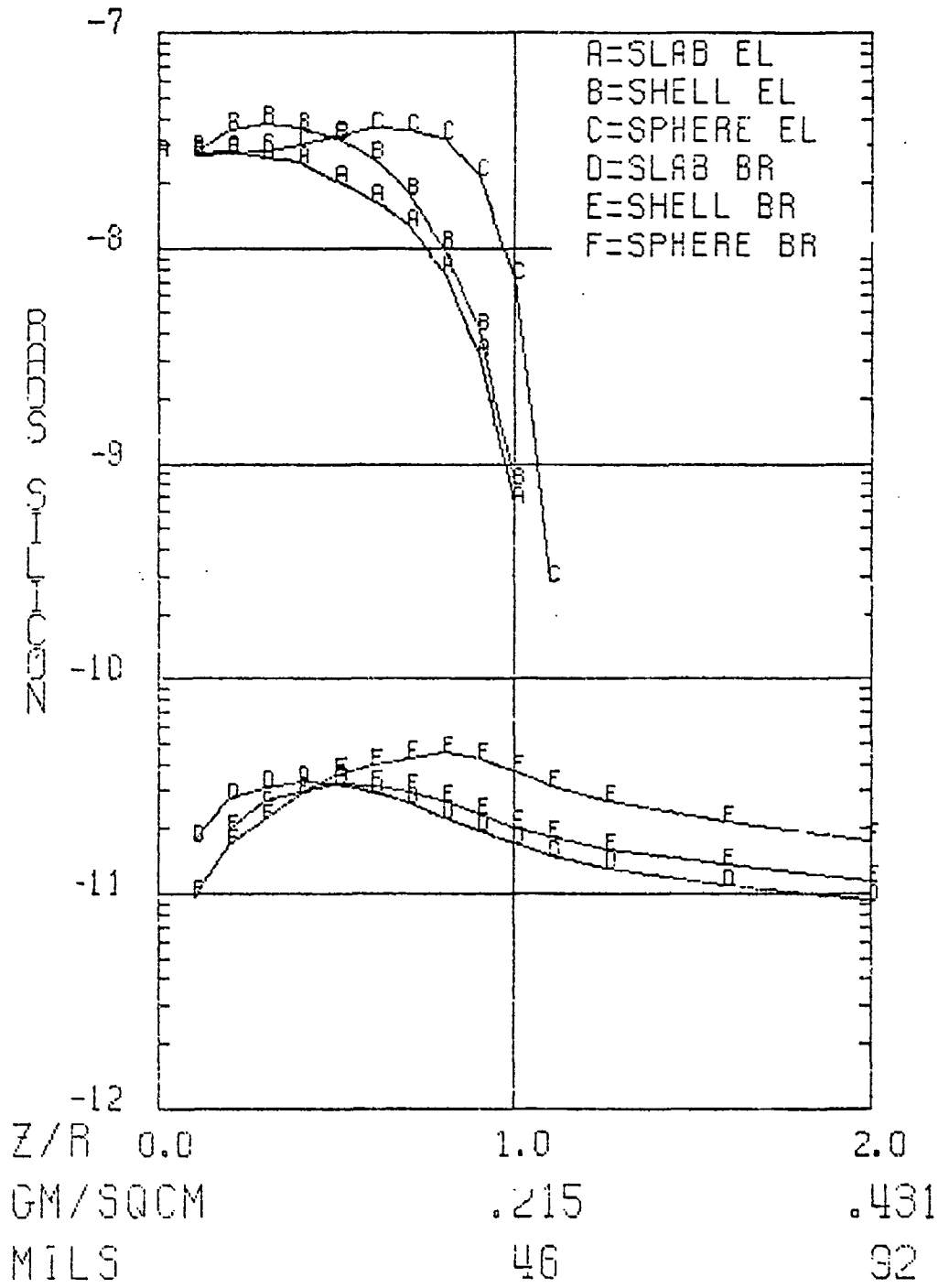
2 MEV, BERYLLIUM



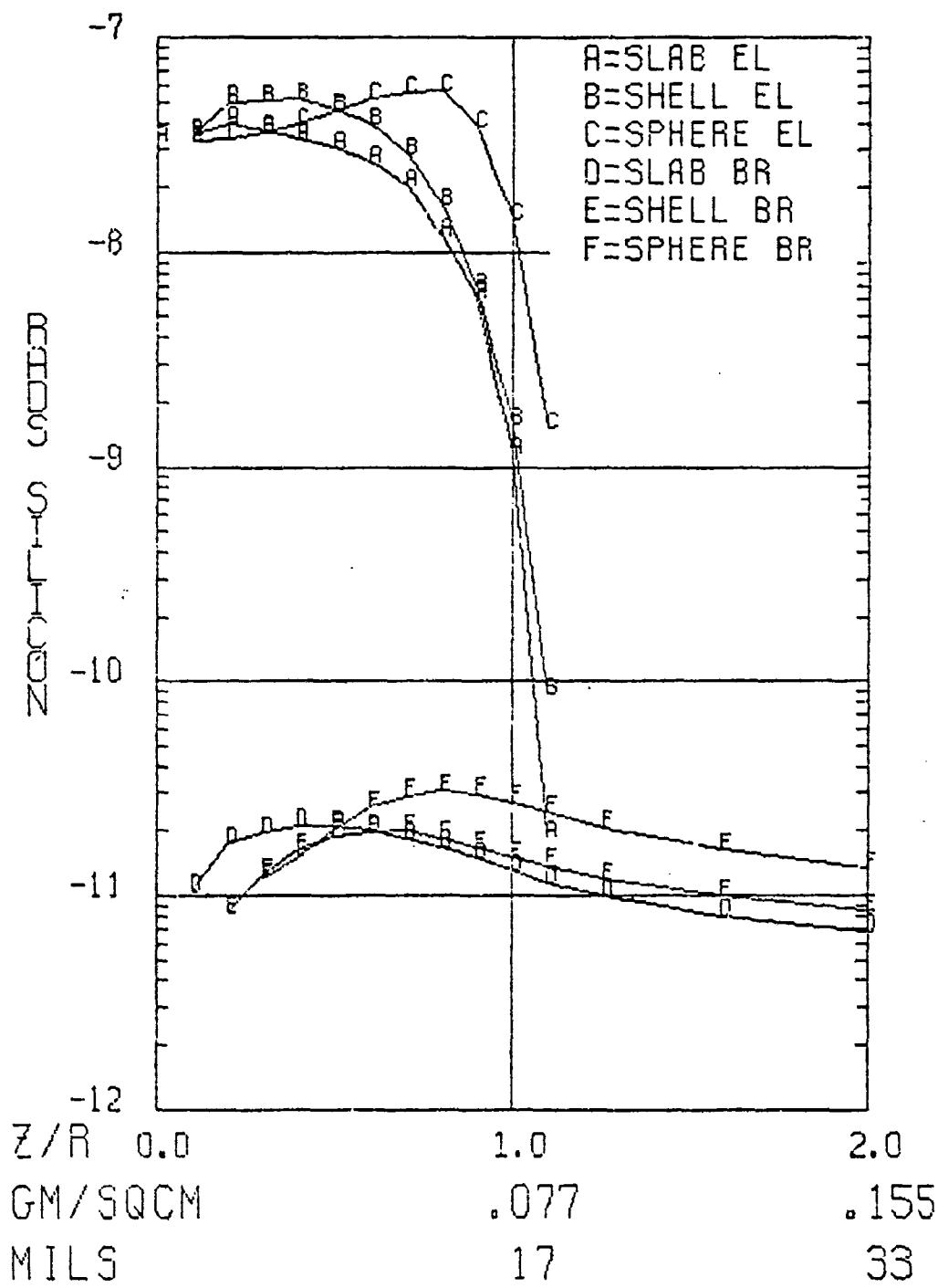
1 MEV, BERYLLIUM



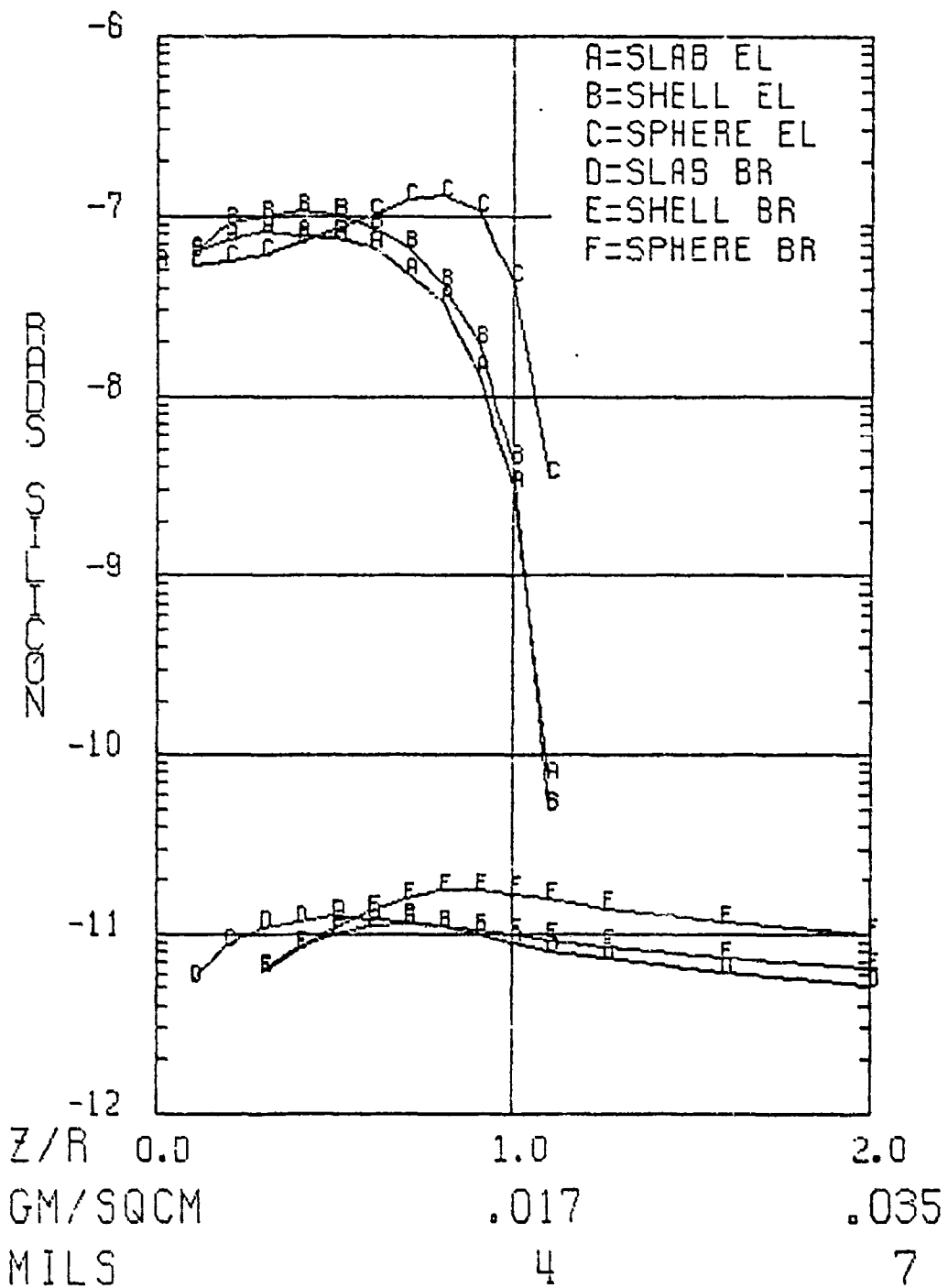
0.5 MEV, BERYLLIUM



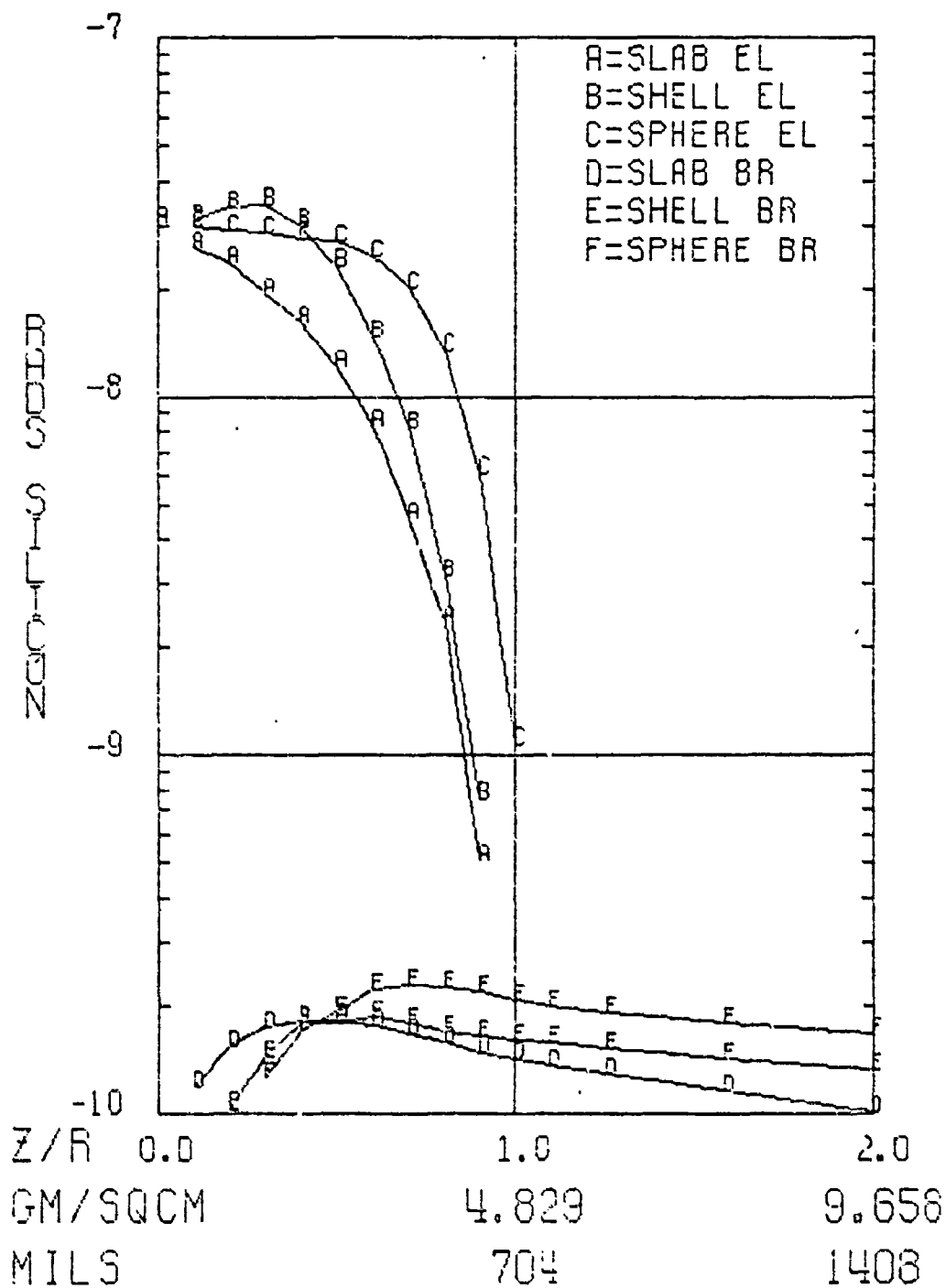
0.25 MEV, BERYLLIUM



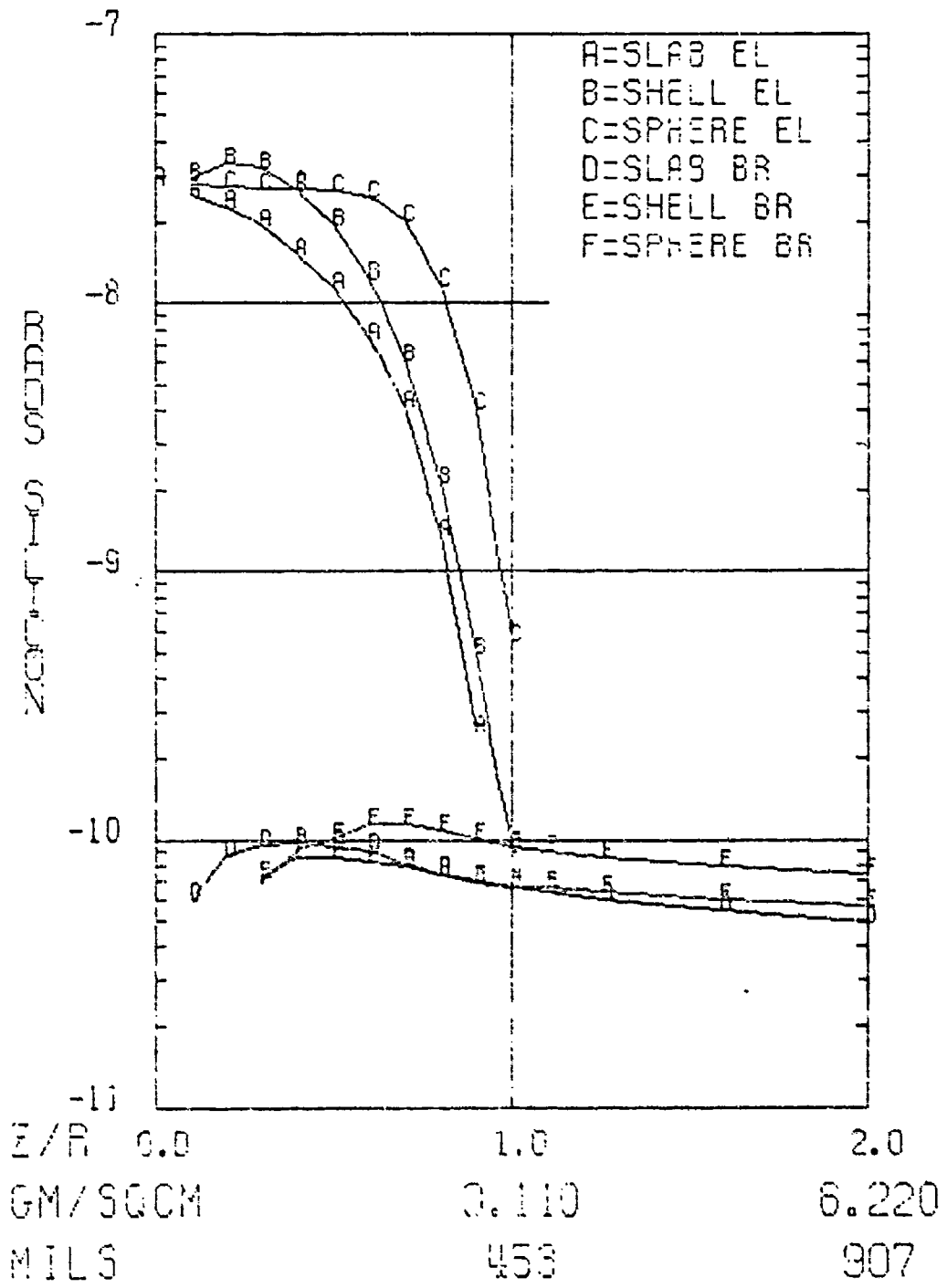
0.1 MEV, BERYLLIUM



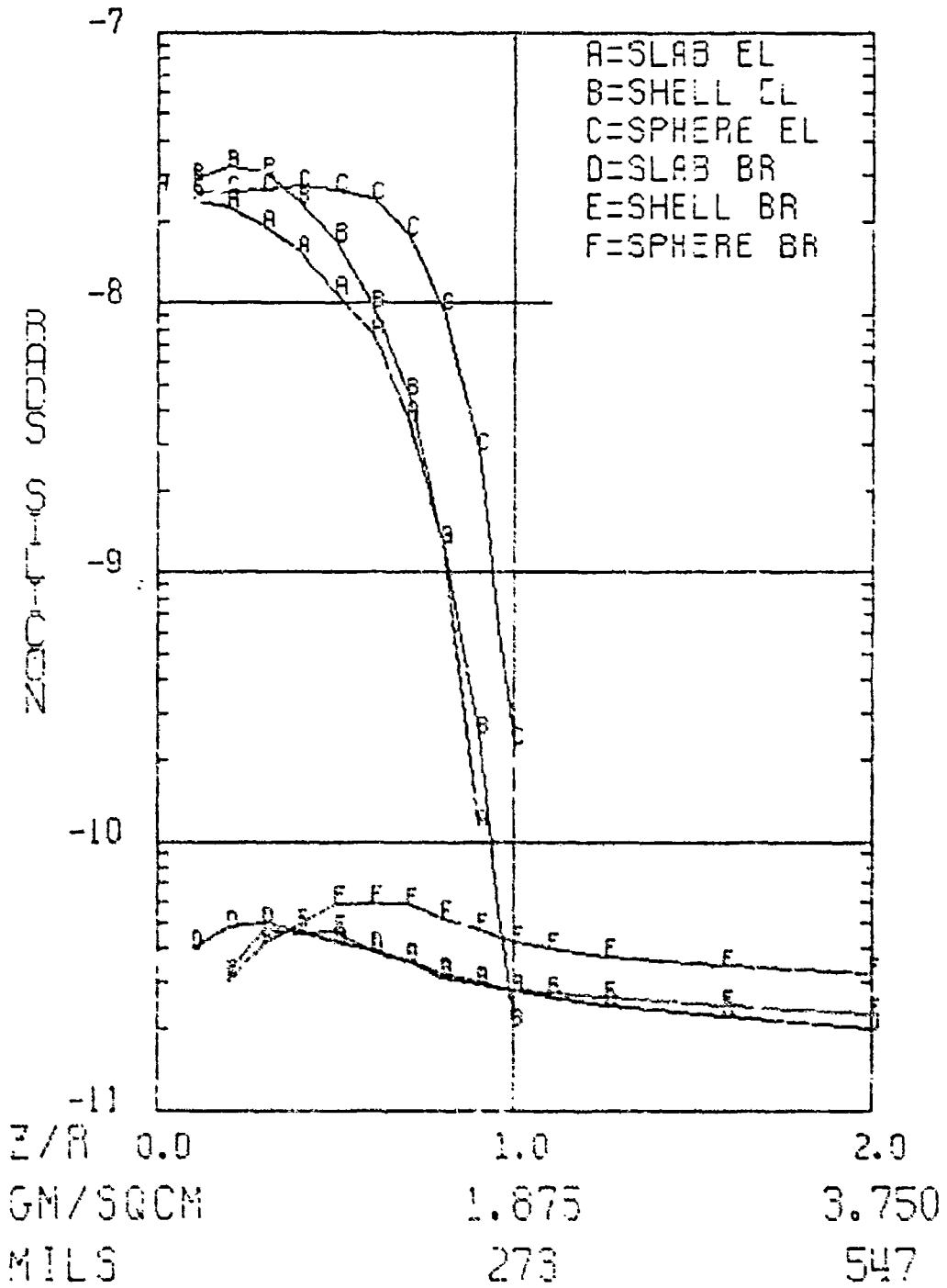
8 MEV, ALUMINUM



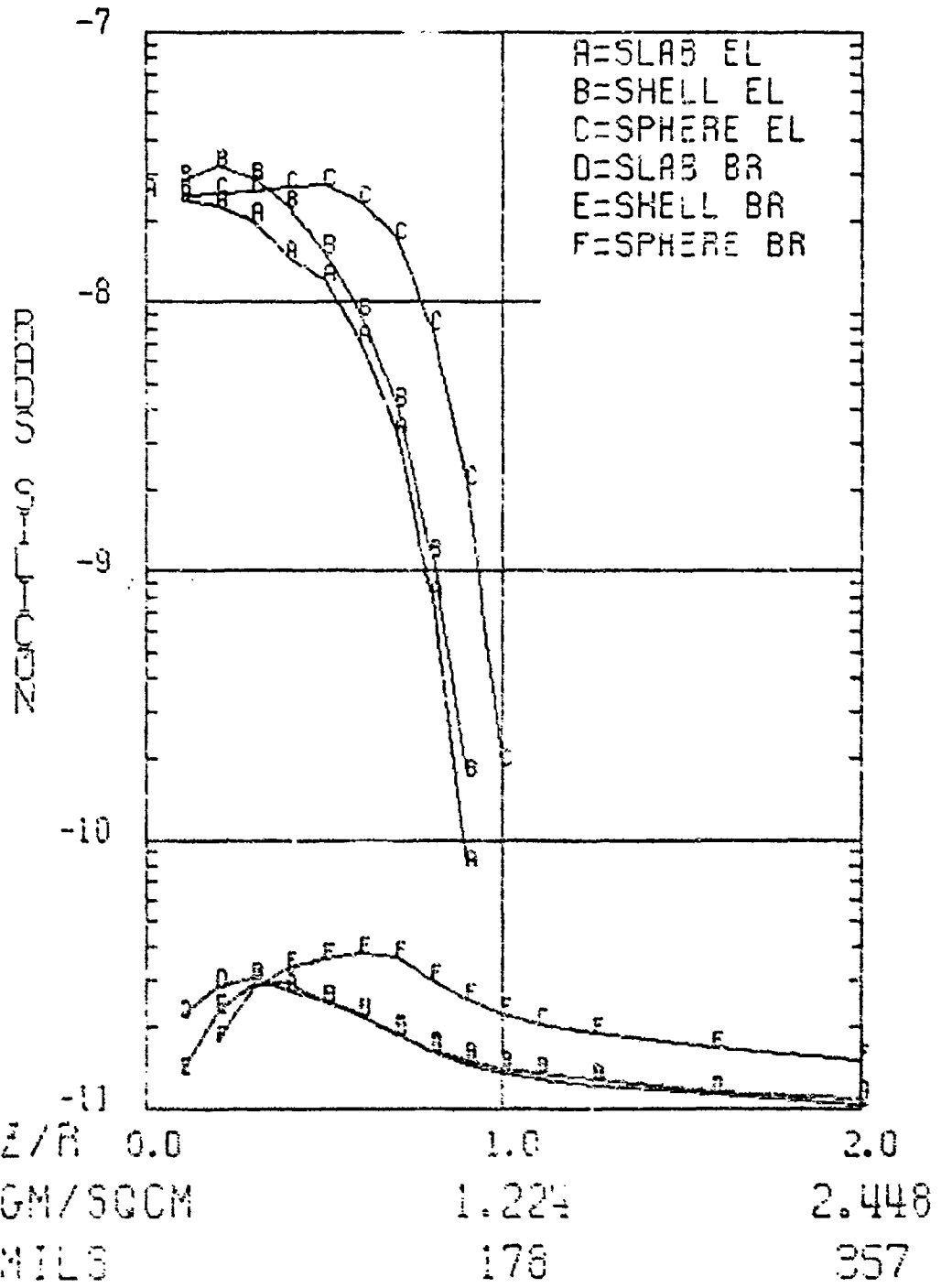
5 MEV, ALUMINUM



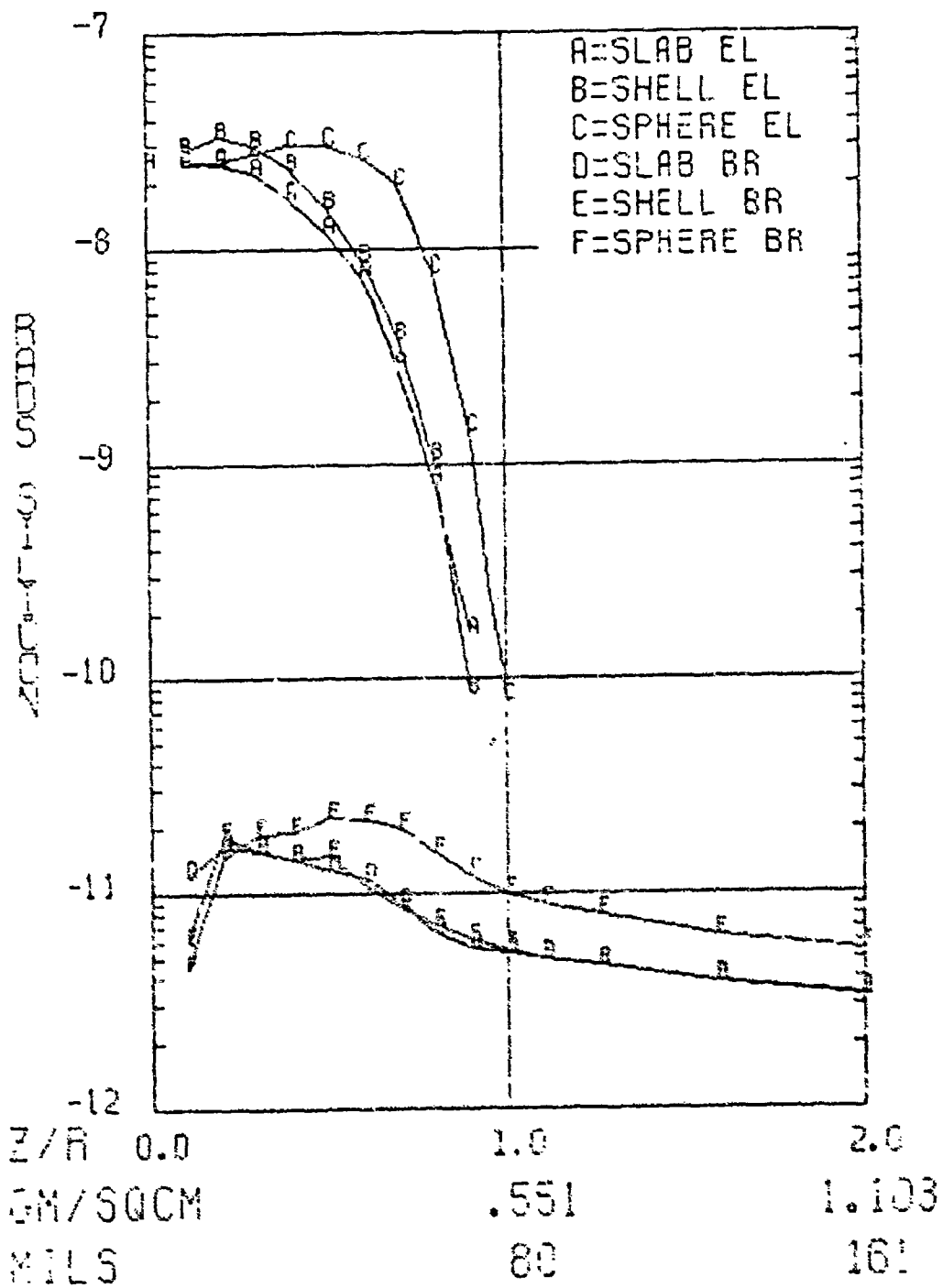
3 MEV, ALUMINUM



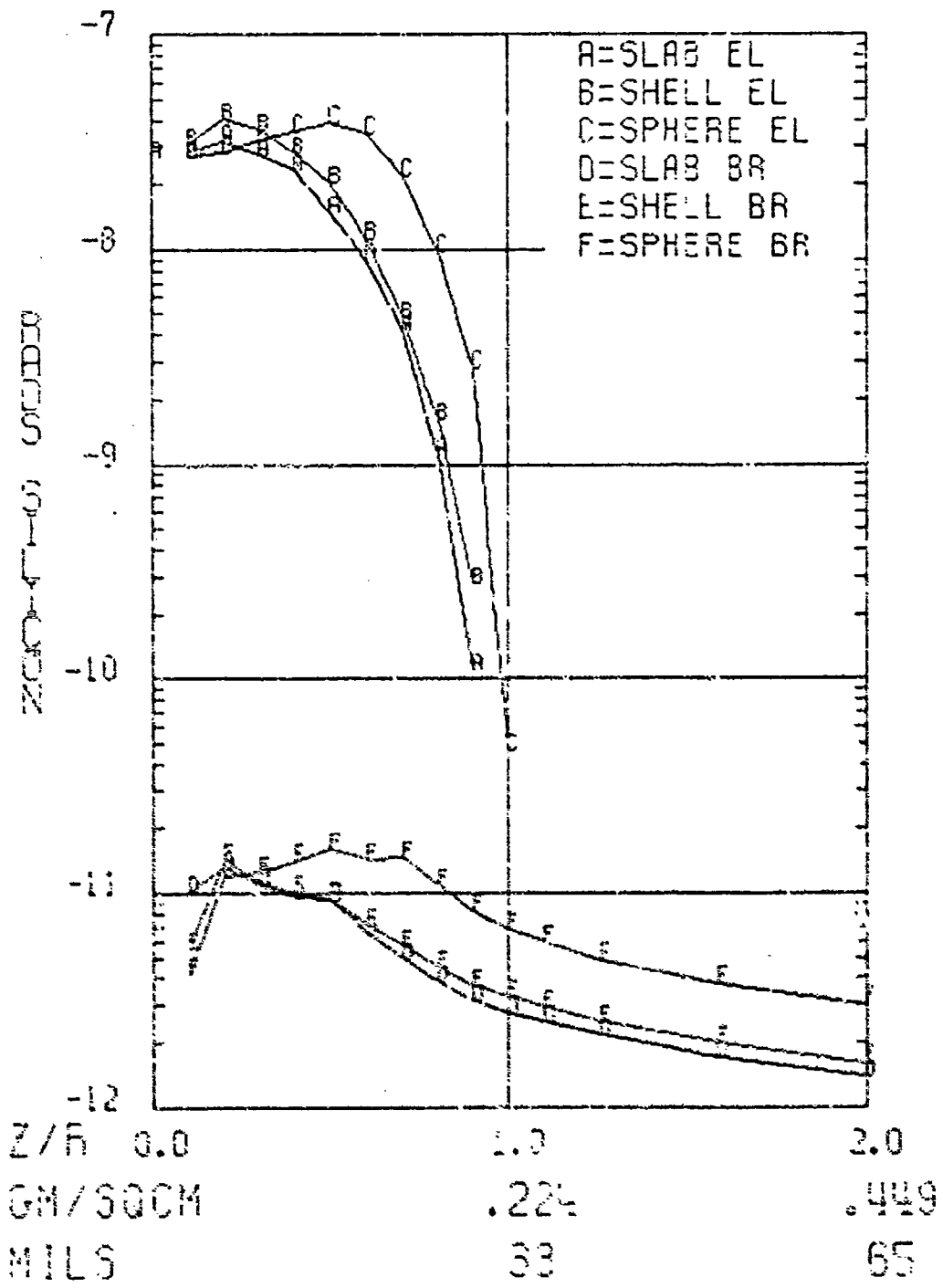
2 MEV, ALUMINUM



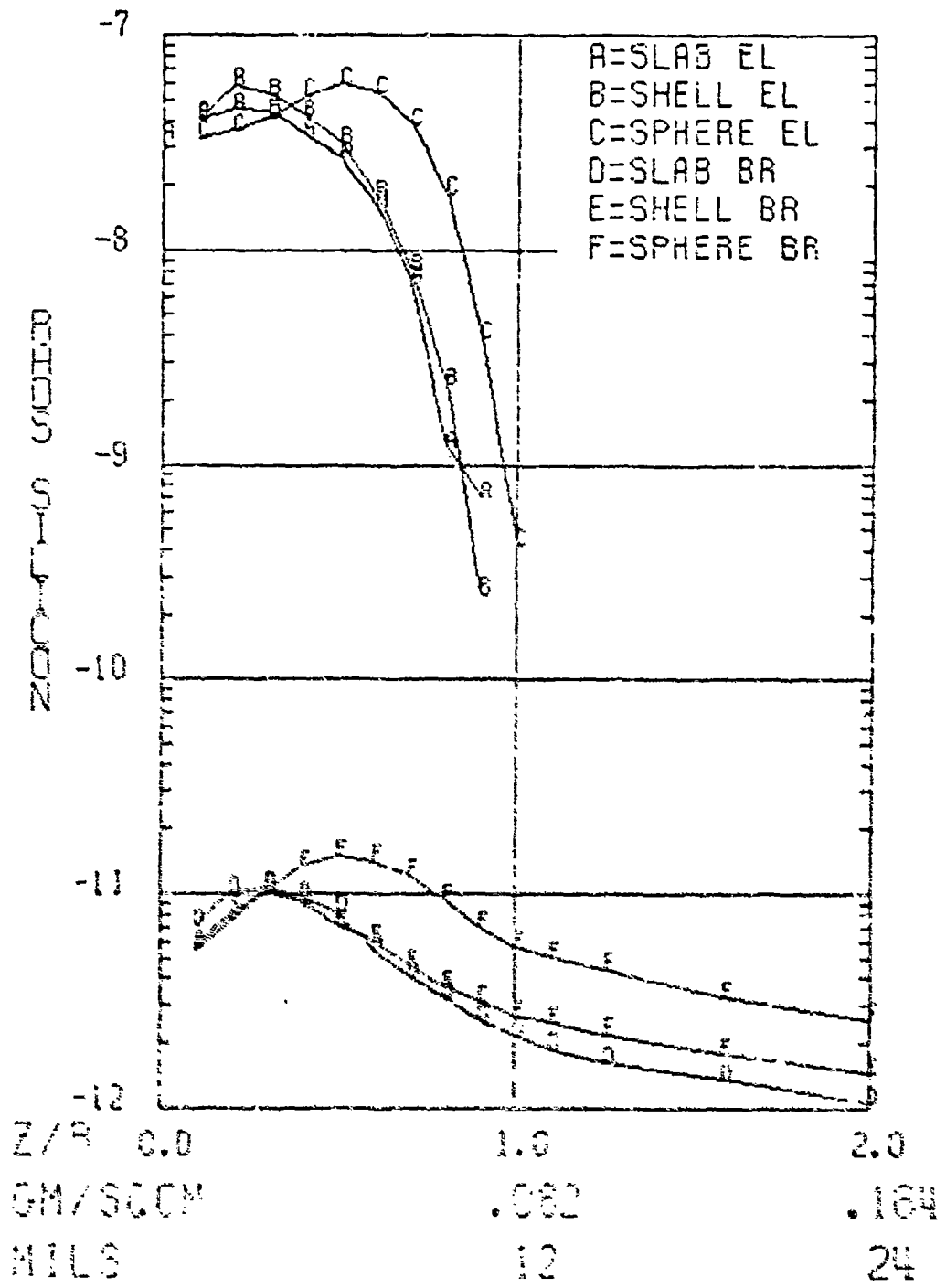
1 MEV, ALUMINUM



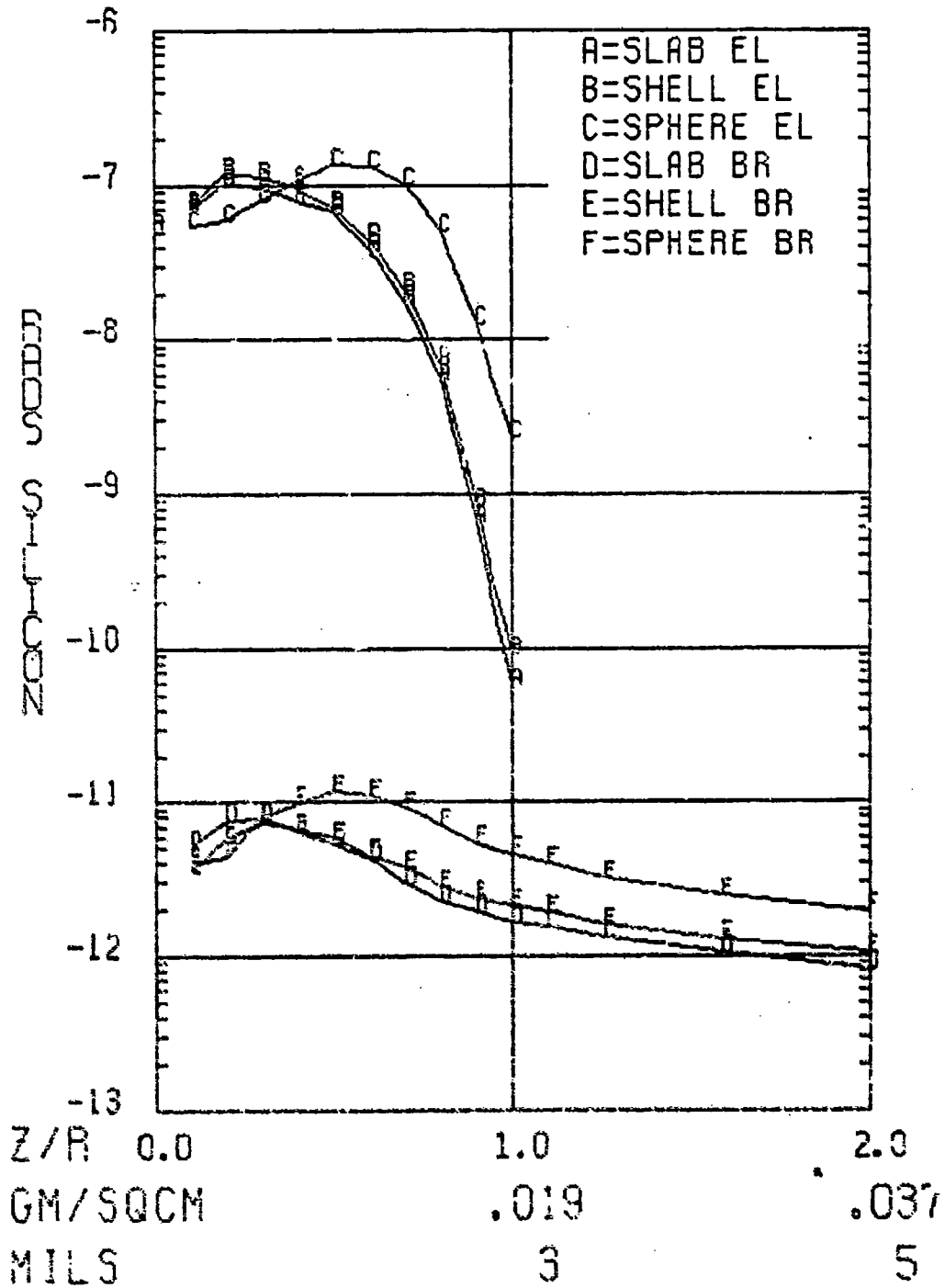
0.5 MEV, ALUMINUM



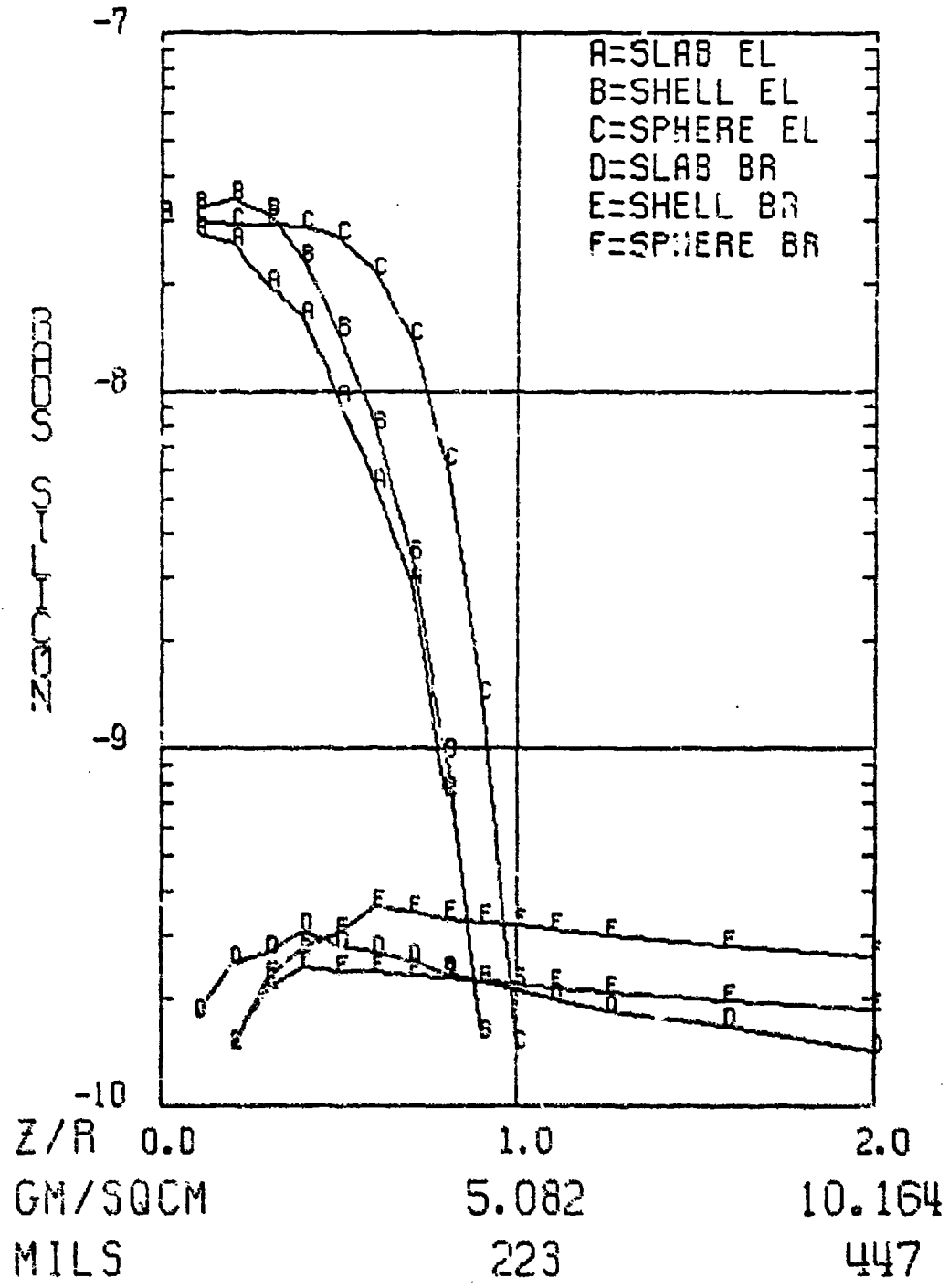
0.25 MEV, ALUMINUM



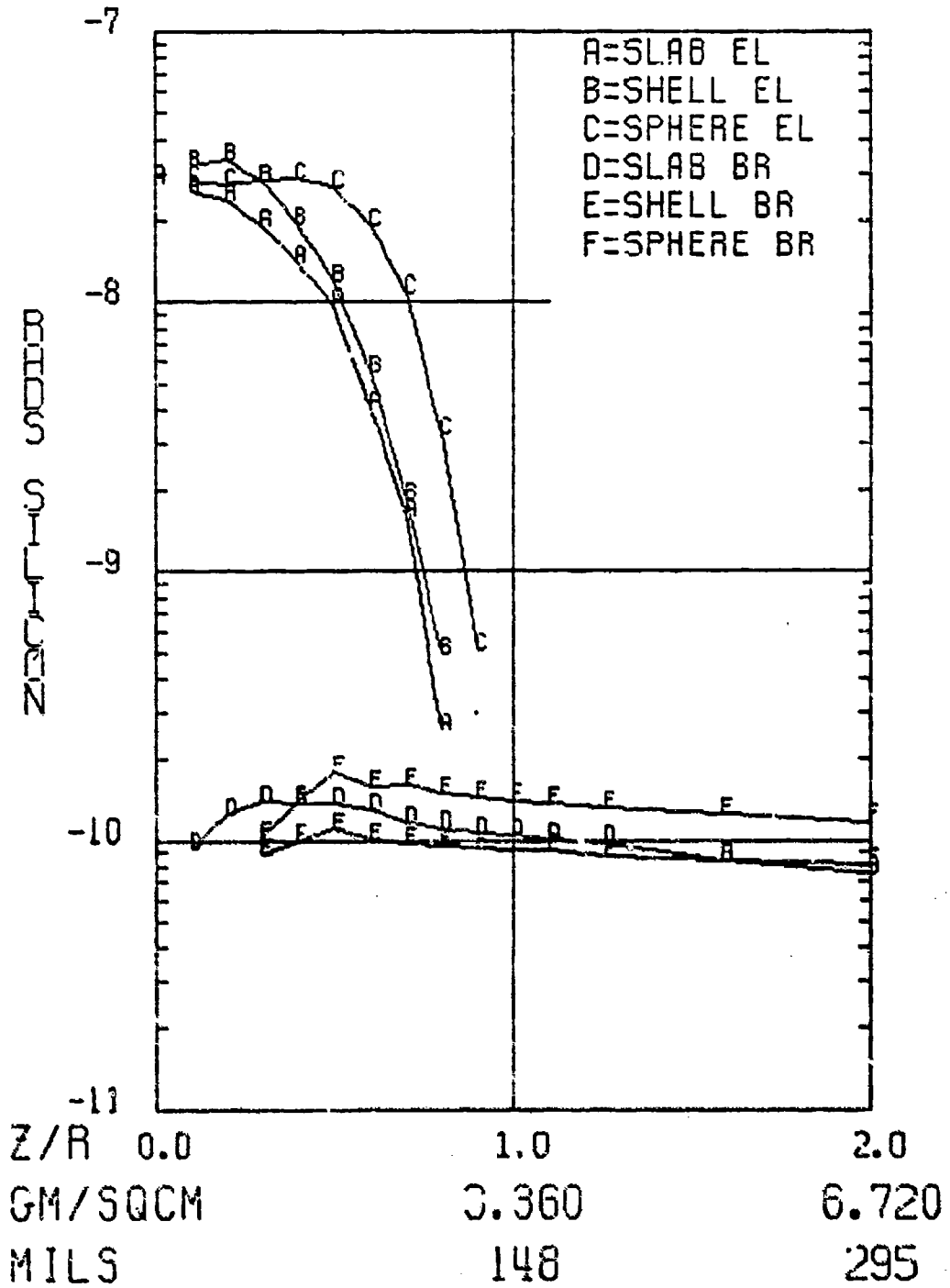
0.1 MEV, ALUMINUM



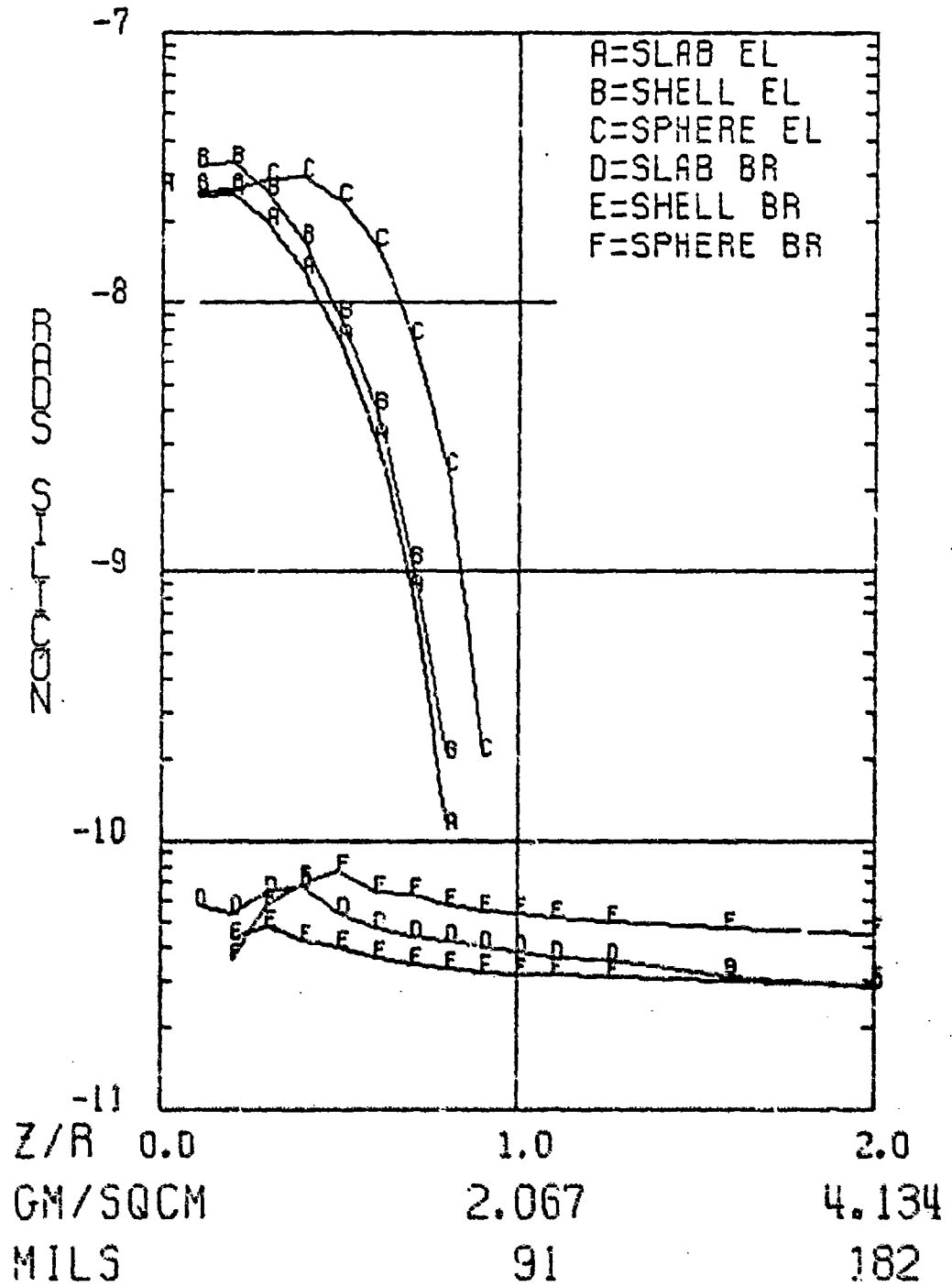
8 MEV, COPPER



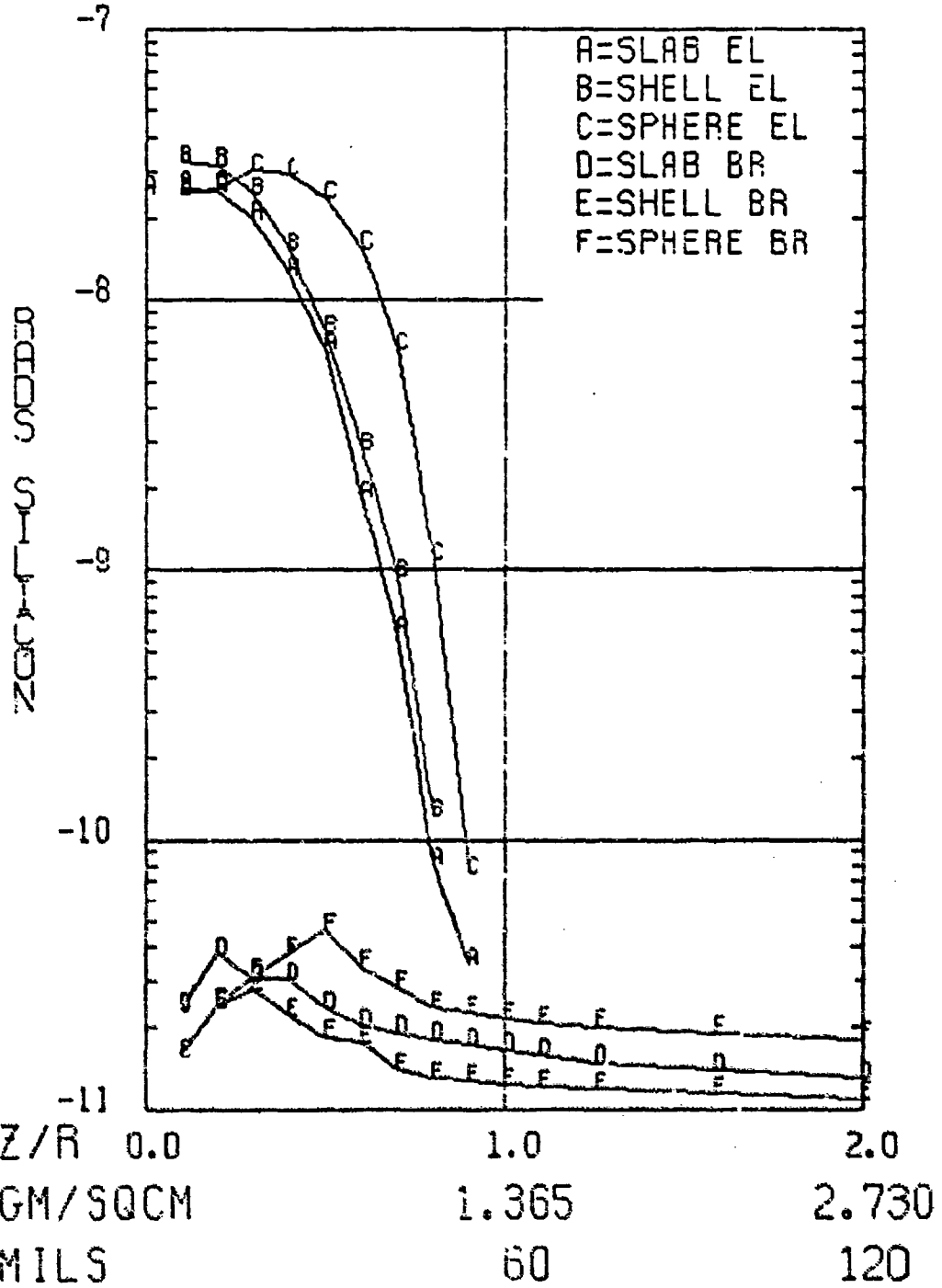
5 MEV, COPPER



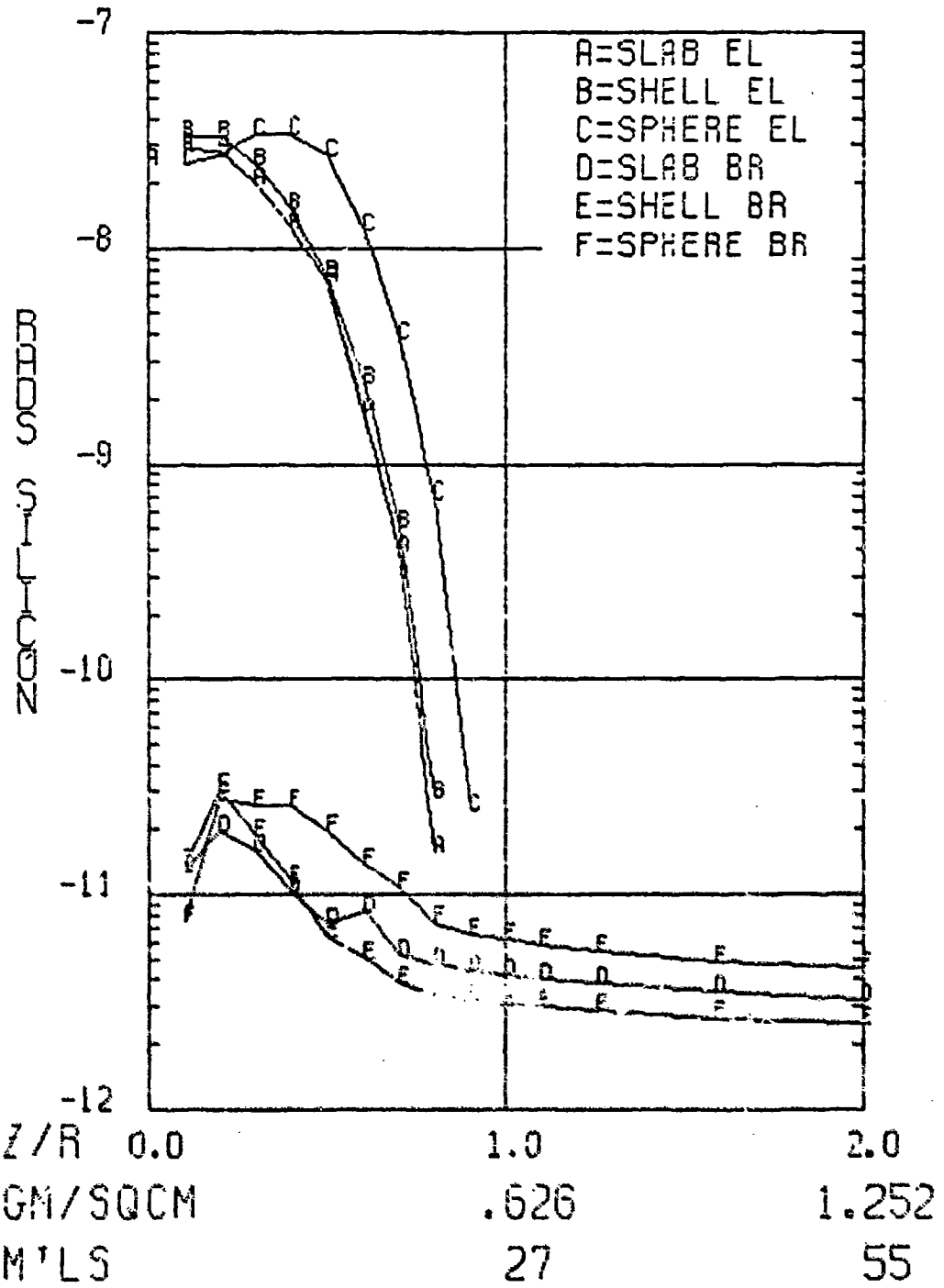
3 MEV, COPPER



2 MEV, COPPER



1 MEV, COPPER



0.5 MEV, COPPER

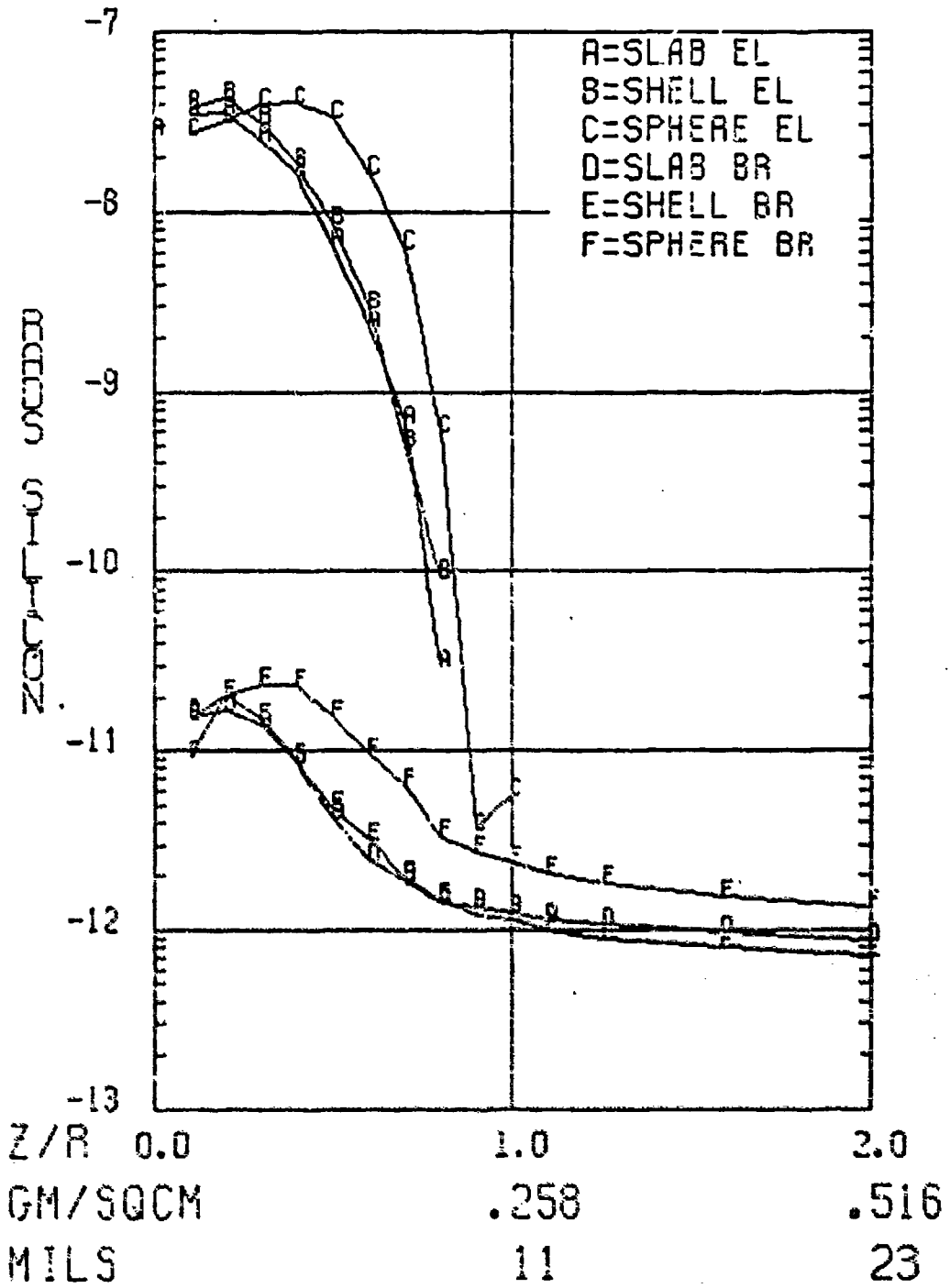
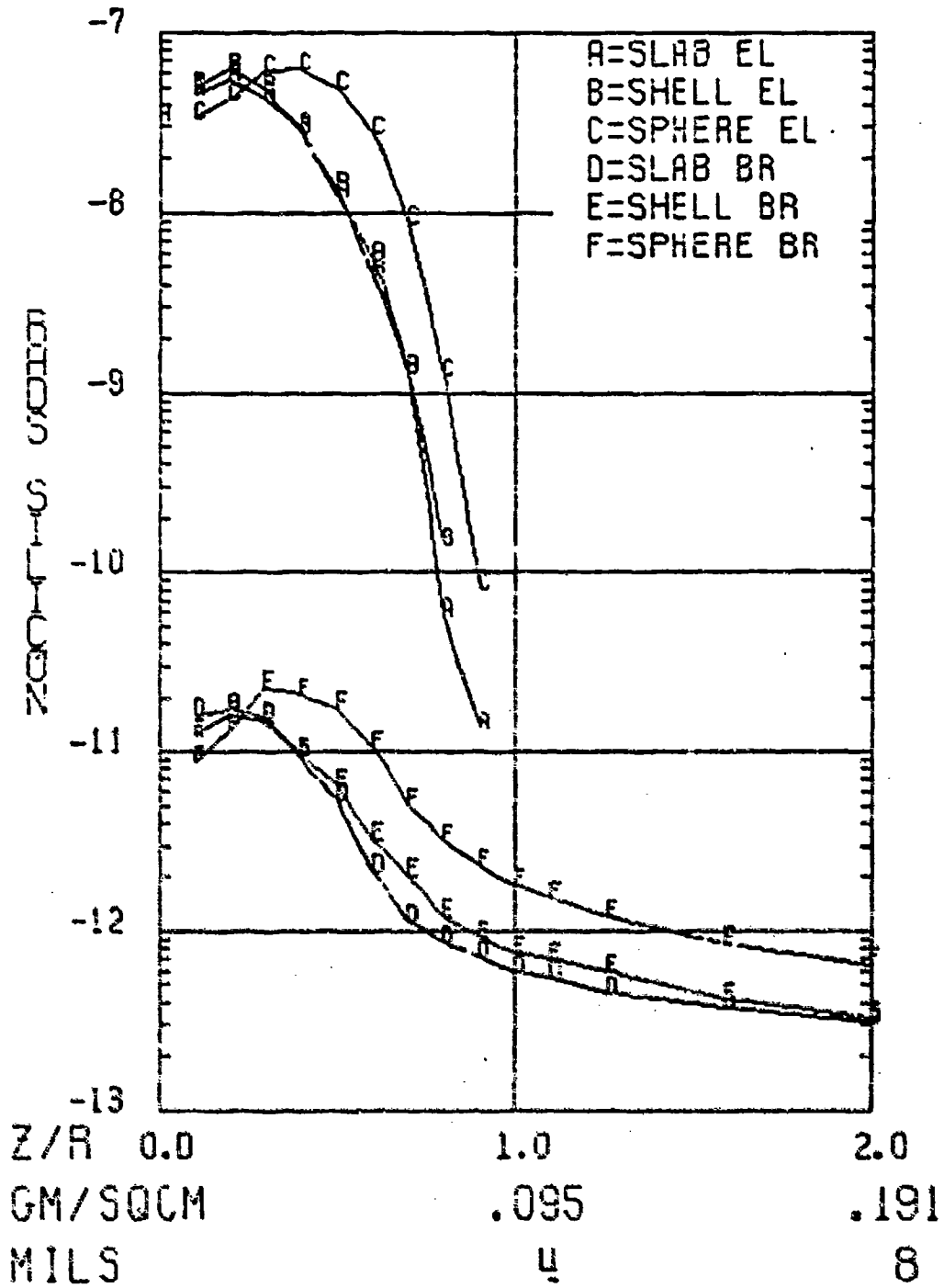
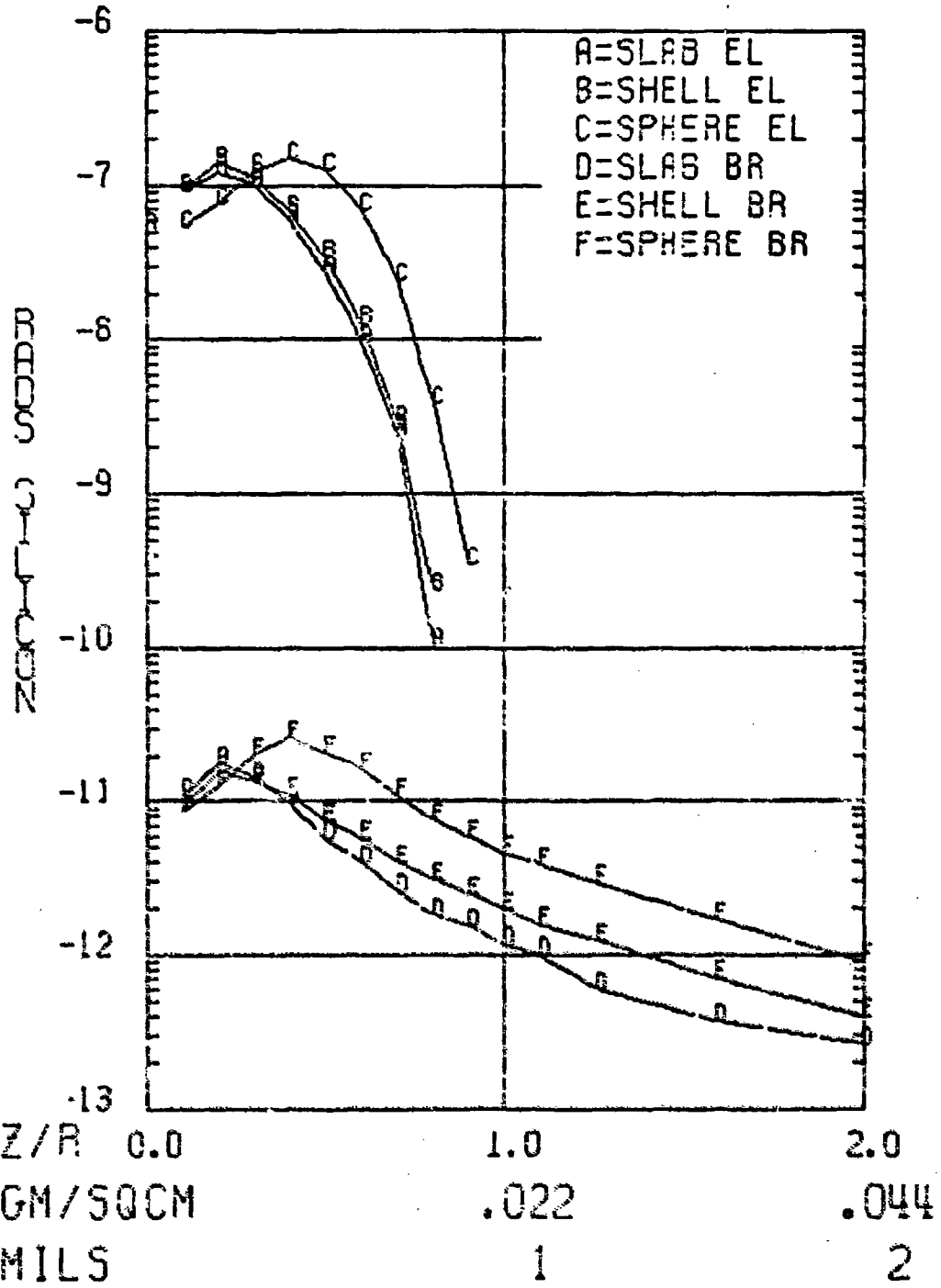


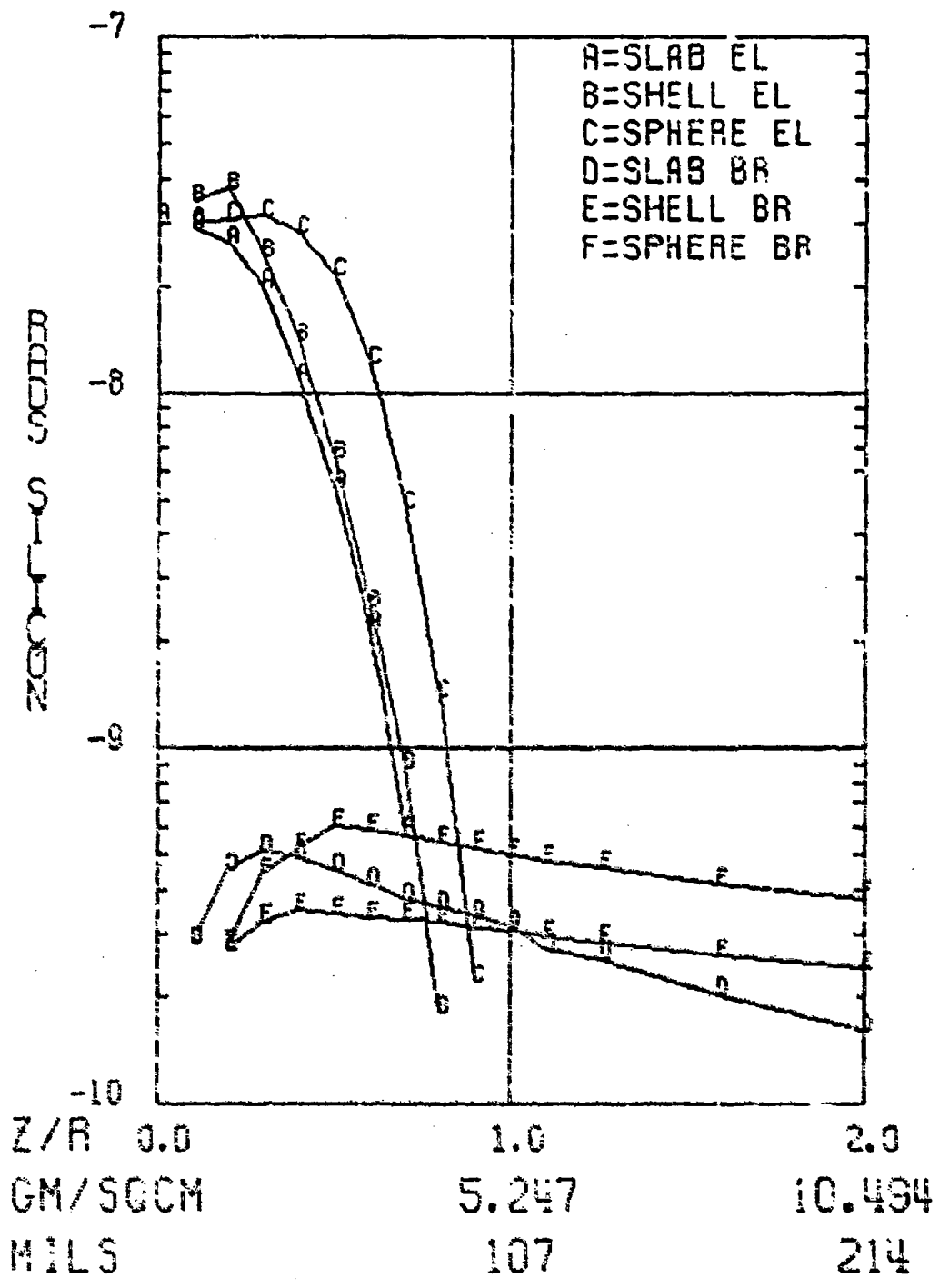
FIGURE 39
0.25 MEV, COPPER



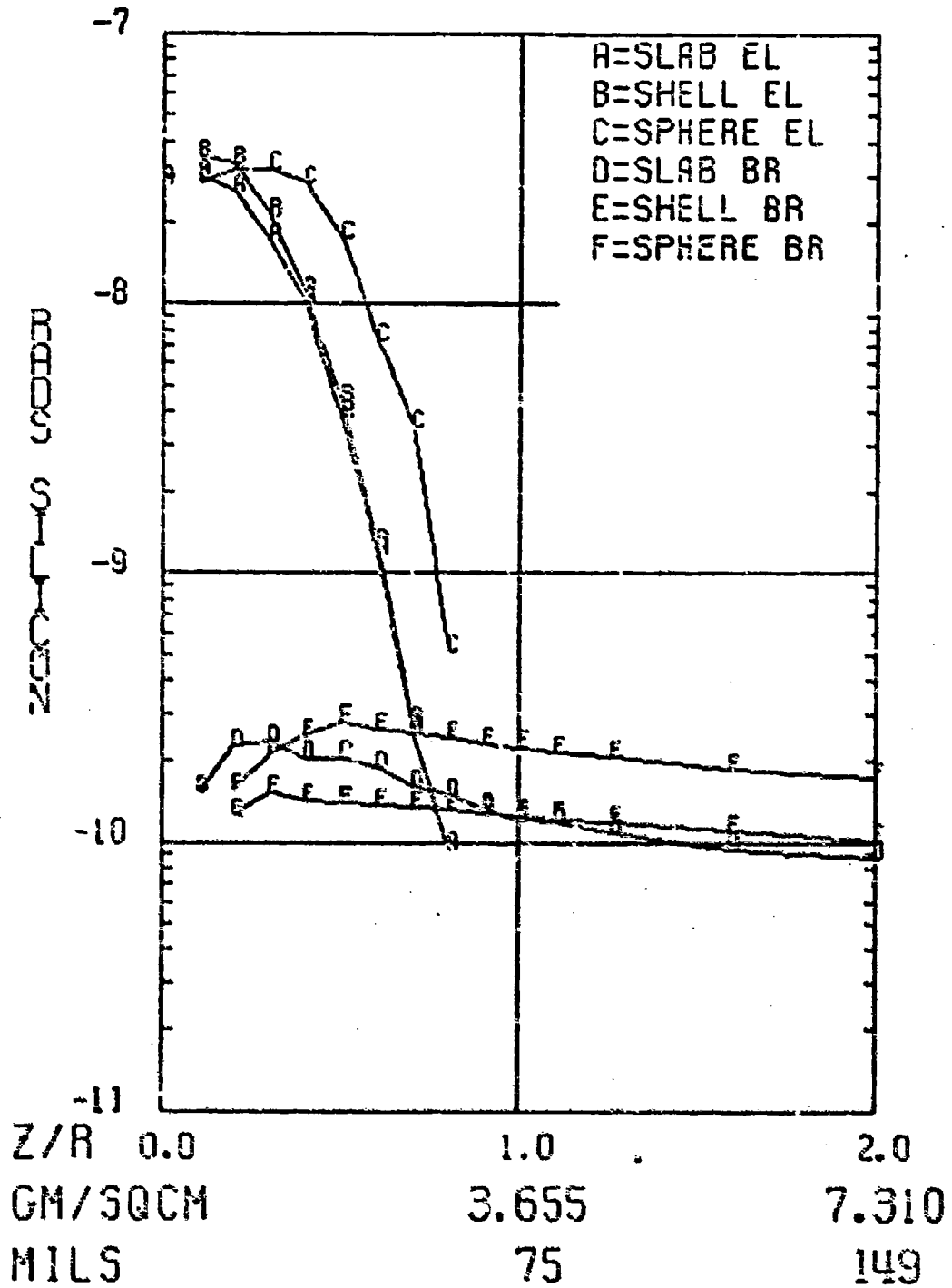
0.1 MEV, COPPER



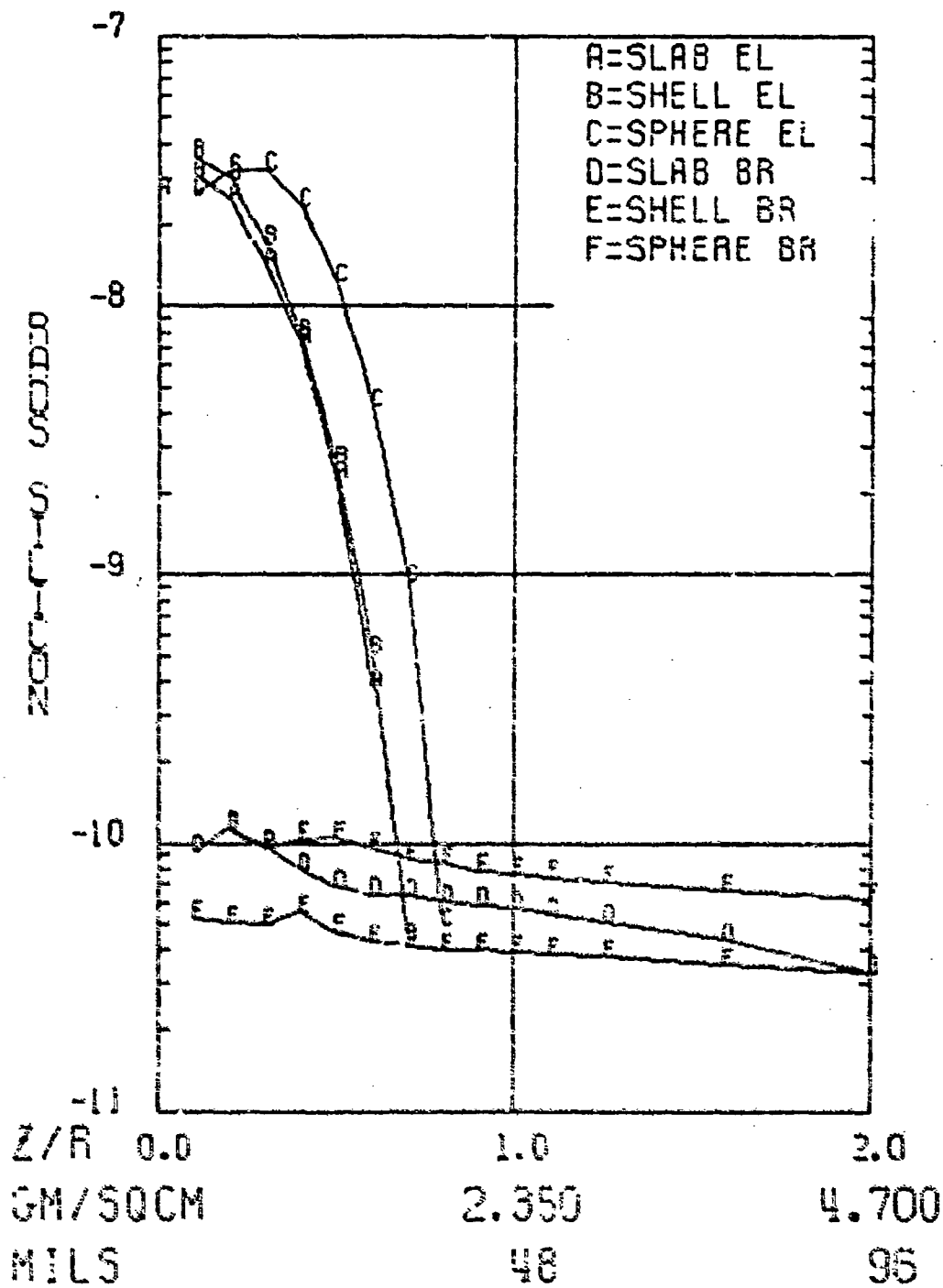
8 MEV, TANTALUM



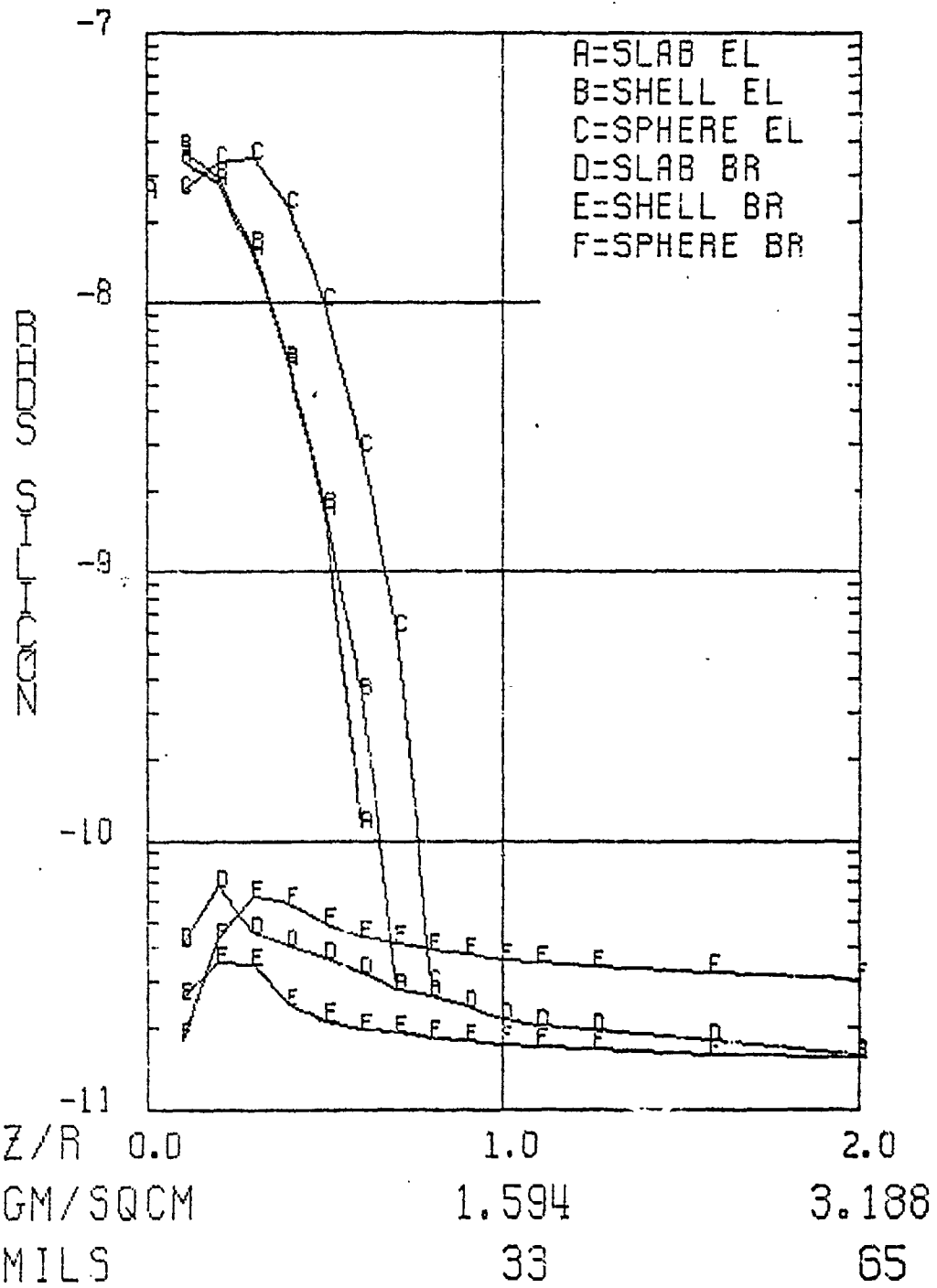
5 MEV, TANTALUM



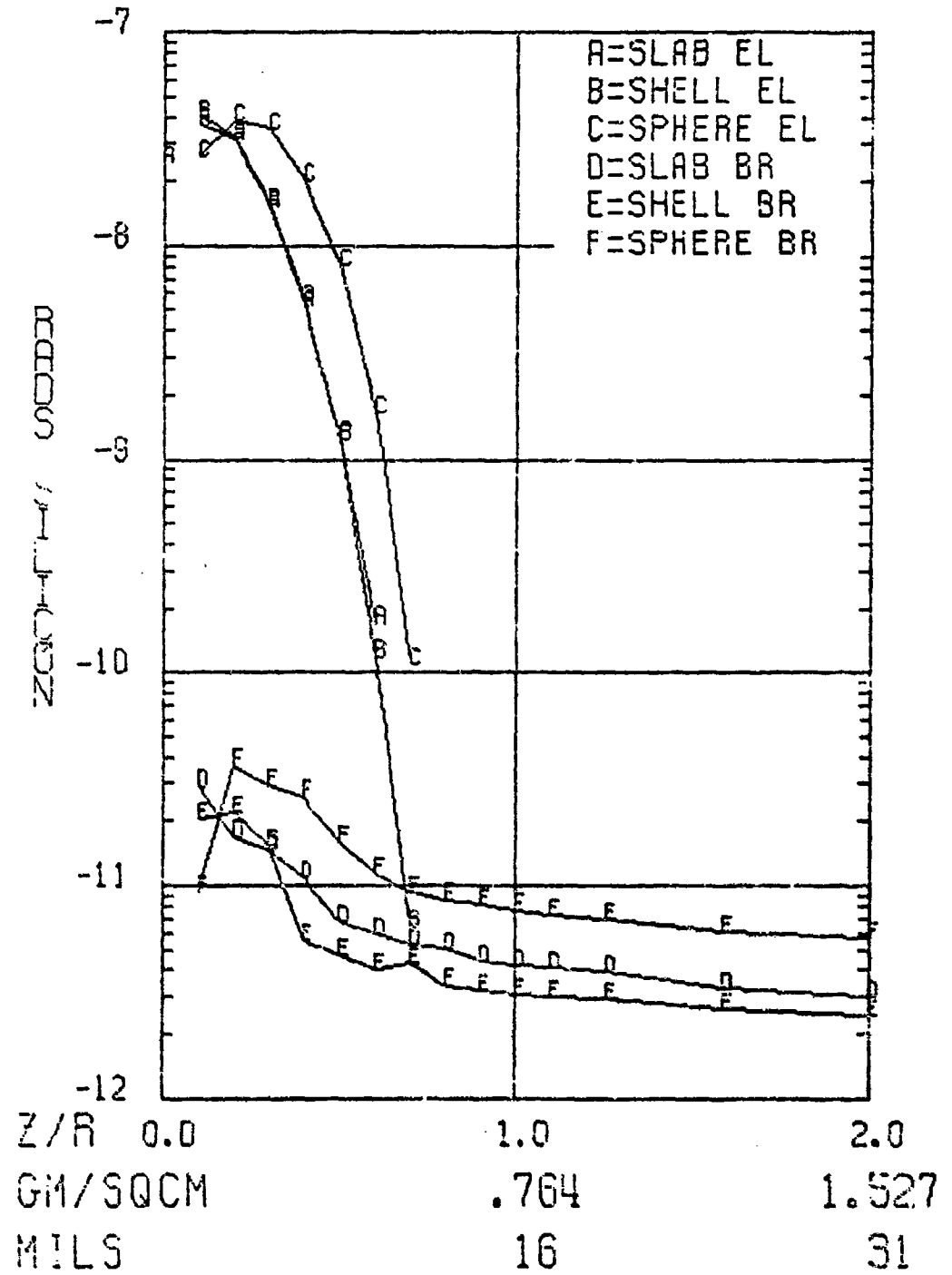
3 MEV, TANTALUM



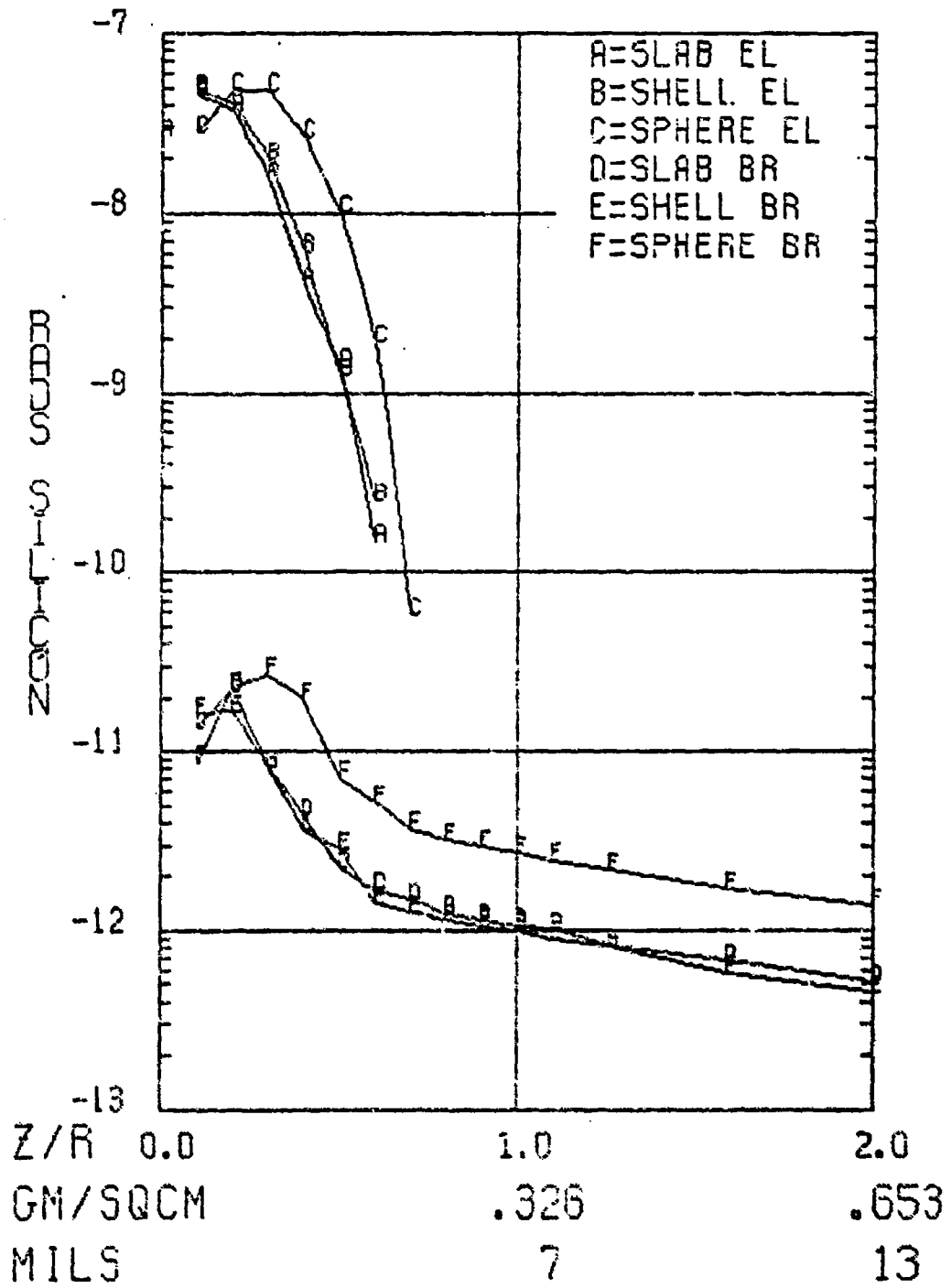
2 MEV, TANTALUM



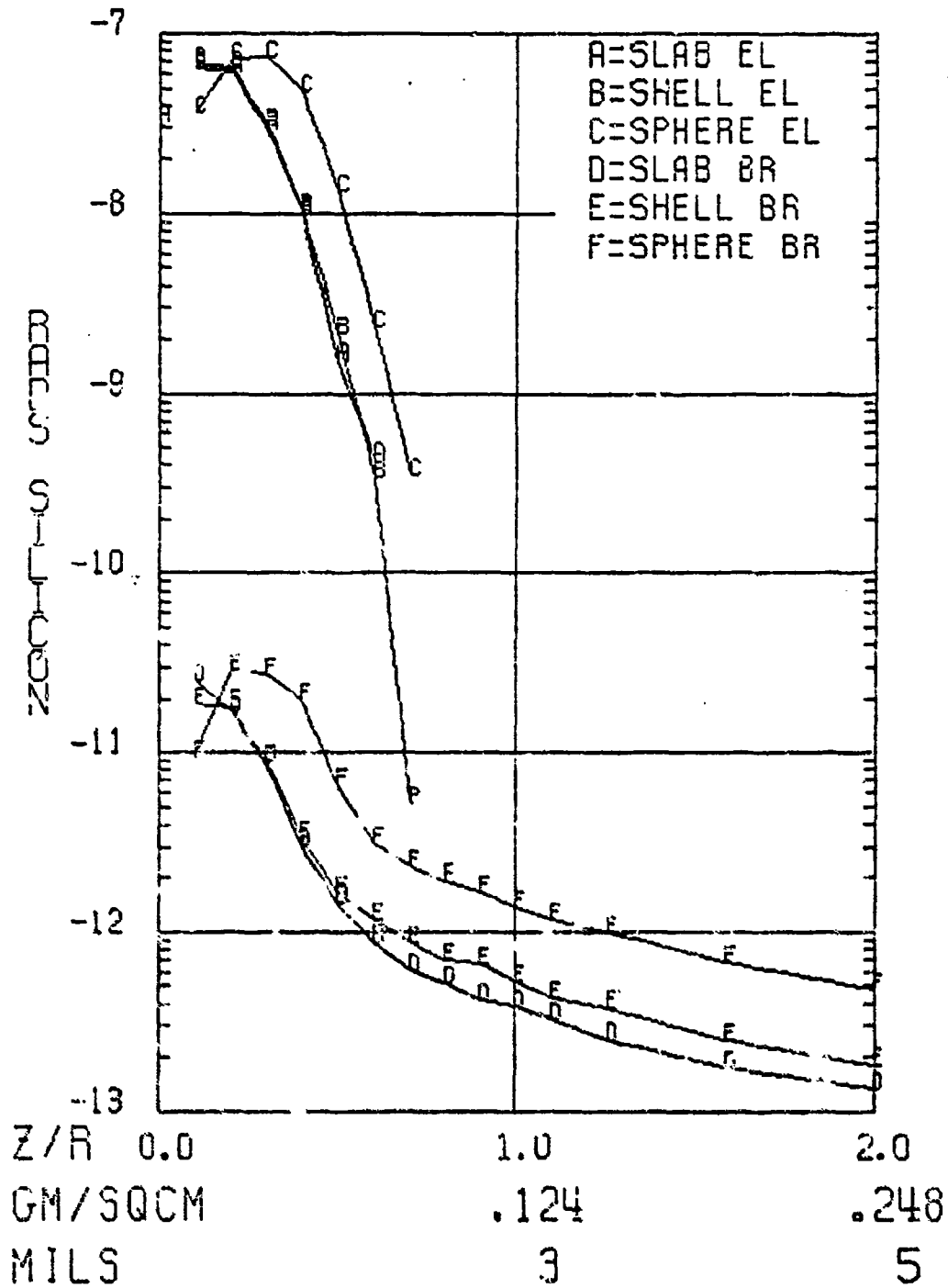
1 MEV, TANTALUM



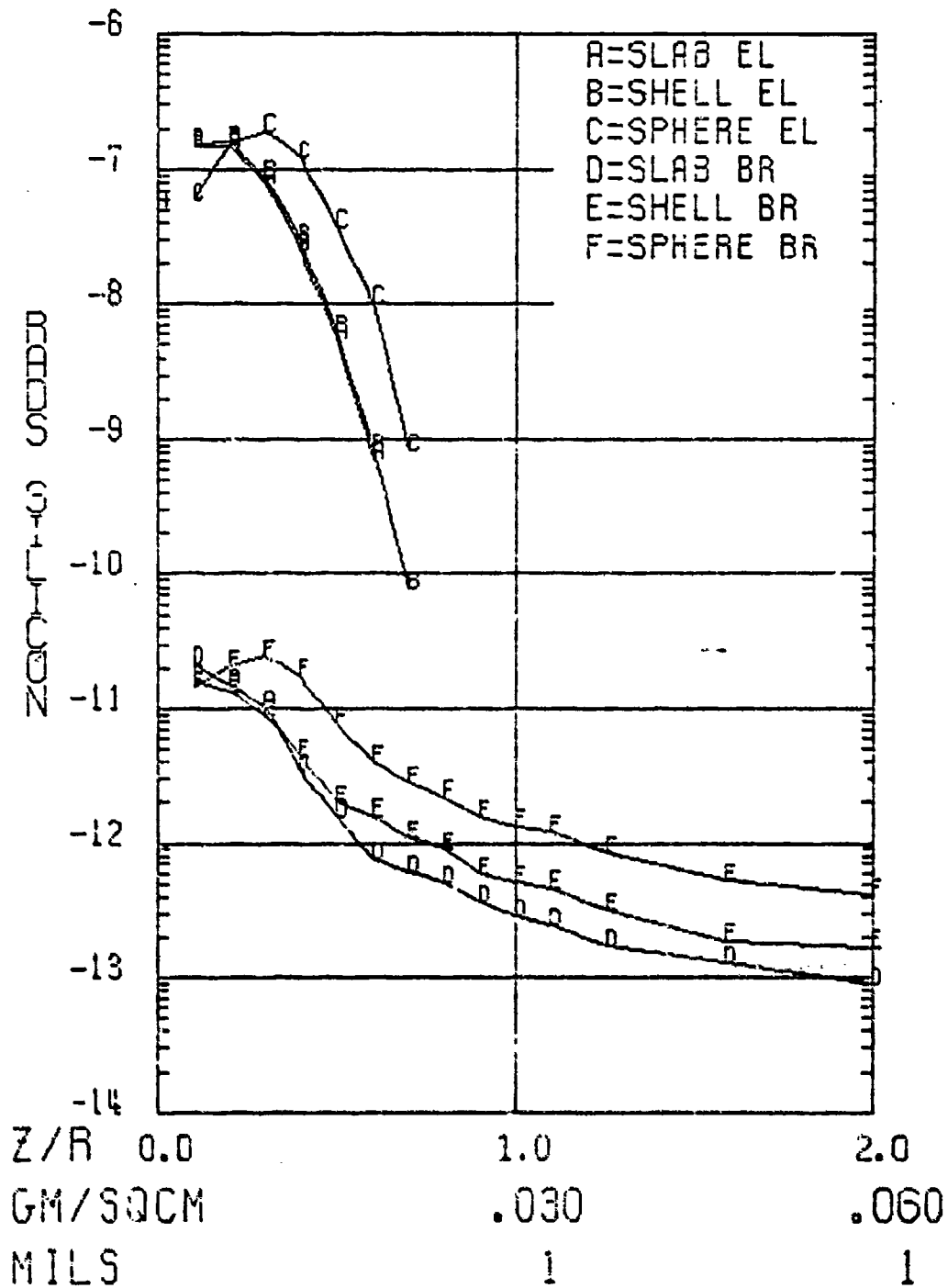
0.5 MEV, TANTALUM



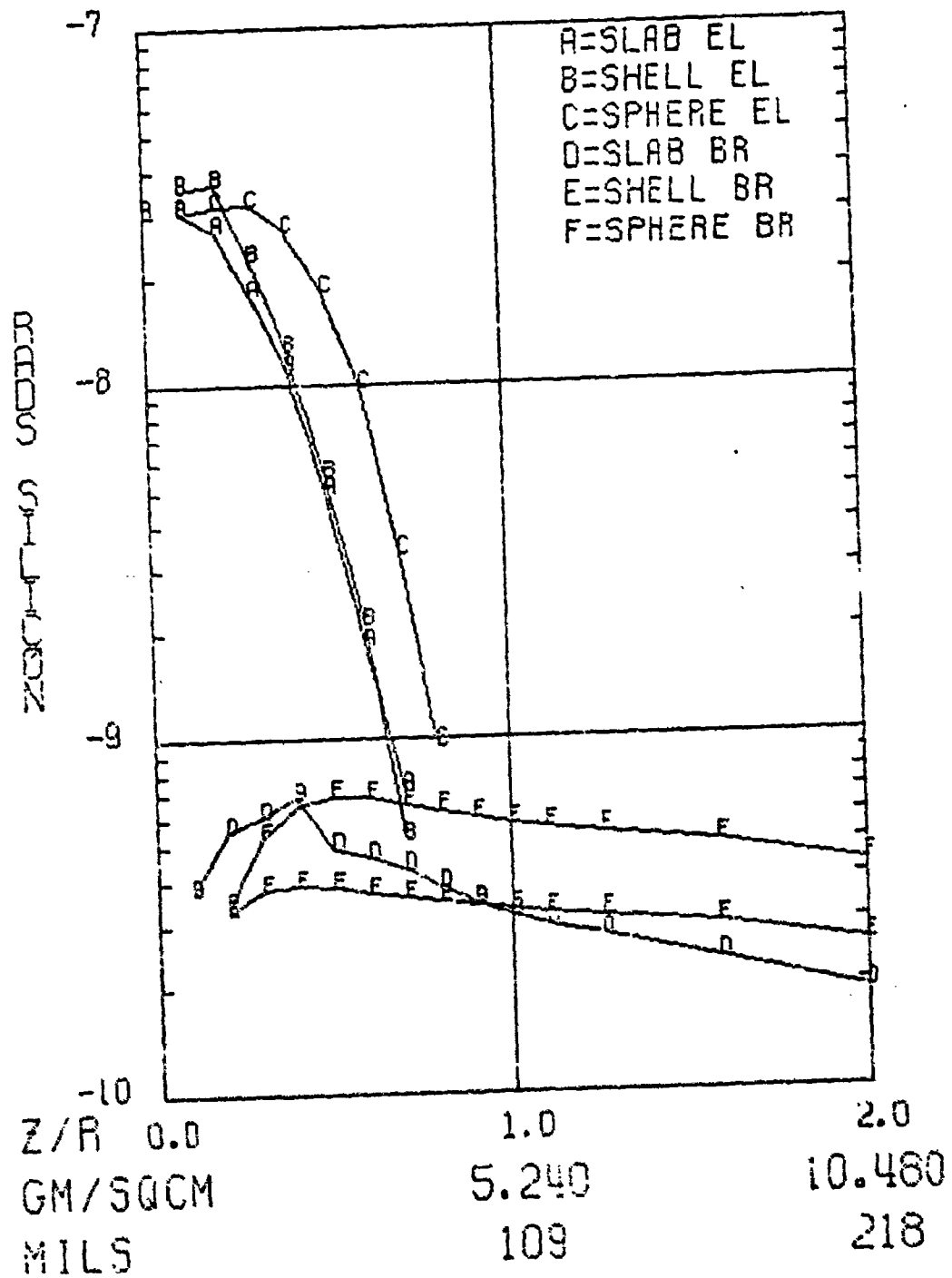
0.25 MEV, TANTALUM



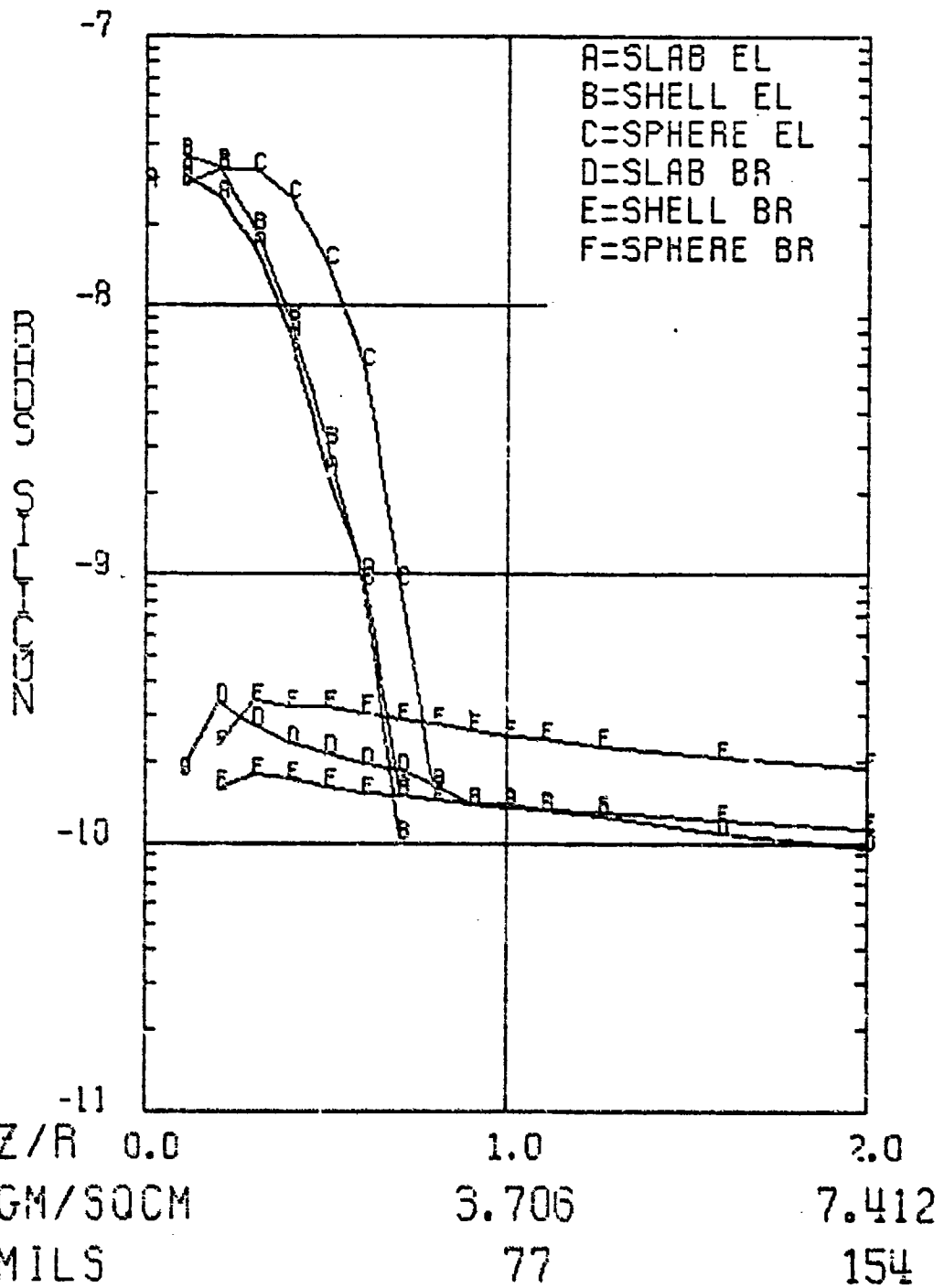
0.1 MEV, TANTALUM



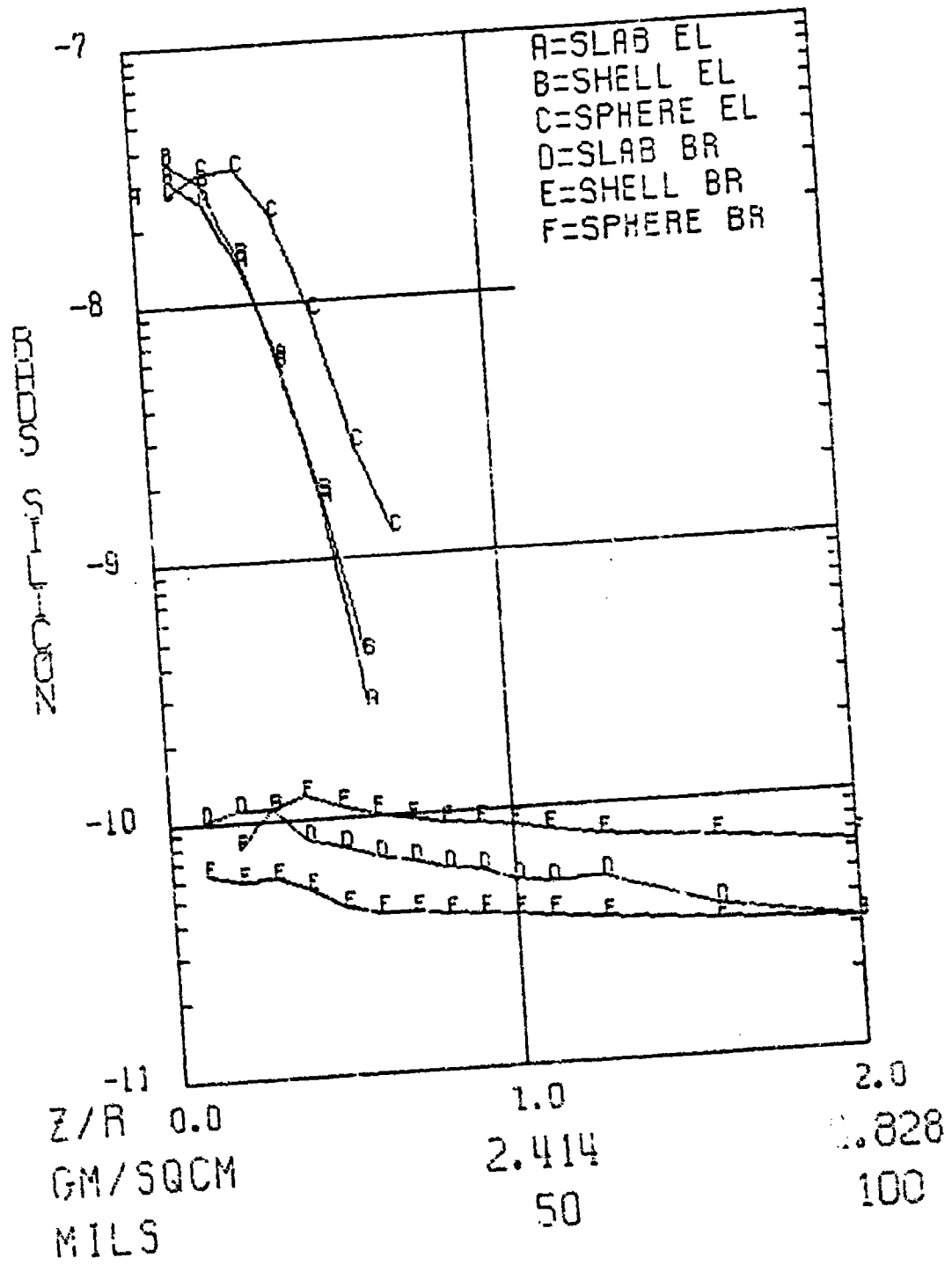
8 MEV, URANIUM



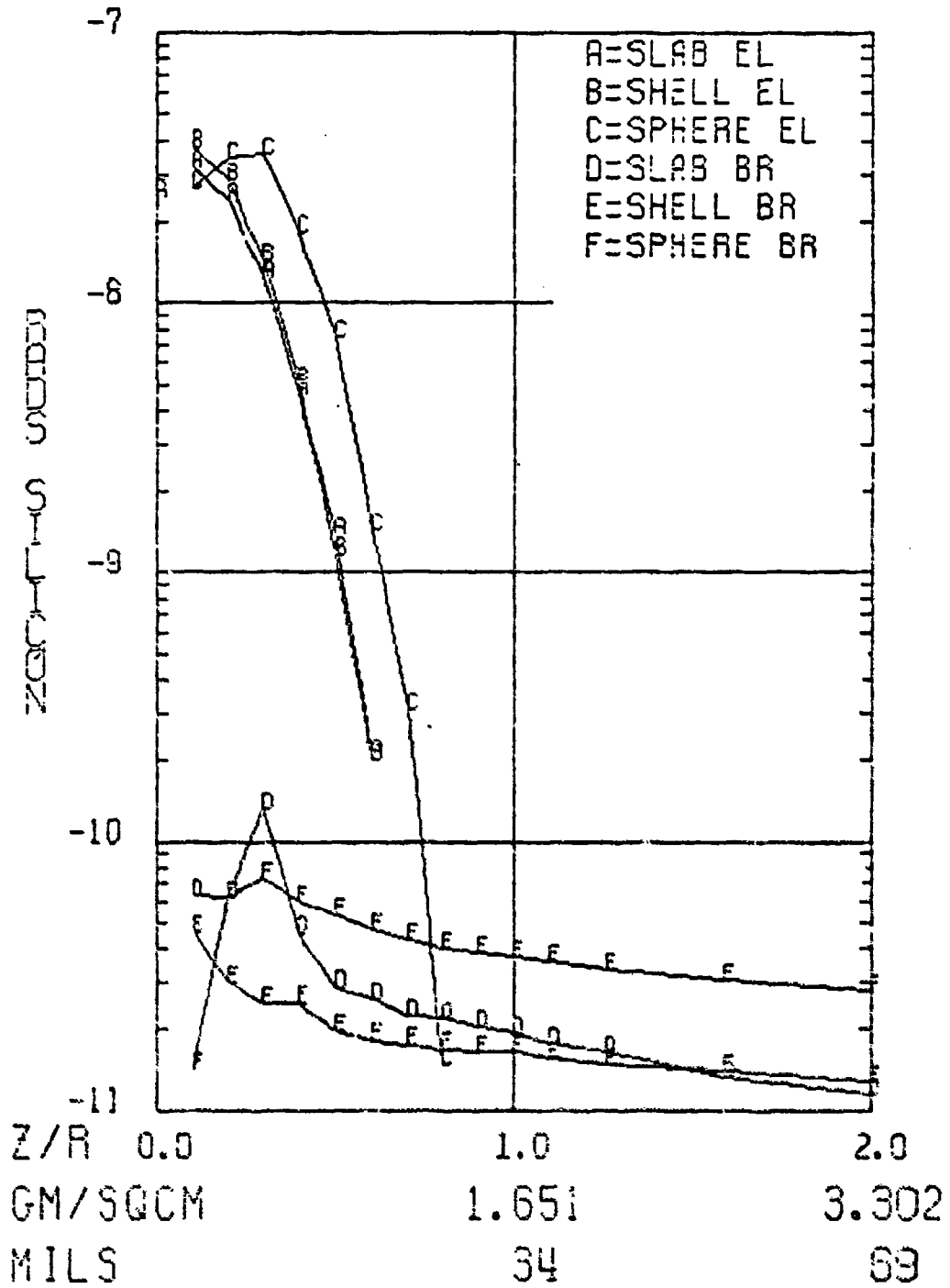
5 MEV, URANIUM



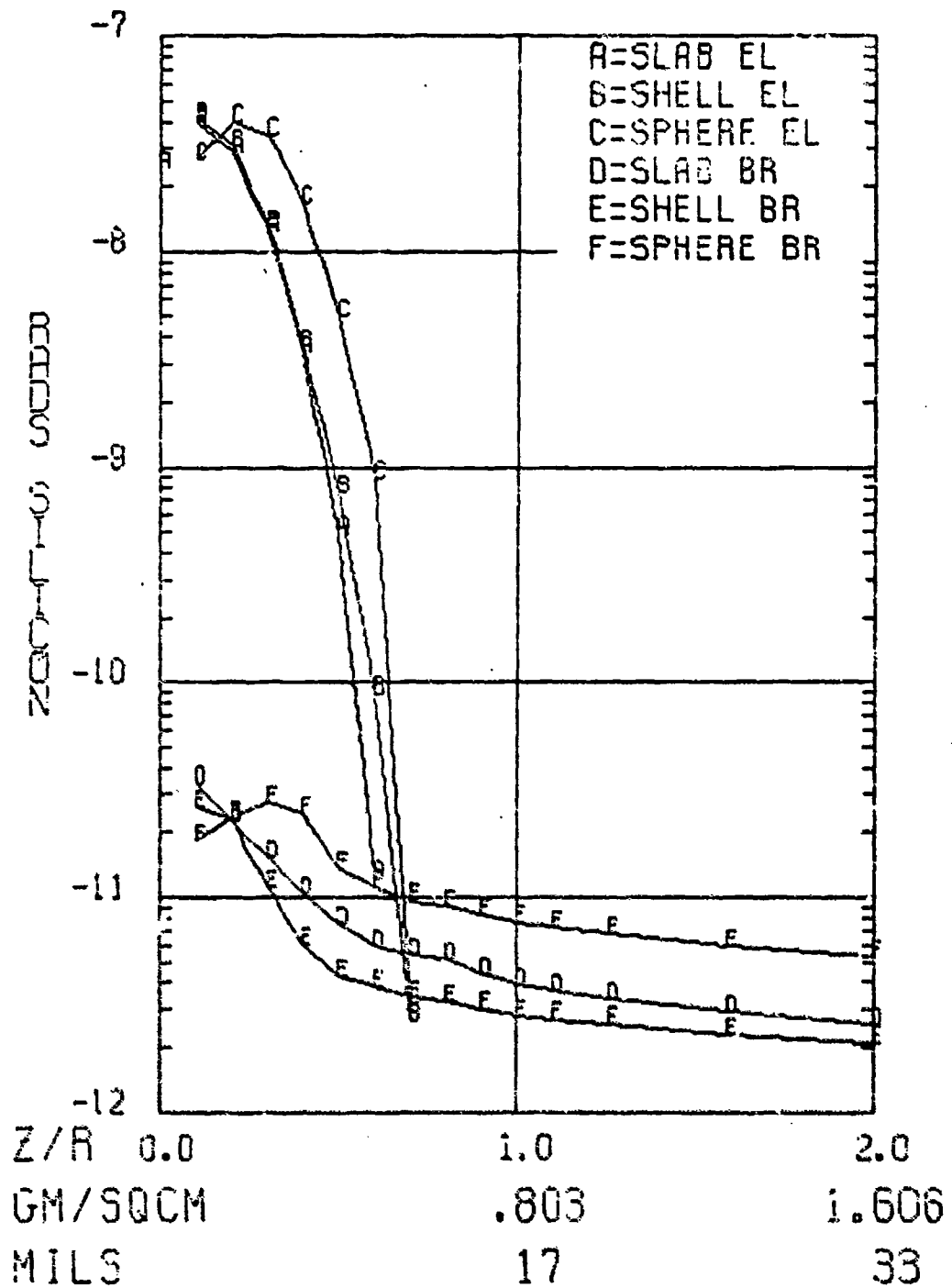
3 MEV, URANIUM



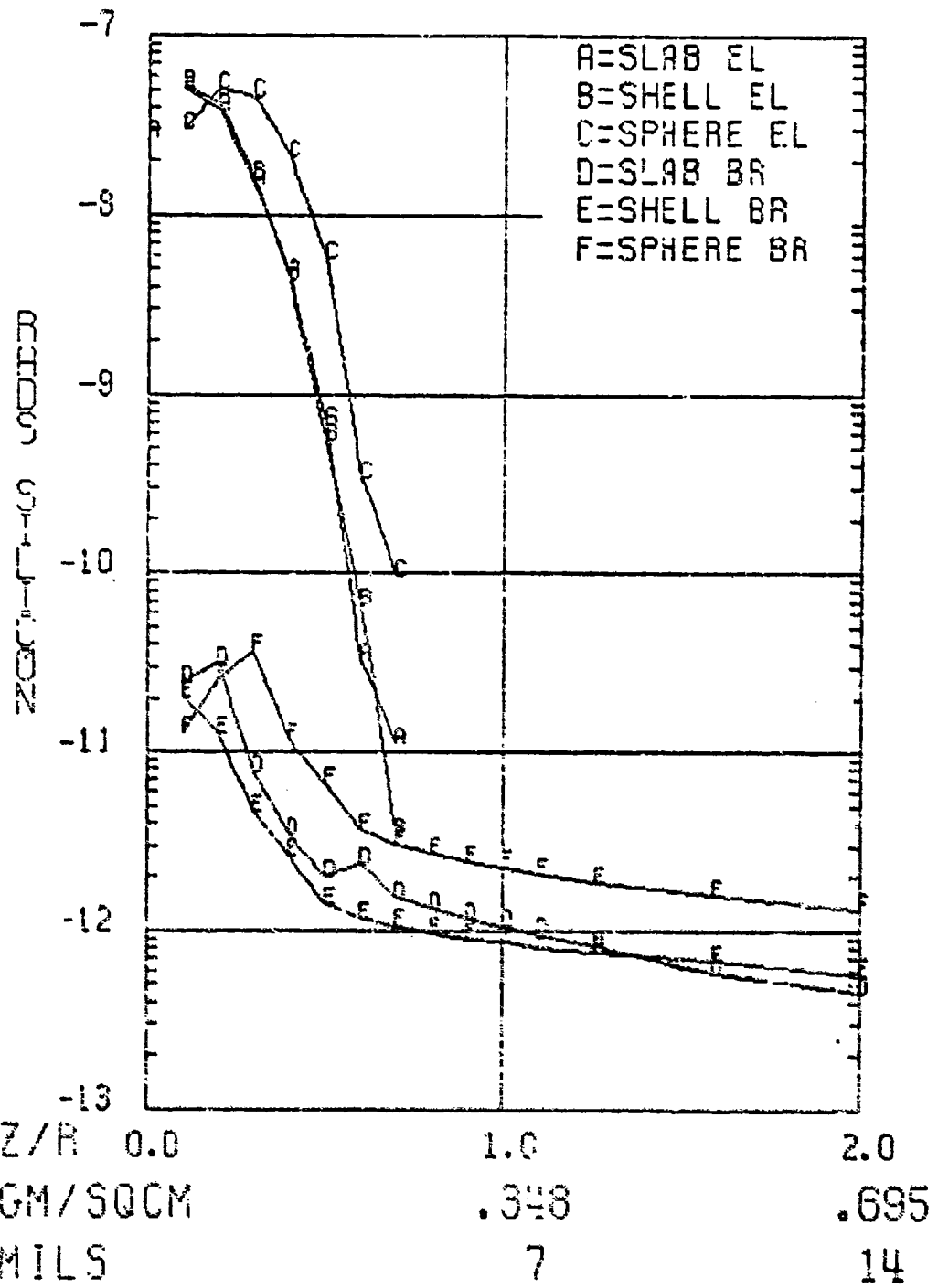
2 MEV, URANIUM



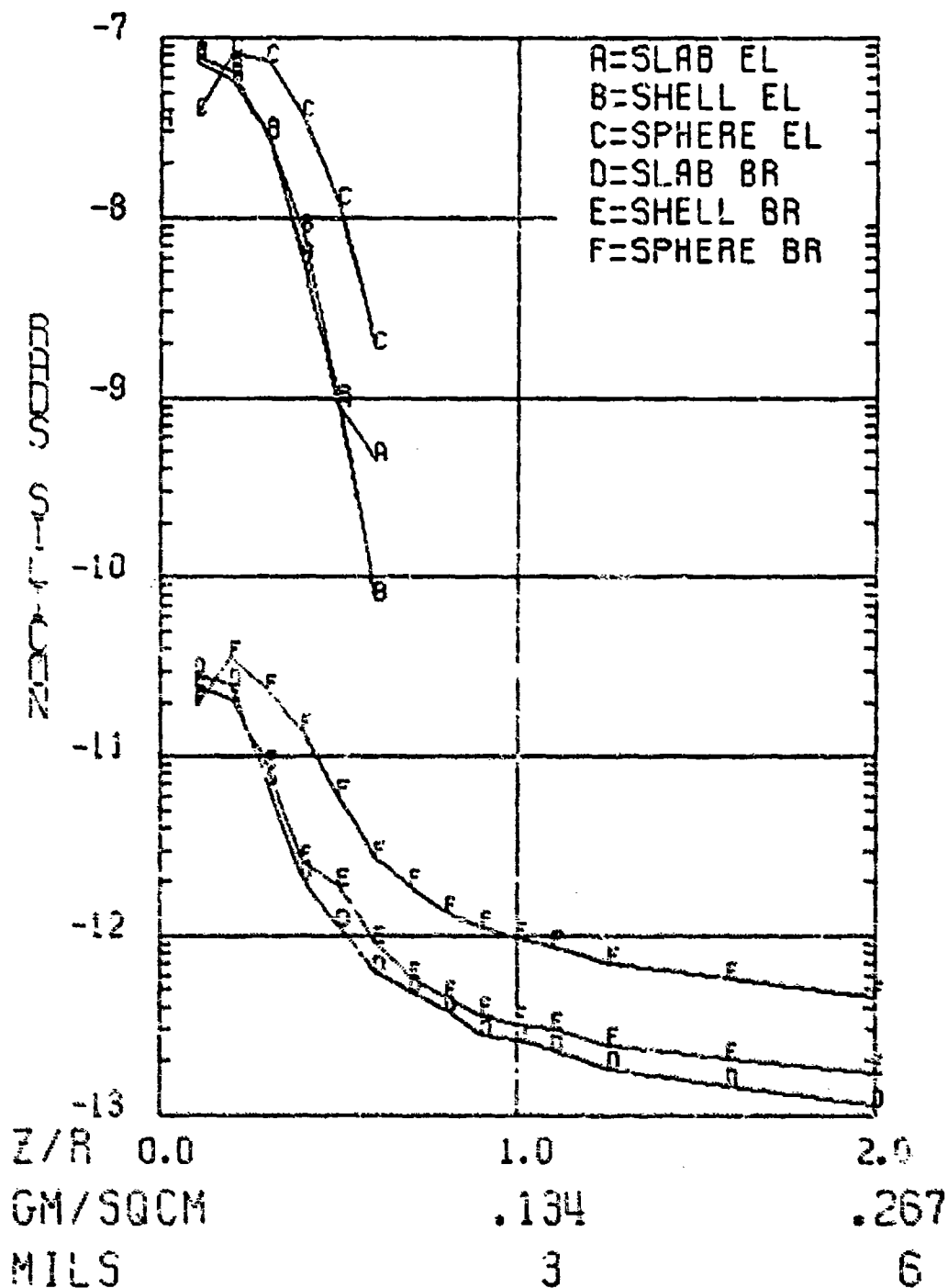
1 MEV, URANIUM



0.5 MEV, URANIUM



0.25 MEV, URANIUM



0.1 MEV, URANIUM

